Multi-Injection Moving Bed Reactors in Cu-Cl Cycle Hydrolysis for Hydrogen Production

by

Jenna M. Broders

A Thesis Submitted in Partial Fulfillment of the Requirements for the Degree of

Master of Engineering

in

The Faculty of Engineering and Applied Science

Mechanical Engineering

Memorial University of Newfoundland and Labrador

November 2023

Newfoundland and Labrador

Abstract

Hydrogen as an energy source has emerged as a promising solution for addressing energy demands while reducing carbon emissions. It has become a focal point of research and innovation in the pursuit of sustainable and clean energy sources. There are several methods of hydrogen production, with thermochemical water splitting through the Copper-Chlorine (Cu-Cl) cycle gaining momentum as a carbon neutral production technique with readily available resources.

A significant challenge for large-scale implementation of the Cu-Cl cycle is the endothermic gas-solid hydrolysis reaction, which requires a large amount of steam in excess of stoichiometry to achieve favourable solid conversion, reducing process efficiency. In this thesis, investigation of the hydrolysis reaction is presented to enhance the understanding of the reaction limitations as well as identify scenarios which improve conversion and minimize steam requirements. Employing the established ideal operating conditions, this thesis aims to develop a kinetic model for a novel reactor design – downdraft multi-injection moving bed reactors (MBR). A detailed literature review highlights current work on techniques that increase CuCl2 conversion and reduce steam to copper ratios (SCR), side reactions and by-products, as well as explores the various types of reactors for the hydrolysis phase.

Applying the established operating ranges and side reactions from the literature, a phase equilibrium simulation is generated to discern conditions that will improve solid conversion and mitigate side reaction progression. From the set of simulations, an ideal temperature of

375℃, pressure of 1 bar, and a molar SCR of 10:1, were utilized to model the behaviour of a downdraft multi-injection MBR through reactors in series. This simulation demonstrated a 17% increase in $CuCl_2$ conversion when compared to a single injection reactor at the same conditions, indicating the viability of an MBR approach to the hydrolysis stage. In terms of steam reduction techniques, a gas recirculation configuration was explored to recycle the unreacted outlet steam. Due to the increasing concentration of HCl gas with every recycle, this configuration requires additional processing to reduce the concentration of HCl.

Building on the results from the phase equilibrium MBR simulation, reaction rates and kinetics were introduced to generate a more realistic predictive model of the hydrolysis reaction in downdraft multi-injection MBR conditions. A comparison to a fixed bed reactor at the same conditions was performed. A 23.4% increase in $CuCl_2$ solid conversion was observed. Applying the same conditions as those used in the phase equilibrium model resulted in a total conversion of 61.1%. Through a sensitivity analysis at varying reactor lengths, injection spacing and steam injection amounts, a maximum conversion of 66.5% was achieved. The sensitivity analysis also demonstrated the importance of reactor design on reaction progression, emphasizing the need to investigate different reactor scenarios to identify conditions for the best conversion and product yield. Overall, this research demonstrated the promising feasibility of the MBR reactor design for the hydrolysis reactor, with the ability to obtain higher solid conversion at lower SCR.

Acknowledgements

I would like to take this opportunity to thank my supervisors, Dr. K. Pope, and Dr. G. Naterer, as well as Dr. K.A. Hawboldt for their continual guidance, encouragement, and advice during this research. The financial assistance of the Natural Sciences and Engineering Research Council of Canada (NSERC) and Canadian Nuclear Laboratories (CNL) is also gratefully acknowledged.

Table of Contents

Nomenclature

a	Stoichiometric coefficient of $CuCl_2$
C_i	Concentration, mol/m^3
C_p	Heat capacity
d	Reactor diameter, m
D_p	Particle diameter, m
F_i	Molar flowrate, mol/s
g	Gravitational acceleration, m^2/s
k	Reaction rate constant, $m^3/mol\text{-}s$
K	Equilibrium constant
L	Reactor length, m
n_i	Moles, mol
p_i	Partial pressure, bar
P	Pressure, bar
r_c	Particle radius, m
r_i	Species reaction rate
R	Reactor radius, m
R_p	Particle radius, m
s	Steam to copper ratio, mol/mol
T	Temperature, (K/℃)
V	Volume, m^3
x	Conversion

Acronyms

AP	Acidification Potential
Cu-Cl	Copper Chlorine
CRM	Continuous Reaction Model
EP	Eutrophication Potential
FBR	Fluidized Bed Reactor

GHG	Greenhouse Gas
GWP	Global Warming Potential
LCA	Life Cycle Assessment
MBR	Moving Bed Reactor
ODE	Ordinary Differential Equation
ODP	Ozone Depletion Potential
PFD	Process Flow Diagram
PFR	Plug Flow Reactor
PSA	Parametric Sensitivity Analysis
RSFB	Recirculation Steam Fluidized Bed
SCM	Shrinking Core Model
SCR	Steam to Copper Ratio
SMR	Steam Methane Reforming
TWSC	Thermochemical Water Splitting Cycles
URM	Uniform Reaction Model
XANES	X-ray Absorption Near Edge Structure Spectroscopy

Greek Letters

ε_{mf}	Void fraction at minimum fluidization velocity
ρ_i	Density, kg/m^3
μ	Viscosity

Subscripts

aq	Aqueous state
g	Gas phase
i	Species
l	Liquid phase
s	Solid phase

List of Figures

List of Tables

Chapter 1 – Introduction

Fossil fuel combustion by-products are the world's most significant contributors to global warming [1]. Generation and usage of fossil fuels contributes to approximately 70% of climate change through the release of Greenhouse Gases (GHG) such as CO_2, CH_4, and NO_x [2]. However, they are fundamental to the current anthropogenic era, as the main sources for the world energy supply.

At the current rate of consumption, the world's supply for fossil fuel is rapidly diminishing. Predictive models suggest between 35 – 50 years remain before oil and gas reserves are significantly diminished, and 150 - 400 years for coal if new reserves are not identified [3-5]. From the World Energy Outlook (WEO) 2022, the world is currently amid a global energy crisis, and with the implications of climate change and global warming, research surrounding sustainable, clean energy alternatives has been magnified [6]. Various energy sources such as solar, wind, and geothermal have growing visibility within the energy market as renewable alternatives to fossil fuels.

Hydrogen is a promising resource that is recognized as a renewable alternative in the energy industry [7]. It has the advantage of existing as an energy carrier and an energy storage medium, thus potentially delivering higher efficiency for power plants and acting as a promising storehouse of excess energy [8]. Hydrogen is recognized as carbon-free when utilized as an energy source, providing opportunity to confront various critical energy challenges such as transportation and air quality, while overall strengthening energy security [9].

As one of the most abundant elements in nature, hydrogen is not naturally found. Processing methods are required to generate hydrogen in a usable form and a key challenge is to generate hydrogen at a large scale in a sustainable manner [7, 10]. Based on previous scholarly work, 76% of the hydrogen today is generated through natural gas reformation, 23% through coal, and less than 1% through renewable methods [9, 11, 12]. Figure (1-1) demonstrates a breakdown in hydrogen production techniques.

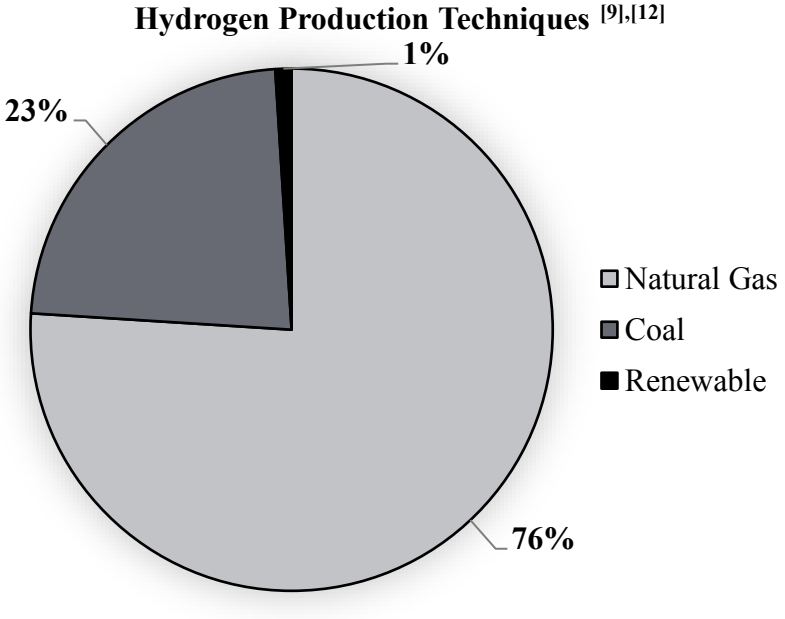

Figure 1-1: Percent breakdown for hydrogen production methods in industry [9, 12].

Steam methane reforming (SMR) is one of the most widespread hydrogen production techniques from natural gas. SMR is an endothermic process in which methane from natural gas reacts with steam in the presence of a catalyst to produce hydrogen [11]. However, combustion of the fuel, conversion of the feed into the final product, and lower energy efficiency, along with a global warming potential ranging between 10 - 13 kg CO2

equivalent per kilogram of net hydrogen, present unfavourable outcomes for the energy market [9, 11-14].

Gasification of coal is another common method for hydrogen generation, there are various approaches for gasification, with the overall process converting coal into synthetic gas using air, water vapour or oxygen [15]. However, hydrogen production using coal produces carbon emissions twice that of natural gas [9]. While there are carbon capture methods that can reduce emissions from SMR and coal up to 90%, clean hydrogen production methods have the potential to become reliable low-cost hydrogen sources [9]. Amongst these clean methods, thermochemical water splitting cycles (TWSC) are promising alternatives for large-scale hydrogen production technologies.

TWSC use thermal and electrical energy to decompose water through a series of reactions that generate hydrogen and oxygen. All chemical intermediate species are recycled, generating a closed-loop cycle [7]. Figure (1.2) presents the interactions between the four reaction steps. While over 200 thermochemical cycles have been identified in past literature, few have been successful in establishing scientific and economic feasibility based on set criteria [16, 17]. These criteria comprise of considerations such as, number of steps, environmental toxicity, energy efficiency, and cost [16, 17]. Of the feasible cycles, the Copper-Chlorine (Cu-Cl) cycle has been identified as a promising lower temperature water splitting cycle for hydrogen production [7, 8, 18]. The lower operating temperature requirement, higher overall conversion efficiency and readily available species present favourable advantages for efficient integration with renewable or waste heat sources. There are a few variations of the Cu-Cl cycle, with the four-step process as the most common presented in Equations (1.1) to (1.4), offering advantages such as improved kinetics, lower

process complexity and reduction in solid handling, further comparison can be found within the Chapter 2 [19 – 21].

Electrolysis: $2CuCl_{(aq)} + 2HCl_{(aq)} \rightarrow 2CuCl_{2(aq)} + H_{2(g)}$ (1.1)

Drying: $2CuCl_{2(aq)} \rightarrow 2CuCl_{2(s)}$ (1.2)

Hydrolysis: $2CuCl_{2(aq)} + H_2O_{(g)} \rightarrow Cu_2OCl_{2(s)} + 2HCl_{(g)}$ (1.3)

Thermolysis: $Cu_2OCl_{2(s)} \rightarrow 2CuCl_{(l)} + {}^{1}/_{2}\, O_{2(g)}$ (1.4)

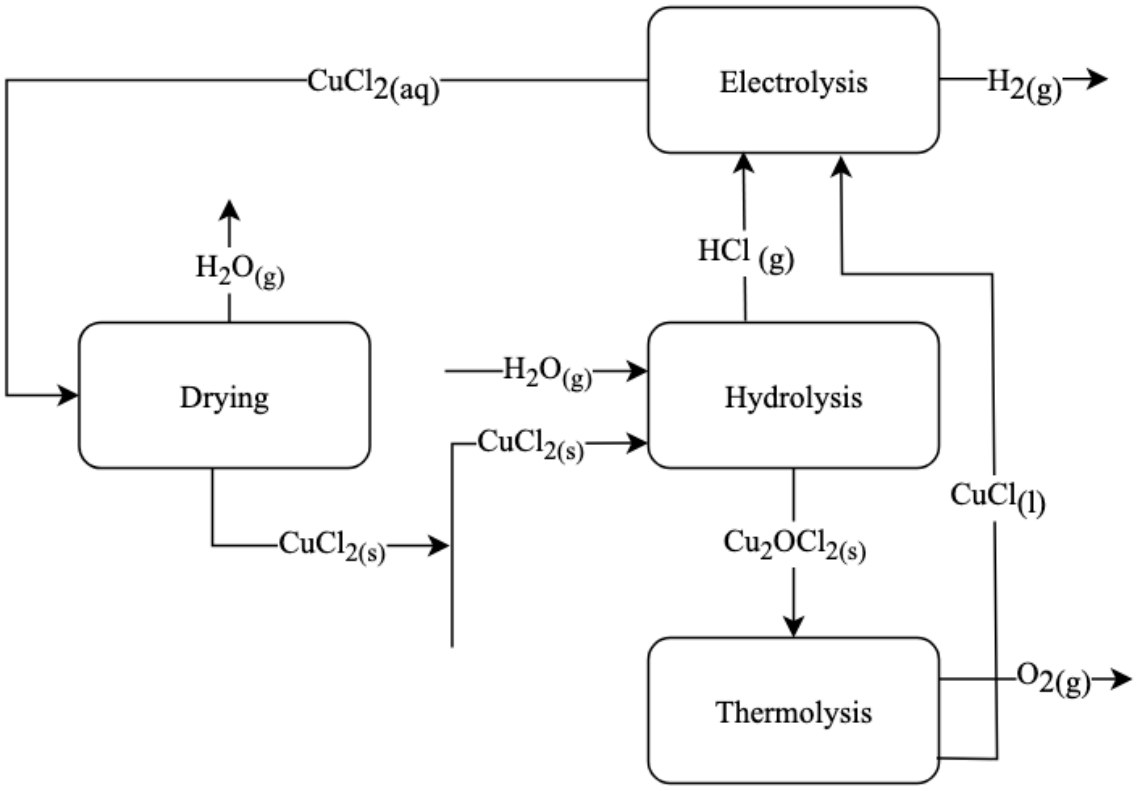

Figure 1-2: Cyclic relationship between the four reactions of the Cu-Cl cycle.

The hydrolysis step (Eq. (1.3)) is considered one of the most challenging steps of the Cu-Cl cycle due to complex decomposition of cupric chloride ($CuCl_2$) and excess steam requirements for complete conversion [7, 20, 22]. High conversion of $CuCl_2$ to Cu_2OCl_2 is key to reducing challenges, however conditions that favour high conversion also favour

side reactions which form undesirable by-products. There is an extensive collection of research studies that have examined techniques that can improve solid conversion while reducing overall steam requirements, including reactor pressure reduction, injection of inert gas, outlet gas recirculation and azeotropic distillation [23 – 26].

Various reactor design configurations have also been considered, such as spray reactors, fluidized beds and packed beds, which all present different advantages for reaction progression and various reaction kinetic data [23, 27, 28]. With limited detailed reaction kinetic data for the hydrolysis stage, further investigation of reactor design and configuration is required to improve predictive models. Research on moving bed reactors (MBR), specifically multi-injection downdraft MBRs, presents promising advantages, such as enhanced heat and mass transfer between particles that could improve solid conversion [29]. Numerical modelling could develop more accurate reaction predictions based on the available reaction data [29].

1.1 Scope and Objectives

A MBR design configuration is novel to Cu-Cl cycles, despite prevalence in gasification processes for biomass and coal [30, 31]. This thesis will investigate the impact of different operating conditions (i.e., pressure, temperature, and steam consumption) on the hydrolysis reaction and its side reactions, through the analysis of equilibrium conversion / concentrations trends. These results will be used to identify conditions that favour the conversion of $CuCl_2$ and minimize side reactions, with the overall goal to reduce steam requirements. This informed selection of reactor design and configuration through

simulations will be used as a tool to improve bed reactor design for the hydrolysis process. The objectives of the thesis are listed below.

- Identify hydrolysis reaction progression with all potential side reactions through simulation of phase equilibrium behaviour and provide preliminary predictions of conversion within the downdraft multi-injection MBR and gas recirculation design.
- Numerically model novel downdraft multi-injection moving bed reactors in a series approach.
- Determine the optimal reactor configuration through sensitivity analysis of the MBR design to achieve maximum conversion at lower SCR.

1.2 Thesis Structure

Chapter 2 presents a detailed literature review surrounding the Cu-Cl thermochemical water splitting cycle. The review begins with an investigation of common thermochemical cycles for hydrogen production, with a review of different variations of the Cu-Cl cycle. Further elaboration regarding the hydrolysis step of the cycle will be presented, with details surrounding gas-solid reaction kinetics, reactor design, and parameters commonly studied in prior published material. This review leads to an investigation of the use of moving bed reactors for the gas-solid reaction, such biogas/coal gasification and naphtha reforming and how it can be introduced with the hydrolysis reaction.

Chapter 3 describes the phase equilibrium analysis of the hydrolysis reaction in the thermochemical Cu-Cl cycle of hydrogen production. Various reactor temperatures, pressures, and steam to copper ratios are simulated within a single reactor to predict $CuCl_2$

conversion with the inclusion of all potential side reactions. Two hydrolysis reactor configurations are also considered, multi-injection MBRs simulated through reactors in series and outlet gas recirculation. A modified version of this chapter has been submitted for publication.

Chapter 4 builds on the MBR results from Chapter 3. The reactor in series simulation of the downdraft multi-injection MBR was improved with the introduction of reaction kinetics and reactor parameters. The validated model is used in a sensitivity analysis to identify optimal reactor configurations to achieve maximum solid conversion. A modified version of this chapter will be submitted for publication.

Chapter 5 provides a summary of the research performed in the preceding chapters and provides concluding remarks and recommendations for future studies.

1.3 Co-Authorship Statement

The principal author of this thesis, Jenna Broders, is the primary author of all chapters included in this thesis and performed all numerical modelling and analysis. Dr. Kevin Pope and Dr. Greg F. Naterer acted as principal supervisors on this thesis and provided technical guidance, analytical support, and additional support in editing the thesis and were listed as co-authors on the manuscripts for chapters 3 and 4. Dr. Kelly A. Hawboldt also provided technical guidance, analytical support and editing of the work performed in Chapters 3 and 4 and is listed as a co-author in these chapters.

References

[1] F. Perera, "Pollution from fossil-fuel combustion is the leading environmental threat to global pediatric health and equity: Solutions exist," *Int. J. Environ. Res. Public Health*, vol. 15, no. 1, 2018.

[2] J. Lelieveld, K. Klingmüller, A. Pozzer, R. T. Burnett, A. Haines, and V. Ramanathan, "Effects of fossil fuel and total anthropogenic emission removal on public health and climate," *Proc. Natl. Acad. Sci. U. S. A.*, vol. 116, no. 15, pp. 7192–7197, 2019.

[3] S. Shafiee and E. Topal, "When will fossil fuel reserves be diminished?," *Energy Policy*, vol. 37, no. 1, pp. 181–189, 2009.

[4] G. Boyle, B. Everett, S. Peake, and J. Ramage, *Energy Systems and Sustainability: Power for a Sustainable Future*, Second. Oxford: Oxford University Press, 2012.

[5] "Coal explained: How much coal is left?," *U.S Energy Information Administration*, 2022.

[6] W. E. Outlook, "International Energy Agency (IEA) World Energy Outlook 2022," 2022. [Online]. Available: https://www.iea.org/reports/world-energy-outlook-2022.

[7] G. F. Naterer, I. Dincer, and C. Zamfirescu, *Hydrogen production from nuclear energy*, 2013.

[8] G. Naterer *et al.*, "Recent Canadian advances in nuclear-based hydrogen production and the thermochemical Cu-Cl cycle," *Int. J. Hydrogen Energy*, vol. 34, no. 7, 2009.

[9] International Energy Agency, "The Future of Hydrogen," 2019.

[10] M. Sterner and I. Stadler, *Handbook of Energy Storage - Demand, Technologies, Integration*. 2019.

[11] B. Chen, Z. Liao, J. Wang, H. Yu, and Y. Yang, "Exergy analysis and CO2 emission evaluation for steam methane reforming," *Int. J. Hydrogen Energy*, vol. 37, no. 4, pp. 3191–3200, 2012.

[12] J. Dufour, D. P. Serrano, J. L. Gálvez, J. Moreno, and C. García, "Life cycle assessment of processes for hydrogen production. Environmental feasibility and reduction of greenhouse gases emissions," *Int. J. Hydrogen Energy*, vol. 34, no. 3, pp. 1370–1376, 2009.

[13] P. Spath, M.Mann*, Life Cycle Assessment of Hydrogen Production via Natural Gas Steam Reforming*, 2003.

[14] F. Suleman, I. Dincer, and M. Agelin-Chaab, "Environmental impact assessment and comparison of some hydrogen production options," *Int. J. Hydrogen Energy*, vol. 40, no. 21, pp. 6976–6987, 2015.

[15] A. Midilli, H. Kucuk, M. E. Topal, U. Akbulut, and I. Dincer, "A comprehensive review on hydrogen production from coal gasification: Challenges and Opportunities," *Int. J. Hydrogen Energy*, vol. 46, no. 50, pp. 25385–25412, 2021.

[16] L. C. Brown *et al.*, "High efficiency generation of hydrogen fuels using nuclear power.," *Gen. At.*, no. June, pp. 29–30, 2003, [Online]. Available: http://www.osti.gov/servlets/purl/814014-tdQyiq/native/%0Ahttps://fusion.gat.com/pubs-ext/AnnSemiannETC/A24285.pdf.

[17] B. W. Mcquillan *et al.*, "High efficiency generation of hydrogen fuels using solar thermal-chemical splitting of water (Solar thermo-chemical splitting for H2)," 2010.

[18] C. Zamfirescu, I. Dincer, and G. F. Naterer, "Thermophysical properties of copper compounds in copper-chlorine thermochemical water splitting cycles," *Int. J. Hydrogen Energy*, vol. 35, no. 10, pp. 4839–4852, 2010.

[19] M. F. Orhan, I. Dinçer, and M. A. Rosen, "Efficiency comparison of various design schemes for copper-chlorine (Cu-Cl) hydrogen production processes using Aspen Plus software," *Energy Convers. Manag.*, vol. 63, pp. 70–86, 2012.

[20] A. Farsi, I. Dincer, and G. F. Naterer, "Review and evaluation of clean hydrogen production by the copper–chlorine thermochemical cycle," *J. Clean. Prod.*, vol. 276, p. 123833, 2020.

[21] A. Ozbilen, I. Dincer, and M. A. Rosen, "Environmental evaluation of hydrogen production via thermochemical water splitting using the Cu-Cl Cycle: A parametric study," *Int. J. Hydrogen Energy*, vol. 36, no. 16, pp. 9514–9528, 2011.

[22] V. N. Daggupati, G. F. Naterer, K. S. Gabriel, R. J. Gravelsins, and Z. L. Wang, "Equilibrium conversion in Cu-Cl cycle multiphase processes of hydrogen production," *Thermochem. Acta*, vol. 496, no. 1–2, pp. 117–123, 2009.

[23] M. S. Ferrandon, M. A. Lewis, F. Alvarez, and E. Shafirovich, "Hydrolysis of $CuCl_2$ in the Cu-Cl thermochemical cycle for hydrogen production: Experimental studies using a spray reactor with an ultrasonic atomizer," *Int. J. Hydrogen Energy*, vol. 35, no. 5, pp. 1895–1904, 2010.

[24] V. N. Daggupati, G. F. Naterer, and K. S. Gabriel, “Diffusion of gaseous products through a particle surface layer in a fluidized bed reactor,” *Int. J. Heat Mass Transf.*, vol. 53, no. 11–12, pp. 2449–2458, 2010.

[25] L. Finney, K. Gabriel, and K. Pope, “A novel fluidized bed suitable for the hydrolysis step in CuCl hydrogen production cycle,” *Int. J. Hydrogen Energy*, vol. 47, no. 71, pp. 30378–30390, 2022.

[26] A. Farsi, Ö. Kayhan, C. Zamfirescu, I. Dincer, and G. F. Naterer, “Azeotropic pressure swing distillation of hydrochloric-water for hydrogen production in the Cu–Cl cycle: Thermodynamic and design methods,” *Int. J. Hydrogen Energy*, vol. 44, no. 16, pp. 7969–7982, 2019.

[27] D. Thomas, N. A. Baveja, K. T. Shenoy, and J. B. Joshi, “Experimental Study on the Mechanism and Kinetics of CuCl2 Hydrolysis Reaction of the Cu-Cl Thermochemical Cycle in a Fluidized Bed Reactor,” *Ind. Eng. Chem. Res.*, vol. 59, no. 26, pp. 12028–12037, 2020.

[28] K. Pope, G. F. Naterer, and Z. L. Wang, “Nitrogen carrier gas flow for reduced steam requirements of water splitting in a packed bed hydrolysis reactor,” *Exp. Therm. Fluid Sci.*, vol. 44, pp. 815–824, 2013.

[29] M. Shirzad, M. Karimi, J. A. C. Silva, and A. E. Rodrigues, “Moving Bed Reactors: Challenges and Progress of Experimental and Theoretical Studies in a Century of Research,” *Ind. Eng. Chem. Res.*, vol. 58, no. 22, pp. 9179–9198, 2019.

[30] A. Schwabauer, M. Mancini, Y. Poyraz, and R. Weber, “On the mathematical modelling of a moving-bed counter-current gasifier fuelled with wood-pellets,” *Energies*, vol. 14, no. 18, 2021.

[31] J. Adánez and F. G. Labiano, “Modeling of Moving-Bed Coal Gasifiers,” *Ind. Eng. Chem. Res.*, vol. 29, no. 10, pp. 2079–2088, 1990.

Chapter 2 - Literature Review

2.1 Introduction

Hydrogen production by thermochemical water splitting cycles (TWSC) is a clean production alternative to natural gas and coal techniques [1, 2]. The objective of this literature review is to offer a comprehensive understanding of the existing scientific achievements in phase equilibrium, reaction kinetics, and reactor design techniques, particularly concerning the Cu-Cl thermochemical cycle and multi-injection downdraft MBRs. Specific topics will include the hydrolysis reaction and side reaction progression, steam reduction techniques, and reactor configurations. This literature review will provide insight with respect to hydrolysis reaction progression and MBR operations, aiding the generation of the phase equilibrium and numerical models presented in this work.

2.2 Overview of Cu-Cl Thermochemical Cycle

There are various TWSC presented in prior literature. Brown et al. [3] and McQuillan et al. [4] both reported on high efficiency generation of hydrogen through thermochemical methods integrated with nuclear power or solar energy as heat sources. Each report evaluated various efficient and cost-effective thermochemical processes for hydrogen production from water. Of the hundreds of cycles investigated, only a few were considered viable based on criteria such as thermal efficiency, simplicity, feasibility (i.e., available materials, number of reaction steps, temperatures), and costs. Table (2-1) presents some of the viable thermochemical cycles discussed in past literature, additional to the Cu-Cl cycle, along with the reaction sequence and typical operating temperatures.

Table 2-1: Alternative thermochemical cycles for hydrogen production

No	Type	Reaction	Max Temp.	Source
1	Magnesium Iodine	$6MgO + 6I_2 \rightarrow Mg(IO_3)_2 + 5MgI_2$ $Mg(IO_3)_2 \rightarrow MgO + 6I_2 + {}^5/_2\, O_2$ $5(MgI_2 \cdot 6H_2O) \rightarrow 5MgO + 25H_2O + 10HI$	600 ℃	Shindo et al. [5]
2	Sulfur Iodine	$I_2 + SO_2 + 2H_2O \rightarrow 2HI + H_2SO_4$ $H_2SO_4 \rightarrow SO_2 + H_2O + {}^1/_2\, O_2$ $2HI \rightarrow I_2 + H_2$	>800℃	Kubo et al. [6]
3	Vanadium Chlorine	$2VCl_2 + 2HCl \rightarrow 2VCl_3 + H_2$ $4VCl_3 \rightarrow 2VCl_4 + 2VCl_2$ $2VCl_4 \rightarrow 2VCl_3 + Cl_2$	760 ℃	Knoche et al. [7]
4	Cerium Chlorine	$2CaO + 2Br_2 \rightarrow 2CaBr_2 + O_2$ $CaBr_2 + H_{2O} \rightarrow CaO + 2HBr$ $Fe_3O_4 + 8HBr \rightarrow 3FeBr_2 + 4H_2O + Br_2$ $3FeBr_2 + 4H_2O \rightarrow Fe_3O_4 + 6HBr + H_2$	730 ℃	Lemont et al. [8]
5	Iron Chlorine	$Cl_2 + H_2O \rightarrow 2HCl + O_2$ $3FeCl_2 + 4H_2O \rightarrow Fe_3O_4 + 6HCl + H_2$ $Fe_3O_4 + 8HCl \rightarrow FeCl_2 + 2FeCl_3 + 4H_2O$ $2FeCl_3 \rightarrow 2FeCl_2 + Cl_2$ $Cl_2 + H_2O \rightarrow 2HCl + {}^1/_2\, O_2$	925 ℃	Safari et al. [9]
6	Hybrid Sulfur	$H_2SO_4 \rightarrow SO_2 + H_2O + {}^1/_2\, O_2$ $2H_2O + SO_2 \rightarrow H_2SO_4 + O_2$	900 ℃	Sattler et al. [10]

While these have potential for large-scale production, the high temperature requirements remain a challenge for process efficiency and implementation. Additional to these feasible cycles, the Cu-Cl cycle is one of the most promising types of thermochemical

cycles that operate in a lower temperature range (a maximum temperature of approximately 550℃)[11]. This cycle presents additional advantages such as higher overall conversion, availability of chemicals, and lower maintenance and material costs, all of which are favourable for integration with renewable or waste energy [12,13].

The Cu-Cl cycle consists of a closed loop of chemical and physical reactions that dissociates water into oxygen and hydrogen through intermediate copper and chloride compounds. There are different variations of the cycle presented in previous literary works depending on the number of reactions in series. The handling and transport of solids within the cycle, as well as reaction kinetics, can be improved through a reduction of main reaction steps [14]. However, a reduction of steps can also lead to challenges such as incomplete reactions, higher heat requirements or increased production of undesirable by-product formation [14]. Table (2.2) presents the different types of Cu-Cl thermochemical cycles found in prior investigations.

Ferrandon et al. [15] identified the Cu-Cl cycle to have three major steps, electrolysis, hydrolysis, and decomposition (thermolysis), as presented in the 3-step cycle of Table (2.2), in their experimental spray reactor setup for the hydrolysis reactor. Farsi et al. [16] identified four reaction steps in their experimental study of the hydrolysis reaction step (4a cycle). Daggupati et al. [17] presented the 5-step cycle in their thermodynamic equilibrium analysis of the cycle. With varying literature for cycle reaction steps, Orhan et al. [14] performed a comparative study of the three, four and five step Cu-Cl cycles through simulation models developed in Aspen Plus. Exergy, energy and yield effectiveness of the different cycles were examined, identifying advantages and disadvantages for each variation. Overall, a reduction of cycle steps can provide better reaction kinetics and

reduces complexity of the cycle. However, there are potential drawbacks, including higher heat grade and incomplete reaction, which ultimately diminish the efficiency of the process. These disadvantages become more evident within the 3-step cycle. However, the 5-step cycle has a major disadvantage of increased solid transport, suggesting that a four-step cycle can integrate advantages found with the higher and lower step cycles.

Ozbilen et al. [18] further investigated the different cycle variations through a Life Cycle Assessment (LCA). The parametric study presented an environmental impact of the various cycle configurations through a "cradle to grave" approach. Four different impact categories were assessed: Acidification Potential (AP), Eutrophication Potential (EP), Global Warming Potential (GWP), and Ozone Depletion Potential (ODP). Based on the presented trends, the 4-step cycle had the lowest rating in all categories due to its lower energy requirement. This further supports the implementation of the 4-step configuration for the Cu-Cl cycle. Ozbilen et al. [19] performed other LCA assessments of the various cycle steps, further emphasizing the reduced environmental impacts of the 4-step cycle. For the remainder of this thesis, the 4a cycle in Table (2.2) will be the reference for the main reactions of the Cu-Cl cycle.

Additionally, Farsi et al. [11] briefly presented a two-step cycle which demonstrates the Cu-Cl cycles through an oxygen generating step and a hydrogen generating step. While this is a valid progression, there is limited research that presents the two-step Cu-Cl cycle. Due to the limitations associated with reduced reaction numbers, this variation may not be suitable for large scale implementation.

Table 2-2: Different variations of the Cu-Cl cycle.

Cycle	Reaction steps
Cu - Cl 3a cycle (three steps)	S1: $2CuCl_{2(s)} + H_2O_{(g)} \rightarrow 2CuCl_{(l)} + 2HCl_{(g)} + H_2O_{(g)} + {}^1/_2\, O_{2(g)}$ S2: $4CuCl_{(aq)} \rightarrow 2CuCl_{2(aq)} + 2Cu_{(s)}$ S3: $2Cu_{(s)} + 2HCl_{(g)} \rightarrow 2CuCl_{(l)} + H_{2(g)}$
Cu – Cl 3b cycle (three steps)	S1: $2CuCl_{(aq)} + 2HCl_{(g)} \rightarrow 2CuCl_{2(aq)} + H_{2(g)}$ S2: $2CuCl_{2(s)} + H_2O_{(g)} \rightarrow Cu_2OCl_{2(s)} + 2HCl_{(g)}$ S3: $Cu_2OCl_{2(s)} \rightarrow 2CuCl_{(s)} + {}^1/_2\, O_{2(g)}$
Cu – Cl 4a cycle (four steps)	S1: $2Cu_{(s)} + 2HCl_{(g)} \rightarrow 2CuCl_{(l)} + H_{2(g)}$ S2: $2CuCl_{2(s)} + H_2O_{(g)} \rightarrow Cu_2OCl_{2(s)} + 2HCl_{(g)} + H_2O_{(g)}$ S3: $Cu_2OCl_{2(s)} \rightarrow 2CuCl_{(l)} + {}^1/_2\, O_{2(g)}$ S4: $4CuCl_{(aq)} \rightarrow 2CuCl_{2(aq)} + 2Cu_{(s)}$
Cu – Cl 4b cycle (four step)	S1: $2CuCl_{(aq)} + 2HCl_{(aq)} \rightarrow 2CuCl_{2(aq)} + H_{2(g)}$ S2: $2CuCl_{2(aq)} \rightarrow 2CuCl_{2(s)}$ S3: $2CuCl_{2(s)} + H_2O_{(g)} \rightarrow Cu_2OCl_{2(s)} + 2HCl_{(g)}$ S4: $Cu_2OCl_{2(s)} \rightarrow 2CuCl_{(l)} + {}^1/_2\, O_{2(g)}$
Cu - Cl 5 cycle (Five steps)	S1: $2Cu_{(s)} + 2HCl_{(g)} \rightarrow 2CuCl_{(l)} + H_{2(g)}$ S2: $2CuCl_{2(s)} + H_2O_{(g)} \rightarrow Cu_2OCl_{2(s)} + 2HCl_{(g)}$ S3: $Cu_2OCl_{2(s)} \rightarrow 2CuCl_{(l)} + {}^1/_2\, O_{2(g)}$ S3: $4CuCl_{(s)} + H_2O \rightarrow 2CuCl_{2(aq)} + 2Cu_{(s)}$ S4: $CuCl_{2(aq)} \rightarrow CuCl_{2(s)}$

2.3 Cu-Cl Hydrolysis

The hydrolysis reaction is an endothermic, non-catalytic gas-solid reaction which converts solid $CuCl_2$ with excess steam to solid copper oxychloride (Cu_2OCl_2) and hydrochloric (HCl) gas for the thermolysis and electrolysis stages respectively [20]. The hydrolysis reaction is represented through Equation (2-1).

$$2CuCl_{2(s)} + H_2O_{(g)} \rightarrow Cu_2OCl_{2(s)} + 2HCl_{(g)} \quad (2\text{-}1)$$

Previous research investigated operating conditions of hydrolysis, with a typical operating temperature range and pressure for hydrolysis between 350 – 400 ℃ and 1 bar respectively, along with examining methods to improve solid conversion and cycle integration [1, 20].

Within the Cu-Cl cycle, the hydrolysis reaction is considered the most challenging step [15, 16, 20]. High solid conversion is key to reducing integration challenges. However, conditions favouring high conversion also favour undesired side reactions, resulting in the formation of potentially toxic by-products. Research has demonstrated that excess steam injection (i.e., higher steam to copper ratio (SCR)) during the hydrolysis stage mitigates the progression of side reactions and increases solid conversion [21]. Singh et al. [22] performed several experiments investigating the impact of the SCR using different operating parameters. Conversions greater than 70% were achieved at SCR ranging from 33 to 44. Daggupati et al. [17] found that an SCR of 27 resulted in an 85% equilibrium conversion at 400 ℃, concluding that the equilibrium conversion of the hydrolysis reaction favours higher temperatures, excess steam, and lower pressures [17].

A challenge with increasing the SCR is the high energy requirement to maintain the steam in a superheated phase - reducing cycle efficiency and impeding large scale implementation [21, 23]. Farsi et al. [24] identified that the SCR and reaction temperature significantly affect the exergy loss of the hydrolysis reaction through their Aspen Plus simulation of hydrolysis reaction. This work identified that an SCR of 19 and temperature of 388 ℃ result in a maximum value of exergy efficiency. This challenge has led to several studies examining methods to reduce the steam requirement of the hydrolysis reaction while also maintaining high solid conversion.

Duggapati et al. [25] generated a model based on the shrinking core model (SCM) to examine the solid conversion during the hydrolysis reaction at various conditions. The operating limit of the total reactor pressure was enhanced and the steam requirement for complete conversion of $CuCl_2$ was reduced when inert gas was added. Ferrandon et al. [26] investigated the impact of reactor pressure on the steam requirement. In experiments from 0.4 – 1 atm, this work demonstrated that decreasing the reactor pressure results in less formation of CuCl, while maintaining $CuCl_2$ conversion. Additionally, Farsi et al. [27] introduced azeotropic distillation as a method to reduce steam requirements of the hydrolysis reaction. It has been identified that a significant amount of input steam is unreacted after the hydrolysis reaction. This work integrates a pressure swing distillation unit to separate HCl from the unreacted water after hydrolysis. The concentrated HCl will continue to the electrolysis phase, while the steam will re-enter the hydrolysis reactor along with additional fresh steam to maintain the overall SCR [27]. Figure (2-1) demonstrates the

integration of the pressure swing distillation column, while Table (2-3) presents past work surrounding reactor conditions and design of the hydrolysis reactor [27].

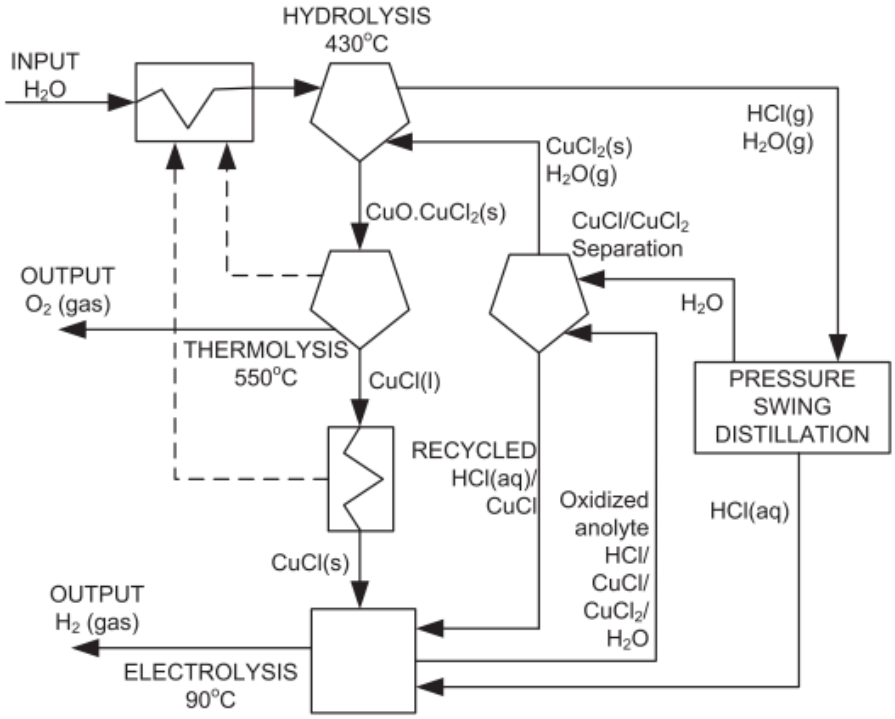

Figure 2-1: Schematic of Cu-Cl cycle with azeotropic separation system [27].

Table 2-3: Overview of various reactor designs in past literature for hydrolysis reaction.

Work	Reactor Temperature	Reactor Pressure	Reactor type	Kinetic Model	Experiment/Model
Sing et al. [1]	400 ℃	1 bar	Fixed-Bed	SCM	Experimental
Daggupati et al. [2]	375 ℃	1 bar	Fluidized-Bed	SCM/ URM	Model
Haseli et al. [3]	400 ℃	-	Fluidized-Bed	SCM/ URM	Model
Pope et al. [4]	365 – 400 ℃	1.1 bar	Packed-Bed	-	Experimental
Ferrandon et al. [5]	390 ℃	1 bar	Spray Reactor	-	Experimental
Farsi et al. [6]	388 ℃	1 bar	Spray Reactor	SCM	Model

2.3.1 Side Reactions

Side reactions and undesired by-products are a challenge for hydrolysis step integration. Toxic by-products such as Cl_2 gas and the decomposition of desired solid products hinder process efficiency and total desired yield. While past literature has identified the various possible side reactions within the hydrolysis reactor and presents data pertaining to the decomposition of $CuCl_2$, there are limited predictive or numerical models of the hydrolysis reaction that include all possible side reactions. These past studies highlight viable reactor conditions, however, unless results were obtained from experimental trails, hydrolysis models typically assume that no side reactions occur.

In the hydrolysis model of Daggupati et al. [25], it was assumed that no side reactions occur, with solid conversion only with respect to the hydrolysis reaction. From Farsi et al. [16], a hydrodynamic model that estimated the residency time of the reactants of the hydrolysis phase also assumed that no side reactions occur. While these studies provide useful information with respect to the progress of the hydrolysis reaction, they had limitations with respect to possible side reactions and by-product generation within the hydrolysis reaction. Thus, encompassing the full progression of actual experimental conditions of the hydrolysis reaction remains a gap in the literature.

Past studies have identified some of the major side reactions present in the hydrolysis stage. Thomas et al. [30] stated that the existence of side reactions creates further challenges in the hydrolysis step. Their experimental work examined the decomposition of $CuCl_2$ and Cu_2OCl_2, as well as reaction kinetics of the hydrolysis process. The addition of inert gases during fluidization and a minimum steam mole fraction of 0.5 were identified to mitigate challenges associated with side reactions. Ferrandon et al. [31] also studied the

decomposition of Cu_2OCl_2 using X-ray Absorption Near Edge Structure (XANES) spectroscopy. By-product formation became noticeable at temperatures greater than or equal to 400 ℃.

Marin et al. [32] highlighted three potential competing reactions in the hydrolysis stage. Theoretical and experimental analyses identified the hydrolysis pathways of reactor conditions and the presence of impurities in the reactants. An analysis of copper extracts by Kekesi et al. [33] identified other potential side reactions and by-products that could occur within a typical hydrolysis reaction temperature range. Their experimental work and thermodynamic analysis of the Cu-Cl-H-O system identified dissociation, reduction, and vaporization of copper compound reactions. Equations (2-2) – (2-7) present the reactants and products for potential side reactions in the hydrolysis process.

$CuCl_2$ decomposition

$$CuCl_2 \rightarrow CuCl + Cl_2 \tag{2-2}$$

Cu_2OCl_2 decomposition

$$Cu_2OCl_2 \rightarrow CuO + CuCl_2 \tag{2-3}$$

Copper chloride generation

$$CuO + Cl_2 \rightarrow CuCl_2 + 0.5O_2 \tag{2-4}$$

Chlorine reaction with excess steam

$$Cl_{2(s)} + H_2O_{(g)} \rightarrow 2HCl_{(g)} + 0.5O_{2(g)} \tag{2-5}$$

$CuCl_2$/CuCl reaction

$$CuCl_2 + CuCl_{(s)} \rightarrow CuCl_2/CuCl_{(l)} \tag{2-6}$$

Melting of CuCl

$$CuCl_{(s)} \rightarrow CuCl_{(l)} \quad (2\text{-}7)$$

Of the several side reactions identified to have an impact on product yield, the most dominant are the decomposition of $CuCl_2$ (Eq. 2-2) and Cu_2OCl_2 (Eq. 2-3), with the reactions occurring at temperatures around 400℃ and higher. Wang et al. [34] performed a thermodynamic analysis on the thermal decomposition of $CuCl_2$ to identify the decomposition temperature of $CuCl_2$. These experiments identified that the decomposition temperature of $CuCl_2$ was higher than predicted, approximately 430 ℃, which broadens the available operating temperature of the hydrolysis reaction [7]. Daggupati et al. [35] investigated the hydrolysis and decomposition reactions with respect to chemical equilibrium conversion and reaction kinetics through the shrinking core model (further details regarding the shrinking core model are found in Section 2.3.2). It was concluded that higher temperature favors higher equilibrium conversions, which increases the decomposition of $CuCl_2$ [35]. These works emphasize that considering side reactions, both dominant and weak, is important to accurate modeling of the hydrolysis reaction progression.

2.3.2 Gas – Solid Reaction Kinetics

The conversion of solid components with a fluid, specifically a gas, is essential to numerous industries including mining, biomass, and steam gasification, etc. In general, gas-solid reactions can be represented in the following three equations [36, 37].

$$A_{(g)} + B_{(s)} \rightarrow C_{(g)} \quad (2\text{-}8)$$

$$A_{(g)} + B_{(s)} \rightarrow D_{(s)} \quad (2\text{-}9)$$

$$A_{(g)} + B_{(s)} \rightarrow C_{(g)} + D_{(s)} \quad (2\text{-}10)$$

For the case of the hydrolysis reaction, the gas-solid reaction is represented by Equation (2-10). This reaction progresses differently than typical gas-liquid, gas-gas, and liquid-liquid reactions, as the solid particles may shrink, grow, or remain unchanged. There are several steps for conversion that must be considered that can make modeling of these reactions a challenge. There are three models available to represent the conversion progression of gas-solid reactions: shrinking core model (SCM), uniform reaction model (URM), and the grain model.

2.3.2.1 Shrinking Core Model

In the shrinking core model, the reaction is visualized to occur in reaction zones. The reaction starts at the outer layer of the particle surface, moving inward as it converts the solid into an "ash" or product layer. Unlike the uniform reaction model, the unreacted material is represented by a core that shrinks in size throughout the reaction [36, 37]. Figure (2-2) demonstrates the reaction progression of the SCM. This progression can be broken down into five conversion steps [36, 37].

Step 1: Film diffusion of the gas to the solid particle.

Step 2: Surface diffusion of the gas through the solid outer surface or ash layer to the reaction front.

Step 3: Surface reaction of the gas with the solid.

Step 4: Diffusion of gas product back through the product layer to the surface.

Step 5: Film diffusion of gaseous product to the main fluid body.

Additional assumptions of the SCM include, unreacted and reacted regions are separated by a sharp interface, pseudo-steady state, and a constant pellet size [35, 38].

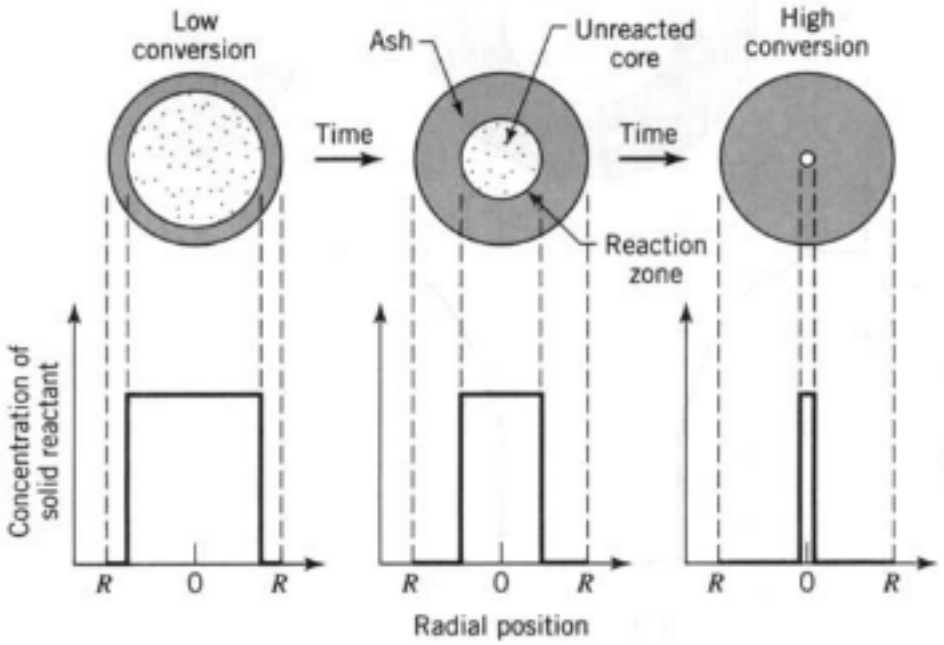

Figure 2-2: Diagram of reaction progression for the shrinking core model [36, 37].

The SCM can be applied to the hydrolysis reactor to generate the reaction rate equation for the non-catalytic reaction. Daggupati et al. [25] utilized the SCM to numerically predict reaction rate constants and time for complete solid conversion. This model predicted that the reaction is controlled by both chemical reaction and diffusion processes through the product layer control for particles size of 200 μm. Singh et al. [22] derived the kinetic rate constant and activation energy from experimental data of the hydrolysis reaction through the use of the SCM. They also concluded that the probable pathways for $CuCl_2$ hydrolysis were found to be diffusion controlled, with the particle size of the reactant affecting the packing and diffusion length. Haseli et al. [39] investigated mass transport phenomena of the hydrolysis reaction and utilized the SCM within a fluidized bed as one of the limiting cases, along with a uniform reaction model (URM) as the other case. The outcomes

indicated that the SCM quantitatively predicted a greater conversion of gas and particles, as well as improved bed effectiveness compared to the URM. Table (2-3) presents the various studies that implemented SCM.

2.3.2.2 Uniform Reaction model

There are two exceptions where the assumptions of a SCM model are not an accurate approximation: (1) the solid is converted by the action of heating without gas contact, and (2) slow reaction of a gas with a very porous solid [37]. In these cases, the uniform reaction model (URM), or continuous reaction model (CRM), is better suited. The URM visualizes gas-solid reaction progression as continuous, even as conversion of the solid particle at all times occurs when the gas enters [37]. Figure (2-3) presents the continuous reaction progression of the uniform reaction model.

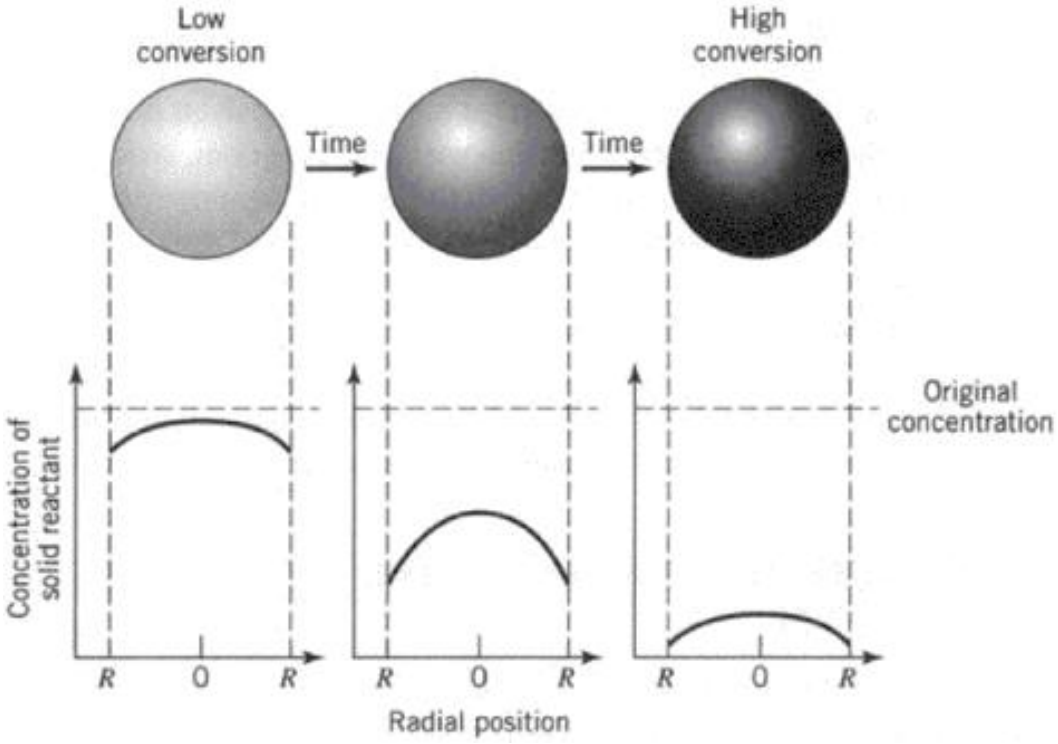

Figure 2-3: Diagram of the progression of Uniform reaction model for gas-solid reactions [37].

In this model, the reactant gas enters the particle and reacts with the solid at various rates along a broad front of the entire particle. The rate of reaction can be limited by (i) diffusion through the porous particle, (ii) chemical kinetics, (iii) diffusion through the external gas film, or (iv) transport of heat across the particle [40].

With respect to the Cu-Cl cycle and the hydrolysis reaction, the URM has been presented numerically in previous studies. Haseli et al. [39] presented both the SCM and URM to investigate the mass transport phenomenon of the hydrolysis reaction. Further investigation by Haseli et al. [28] on hydrolysis transport phenomena incorporated the URM as an assumption for the numerical results. This model presented similar results as their previous work, indicating improved conversion with the SCM.

2.3.2.3 Grain Model

The grain model was first established by Szekely and Evans [38], to improve the description of noncatalytic gas-solid reactions by incorporating structural properties of the solid into the model [38]. This model considers the solid particle to consist of uniformly sized spherical particles. The model assumes that there are reaction zones, rather than reacted and unreacted regions separated by a sharp boundary, as assumed in the SCM. It is implemented to allow incorporation of structural parameters into the overall reaction scheme and define physical criteria that affect reactivity of porous solids (neglected in both the SCM and URM).

Assumptions within the grain model include [38]:

(1) Gas phase mass transfer resistance is negligible.

(2) Semi-infinite porous solid, with a macroscopically unidirectional movement of the reaction zone

(3) The heterogeneous chemical reaction is considered first order and irreversible.

(4) Isothermal system.

(5) Initial structure is maintained and unaffected by reaction progression.

While the reaction mechanism of the grain model is different, the reaction between the gas and solid proceeds in accordance with the SCM [38]. Currently the grain model is not implemented within the Cu-Cl cycle. However, through further research, introducing this method could identify more realistic progression of the hydrolysis reaction. Rahimi et al. [41] utilized the grain model in their development of a general model for moving bed reactors with multiple non-catalytic gas-solid reactions for the reduction of hematite.

2.4 Reactor Design

Reactor design can have a major impact on reaction progression, operating conditions, and reaction kinetics. There are various reactor configurations presented for the hydrolysis reactor in past literature, including fluidized bed reactors (FBR), spray reactors and packed bed reactors. A common reactor design in gas-solid systems is a moving bed reactor (MBR). This design is novel for the hydrolysis reaction but presents intriguing advantages for solid conversion and reduction in overall steam requirement. This section will present the various hydrolysis reactors presented in current research, as well as an overview of the novel MBR design.

2.4.1 Fluidized Bed Reactors

When flow conditions are above the minimum fluidization velocity, the fluid flow in the reactor can be represented by a fluidization regime. Equation (2-11) represents the minimum fluidization velocity [29],

$$V_{mf} = \frac{D_p^2(\rho_s - \rho_v)g}{150\mu}\frac{\varepsilon_{mf}\phi_s^2}{1-\varepsilon_{mf}} \tag{2-11}$$

where $D_p, \rho_s, \rho_v, g, \mu, \varepsilon_{mf}$, and ϕ_s represent particle diameter, solid density, vapor density, gravity, gaseous viscosity, void fraction (at minimum fluidization velocity), and sphericity [29].

FBR is a common reactor design in the hydrolysis step of the Cu-Cl cycle. The required solid conversion depends on the particle size, bed height, reaction temperature and superficial velocity of steam with respect to the required steam to copper mole ratio [42]. Daggupati et al. [25] presented numerical modeling of the hydrolysis reaction in a fluidized bed and reported the effects of various operating parameters on the steam requirements. Dagguptai et al. [42] performed further numerical modelling within a fluidized bed. Parameters such as time to heat solid particles and SCR were presented with respect to fluidization velocity. The main findings presented an increase in minimum fluidization velocity at higher SCR; however, the minimum fluidization velocity can be reduced while maintaining the SCR through the introduction of smaller solid particles. Finney et al. [43] presented experimental results for the hydrolysis reactor within a fluidized bed, along with the integration of steam recirculation, i.e., Recirculating Steam Fluidized Bed (RSFB). This

design presented an ability to maintain high effective SCR while keeping the system SCR low. Thomas et al. [30] also presented experimental results of the hydrolysis reaction within a fluidized bed. These identified the minimum steam mole fraction required to mitigate the progression of undesired side reactions.

2.4.2 Packed Bed Reactors

When flow conditions are below the minimum fluidization velocity, the fluid flow in the reactor can be represented by a packed regime [29]. Equation (2-11) can again be utilized to determine this value. In the hydrolysis phase, packed bed reactors have been implemented in both the horizontal and vertical axis. Pope et al. [44] utilized a packed bed reactor to investigate the steam conversion limit of the hydrolysis reaction through the introduction of humidified nitrogen for the reactor's conditions. It was identified that lower SCR was possible to generate HCl and Cu_2OCl_2, which is a significant result in reducing hydrolysis steam requirements. Pope et al. [29] further investigated nitrogen carrier gas flow for reduced steam requirements through additional experimental results of a PBR.

2.4.3 Spray Reactors

Spray reactors have been used in both catalytic and non-catalytic gas-solid/liquid-solid reactions. They have been implemented for catalytic oxidation processes [45], which have improved the production quantity and quality, along with sufficient contact surface area. Within the Cu-Cl cycle, there have been some accounts of the spray reactor implementation for the hydrolysis reaction. Ferrandon et al. [15, 26] conducted multiple experiments of the hydrolysis reaction utilizing a spray reactor. In this design, steam/Ar are injected, in a co- and counter-current flow, into a heated zone where aqueous $CuCl_2$ is atomized. Upon

injection and atomization of the $CuCl_2$ solution, water is vaporized rapidly, forming small $CuCl_2$ particles [26]. These particles either react with steam or thermally decompose as they travel along the length of the reactor, with solid reaction products deposited at the bottom of the reactor.

Initial work of Ferrandon et al. [15] presented the spray reactor, both co- and counter-current design, and tested for the hydrolysis of $CuCl_2$. The counter-current flow design led to higher yields of Cu2OCl_2 compared to co-current flow due to enhanced mass-transfer. These experiments also highlighted the importance of atomizer design for successful operation of the spray reactor and reduced challenges such as clogging due to solid residues and reduction in the extent of reaction due to the relationship between the expanding spray cone and nebulizer location.

Ferrandon et al. [15] also suggested an ultrasonic nozzle to overcome these problems, providing small droplets and a cylinder of mist that does not expand as the cones exhibit with the pneumatic nebulizer. Their preliminary testing confirmed that this nozzle design and spray geometry prevent clogging. This work was continued in their experimental investigation of the influence of reactor pressure on the amount of steam required for complete conversion to Cu_2OCl_2 and HCl [26]. Ferrandon's experimental setup investigated the hydrolysis reaction at varying reduced reactor pressures (0.4 - 1 atm). The authors identified that as the reactor pressure decreases, less formation of CuCl was observed along with a shift in the maximum formation of Cu_2OCl_2 at lower SCR. This result presented as favourable method to reduce steam requirements and thus lower energy requirements.

2.4.4 Moving Bed Reactors

A common reactor design in gas-solid systems is a moving bed reactor (MBR) [46]. MBRs have the potential to improve the conversion of $CuCl_2$, while also reducing the steam consumption, through improved heat and mass transfer and availability of different flow configurations (e.g., multiple injection sites, recycling, co /counter current flow, cross flow) [46]. From past studies in biomass and coal gasification processes, co-current, or downdraft, MBR are widely used in these processes [47, 48]. However, from the previous sections, there has been a lack of investigation of downdraft MBR modeling for the Cu-Cl cycle. Simulations providing new insight would be useful in identifying experimental and large-scale viability of this design.

2.4.4.1 Operation

Moving bed reactors are frequently implemented in gas-solid systems where the solids typically act as a catalyst, such as fluid catalytic cracking, naphtha processes, etc. However, these reactors are becoming more prominent in non-catalytic systems such as coal / biomass steam gasification [46].

The premise of a chemical moving bed reactor is not unlike a fluidized bed, where a chemical reaction occurs through the contact of solid and fluid streams [46]. However, in an MBR, the solid stream is not fluidized by the fluid stream (i.e., fluid is not flowing at a velocity that would cause the solid particles to flow like a fluid), rather the solid phase is moving due to the downward effects of gravity [46]. With respect to catalytic processes, the exiting solid mass can be regenerated and continuously re-enter the top of the reactor through external equipment (i.e., regenerators) [49]. Figure (2-4) shows a process flow

diagram (PFD) of an MBR for an updraft and downdraft configuration for a gas-solid phase operation.

In terms of operation conditions, MBRs typically have a continuous flow of both the solid and gas phase, and thus can be assumed to operate at steady state, as well as an open system [50]. Furthermore, plug flow operations can also be assumed, providing simplifications in equation generation and mathematical modeling. Additional to these simplifications, there are several advantages in using MBRs [46],

- Low energy consumption,
- Low pressure drop,
- Reduction of maintenance and capital costs,
- Improvement of process performance,
- Enhancing the contact surface of gas-solid systems,
- Higher equilibrium yield and performance when considering continuous catalytic regeneration (CCR).

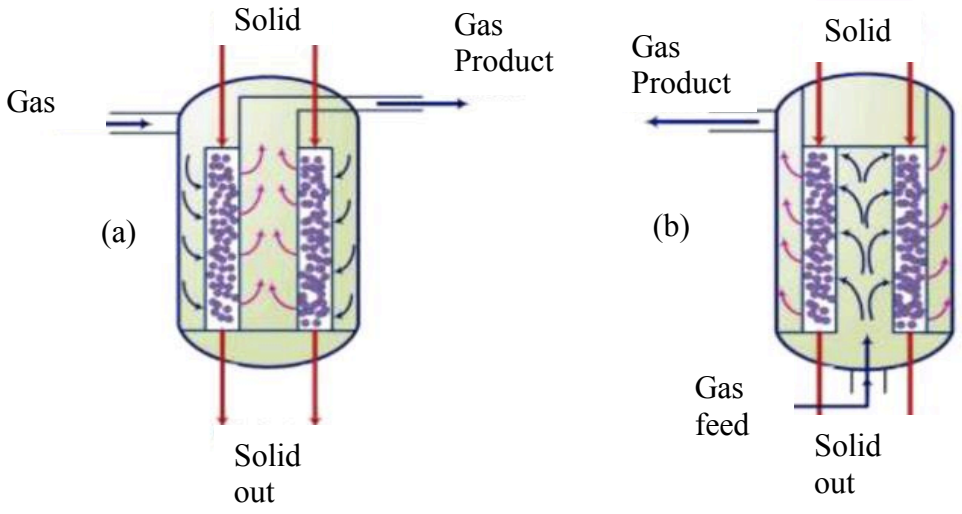

Figure 2-4: Moving bed reactor flow types: (a) downdraft (co-current) and (b) updraft (counter current) [46]

Modelling and optimization of MBRs has been studied extensively, both from an industrial and a hypothetical perspective. These models allowed for detailed investigation of flow configuration and patterns, feed types, particle size, catalyst application, etc., through the investigation of mass and energy balances, kinetics, equilibrium, and physical properties [46]. While the above assumptions can be applied to the process, further details are required on the operating conditions and goals of the specific process. Nonetheless, the above stated techniques can be used in processes such as reduction of iron ore pellets [51], coal steam gasification [52], and biomass gasification [47, 48, 53].

2.4.4.2 Implementation in Literature

There are numerous published literatures that implement MBR for non-catalytic gas-solid systems, with the SCM occasionally implemented to numerically represent reactions within MBR. Arabi et al. [51] utilized the SCM to simulate a countercurrent (updraft) MBR for the reduction of iron ore pellets. Solving the system of ordinary differential equations (ODE) and rate equations generated from the SCM, the temperature and concentration profiles for all species were predicted. Adanez et al. [54] also implemented the SCM to generate the reaction rate for the modelling of coal gasification in an MBR. This representation of the reaction rate through the SCM is promising for the introduction of MBR into the hydrolysis reaction.

Kulkarni et al. [52] presented a model for moving bed gasifiers including an excess gas stream of coal gasification. The model showed good agreement with available data and highlighted a potential for experimental moving bed reactor tests. Schwabauer et al. [47], Mandl et al. [48], and Di Blasi et al. [53], all analyzed Wood-pellet gasification in counter-

current moving beds. Mandl et al. [48] and Di Blasi et al. [53] presented a 1-D model, while Schwabauer et al. [47] presented both 1-D and 3-D models that agreed with past results of Mandl et al. [48] and Di Blasi et al. [53]. The models provided further agreement with experimental data as well as quantitative predictions for future small-scale moving bed reactors. All models from [47], [48], and [53] utilized systems of ordinary differential equations, representing the mass and energy balance equations, to model the boundary conditions and main reaction rate equations. Additionally, due to the non-isothermal and non-isobaric conditions considered in these works, a two-point boundary value method was introduced to solve the ODES. While the models from [47], [48], and [53] are with respect to counter-current, or updraft, MBRs, and considered varying boundary conditions along the reactor length, the numerical setups aid in outlining the system of equation and pathways for solving the downdraft MBR design of this thesis.

MBRs are also implemented in catalytic reaction process and are commonly found in Naphtha reforming. This is the main industrial process to obtain high-octane gasoline and aromatic hydrocarbons for gasoline blending [46]. Krane et al. [55] developed a kinetic model for the principal reactions of naphtha through continuous fixed catalytic beds. These generated product compositions and yields that compared well with experimental data. Bijani et al. [56] modelled a radial flow moving bed reactor for the dehydrogenation of Isobutane. Similar to most models, the model parameters were obtained from lab-scale fixed bed reactors and fair agreement was observed.

2.4.4.3 Reactors in series

An MBR configuration that has shown promise in previous studies for achieving enhance conversion is a multi-injection MBR. This configuration incorporates gas injection sites along the length of the reactor to shift the equilibrium through fresh steam injection and improve heat recovery [57]. Reactors in series can be implemented to mimic the behaviour of multi-injection MBR conditions. Figures (2-5) and (2-6) show the multi-injection MBR and the reactor in series configurations.

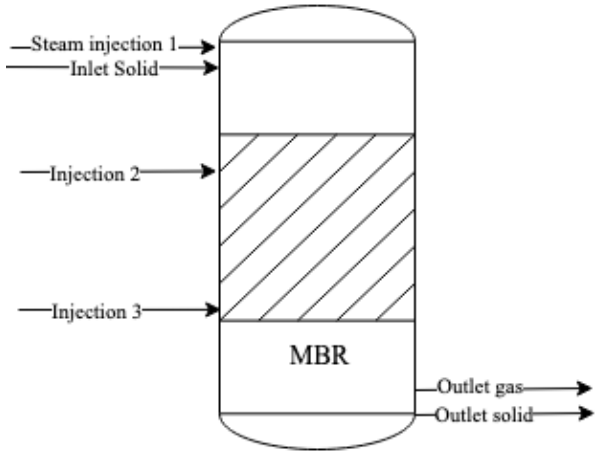

Figure 2-6:Schematic of multi-injection downdraft moving bed reactor.

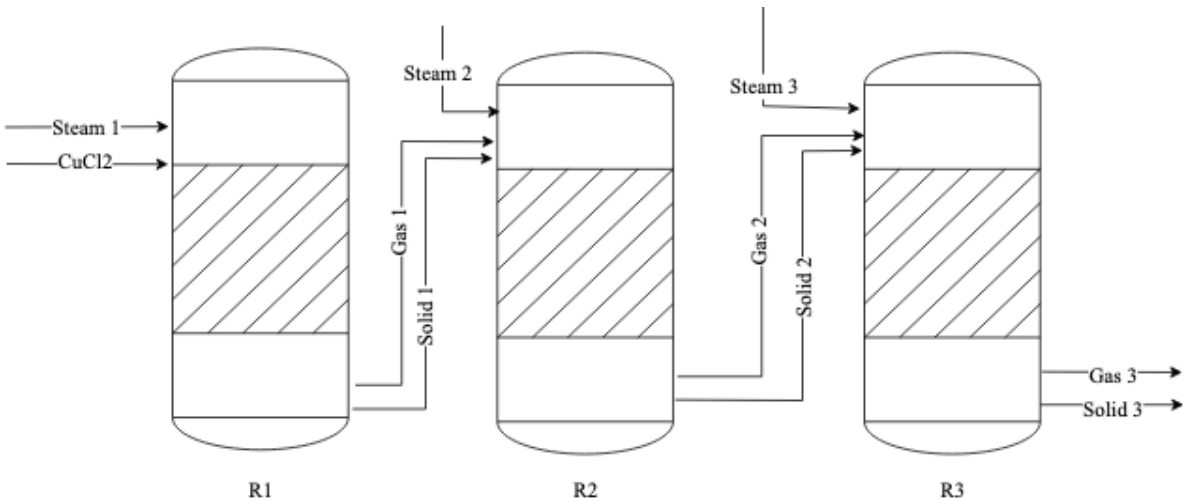

Figure 2-5: Schematic of plug flow reactor in series configurations to simulate multi-injection downdraft MBR behaviour.

Hongjun et al. [58] analyzed an MBR for catalytic naphtha reforming through a series of four catalytic reactors. The model showed good agreement with commercial plant data. Similarly, Ancheyta-Juárez et al. [59] used four catalytic reactors in series for naphtha reforming within an MBR and compared predictions with reactor data from a plant. The reactor in series approach matched the plant data. Karimi et al. [60] modelled four adiabatic reactors in series for naphtha reforming in moving bed conditions. The model results were compared to conventional models, whereby an appreciable reduction in operational costs and enhancement in net plant profit was identified. These studies further suggest the potential benefits for multi-injection MBR integration within the hydrolysis process.

2.4.4.4 Reaction Kinetics

Of the available experimental data for hydrolysis reaction there is limited consistency with respect to reaction rate equations and reaction rate constant values. With respect to reaction rate constants, in the experimental results of Singh et al. [22], for varying $CuCl_2$ particle size, numerous rate constants were generated, ranging from 0.42 h^{-1} to 2.84 h^{-1}. Thomas et al. [30] presented the hydrolysis reaction rate constant in terms of the Arrhenius equation for their experimental investigation of mechanism and kinetics of the hydrolysis reaction, reflected in Equation (2-12).

$$k = 2.4 \times 10^4 e^{-44800/RT} \quad (2\text{-}12)$$

Where, Reynolds Number is represented by R and temperature is represented by T. Further variation in presentation of experimental results is seen in Pope et al. [61], where the generated hydrolysis reaction rate is between 0.05 to 0.03 mol/m^3-min. Hydrolysis reaction rate constant value can likewise be generated from the experimental work of Ferrandon et

al. [62]. The experiments conducted at high SCR conditions presented a reaction rate constant of 0.00063 m^3(STP)/mol-min for solid conversion.

While all the above referenced experimental works are acceptable, they emphasize the importance of identifying suitable validation equations and constants based on chosen operating conditions. This will aid in capturing realistic hydrolysis reaction progression when creating predictive reactor design models. Additionally, it is important to select validation data within the desired operating range, especially in the case for the novel MBR design. Table (2-4) presents some of the available experimental conditions presented within literature, emphasizing the variation in results.

Table 2-4: Hydrolysis reaction conditions for various experimental studies in past literature.

Reference Work	Temperature Range (℃)	Pressure Range (bar)	SCR Range	Particle Size (μm)	Reaction Time (mins)
Singh et al. [22]	370 - 400	1 bar	11 - 88	0.02-0.045	15 - 120
Ferrandon et al. [26]	400	0.4 - 1 bar	15 -23	6 - 23	2
Thomas et al. [30]	300- 375	1 bar	2 - 15	350	10 - 180
Pope et al. [61]	350 - 400	1 bar	95	265	50
Ferrandon et al. [62]	300 - 400	1 bar	27 - 66	150 - 250	20 - 60

Reaction data is influenced by numerous factors, including operating temperature and pressure, reaction time, and steam to copper ratio. Consequently, different experimental setups, parameters, and operating conditions will impact the reaction kinetic parameters developed from the experimental data. This can be observed in the validation of hydrolysis numerical modeling from Daggupati et al. [35] with the experimental results from Ferrandon et al. [62]. From the conversion trends generated by the numerical model, the experimental data only validates longer reaction times within the model (further details can be found in Chapter 4). While this does not indicate that the model or experimental results

are incorrect, it accentuates the need for a larger range of experimental datapoints of the hydrolysis reaction and the significance of selecting suitable validation data for the desired conditions. Given the absence of experimental or predictive results concerning the multi-injection MBR design in the Cu-Cl cycle, a set of data will be chosen that aligns with the desired operating conditions of the MBR model regardless of the reactor type used.

2.4.5 Gas Recirculation

Increasing reactant conversion, improving separation, and recovery of catalysts and reagents, particularly for reversible reaction, are identifiable benefits of recirculation streams [63]. From the objectives, various reactor design configurations will be modelled through the phase equilibrium simulations to analyze their influence on hydrolysis progression and steam consumptions. Additional to the novel multi-injection MBR design, outlet gas recirculation techniques could potentially improve the conversion of $CuCl_2$, while also reducing the steam consumption as any unreacted steam could be further converted. A challenge, however, is the high HCl content in the gas after the hydrolysis reaction.

Farsi et al. [64] proposed recycling of outlet gas stream within the Cu-Cl cycle is necessary to achieve lower operating costs and higher efficiency. HCl was concentrated by simulating a pressure swing distillation (PSD) process in Aspen Plus to separate HCl and water, allowing for recycling of unreacted steam. Finney et al. [43] performed Aspen Plus modeling of gas recirculation within a fluidized bed. The model operated under the assumption that no side reactions occurred, reinforcing the importance of incorporating side reaction data for accurate estimates. Overall, the results highlighted that a high HCl

concentrated gas stream could still progress the hydrolysis reaction in the forward direction and yield a potential steam reduction through gas recirculation. Considering the outlet gas recirculation design concept from [43] and incorporating the side reactions identified in this literature review with the phase equilibrium simulations of this work, more precise predictions of the hydrolysis reaction progression with high HCl concentrated gas can be generated.

2.5 Conclusions

Having zero harmful emissions when expended as a spent fuel, hydrogen presents as a promising pathway to reduce global emissions while continuing to provide sufficient energy on a global scale. Current production methods, such as steam-methane reforming and coal gasification provide a large portion of hydrogen generation. However, these approaches contribute to global carbon emissions, negating the benefits of hydrogen fuel. Investigations of alternative and clean production methods have been presented, with thermochemical water splitting cycles offering a promising production option in yielding clean hydrogen. Of the hundreds of thermochemical cycles for hydrogen production, only a few have been deemed feasible for large scale implementation through various criteria assessments. From these realistic methods, the Cu-Cl thermochemical water splitting cycle presents favourable advantages over other thermochemical cycles due to lower process temperatures, readily available species, and integration with waste heat production facilities.

The main upscaling challenge for the Cu-Cl cycle derives from the large excess steam requirement of the hydrolysis reaction. Past studies have investigated methods to improve

solid conversion while reducing SCR. Numerous research studies have considered adjustments to the hydrolysis reactor design and operating parameters. Various reactor types have been presented such as a fluidized bed, packed bed, and spray reactors, with examination of the impact of particle size, reactor pressure and reactor temperature on solid conversion and steam requirements. From research on gas-solid reactor types, the downdraft multi-injection MBR showed high potential for integration into the hydrolysis reaction due to improved heat and mass transfer, along with an ability for different particle contact through various flow configurations.

Additionally, through literature review it was identified that there are limited past predictive models that present progression of the hydrolysis reaction along with the potential side reactions. Understanding of side reaction progression is important to hydrolysis reaction integration within the Cu-Cl cycle. Mitigation of side reactions, and undesired by-products, can improve product yield and overall efficiency of the cycle. Further study of the impact of side reactions within the hydrolysis cycle through the predictive models of this thesis can aid in the identification of scenarios and reactor conditions to mitigate undesired reactions and by-products.

This research identified potential improvement in $CuCl_2$ conversion and steam requirements. Through the study of the novel multi-injection MBR design and the reactor in series approach to mimic MBR conditions, predictive modeling can be generated to present reaction progression within the reactor. Initial simulation of this reactor design was examined. Various reaction conditions, reactor design parameters and operating conditions were investigated to obtain an overview of the hydrolysis reaction and present scenarios that can improve solid conversion along with reducing SCR.

References

[1] G. Naterer *et al.*, "Recent Canadian advances in nuclear-based hydrogen production and the thermochemical Cu-Cl cycle," *Int. J. Hydrogen Energy*, vol. 34, no. 7, 2009.

[2] International Energy Agency, "The Future of Hydrogen," 2019.

[3] L. C. Brown *et al.*, "High efficiency generation of hydrogen fuels using nuclear power.," 2003. [Online]. Available: http://www.osti.gov/servlets/purl/814014-tdQyiq/native/%0Ahttps://fusion.gat.com/pubs-ext/AnnSemiannETC/A24285.pdf.

[4] B. W. Mcquillan *et al.*, "High efficiency generation of hydrogen fuels using solar thermal-chemical splitting of water (Solar thermo-chemical splitting for H2)," 2010.

[5] Y. Shindo, N. Ito, K. Haraya, T. Hakuta, and H. Yoshitome, "Thermal efficiency of the magnesium-iodine cycle for thermochemical hydrogen production," *Int. J. Hydrogen Energy*, vol. 8, no. 7, pp. 509–513, 1983.

[6] S. Kubo *et al.*, "A pilot test plan of the thermochemical water-splitting iodine- sulfur process," *Nucl. Eng. Des.*, vol. 233, no. 1–3, pp. 355–362, 2004.

[7] K. F. Knoche, P. Schuster, and T. Ritterbex, "Thermochemical production of hydrogen by a vanadium/chlorine cycle. Part 2: Experimental investigation of the individual reactions," *Int. J. Hydrogen Energy*, vol. 9, no. 6, pp. 473–482, 1984.

[8] F. Lemont, "Promising optimization of the CeO2/CeCl3 cycle by reductive dissolution of cerium (IV) oxide," Int. J. Hydrogen Energy, vol. 33, no. 24, pp. 7355–7360, 2008.

[9] F. Safari and I. Dincer, "A study on the Fe–Cl thermochemical water splitting cycle for hydrogen production," Int. J. Hydrogen Energy, vol. 45, no. 38, pp. 18867–18875, 2020.

[10] C. Sattler, M. Roeb, C. Agrafiotis, and D. Thomey, "Solar hydrogen production via sulphur based thermochemical water-splitting," Sol. Energy, vol. 156, pp. 30–47, 2017.

[11] A. Farsi and A. Science, "Development and Modeling of a Lab-scale Integrated Copper-Chlorine Cycle for Hydrogen Production," no. August, 2020.

[12] A. Farsi, I. Dincer, and G. F. Naterer, "Review and evaluation of clean hydrogen production by the copper–chlorine thermochemical cycle," J. Clean. Prod., vol. 276, p. 123833, 2020.

[13] A. Ozbilen, I. Dincer, and M. A. Rosen, “A comparative life cycle analysis of hydrogen production via thermochemical water splitting using a Cu e Cl cycle,” Int. J. Hydrogen Energy, vol. 36, no. 17, pp. 11321–11327, 2011.

[14] M. F. Orhan, I. Dinçer, and M. A. Rosen, “Efficiency comparison of various design schemes for copper-chlorine (Cu-Cl) hydrogen production processes using Aspen Plus software,” Energy Convers. Manag., vol. 63, pp. 70–86, 2012.

[15] M. S. Ferrandon et al., “Hydrogen production by the Cu-Cl thermochemical cycle: Investigation of the key step of hydrolysing CuCl2 to Cu2OCl2 and HCl using a spray reactor,” Int. J. Hydrogen Energy, vol. 35, no. 3, pp. 992–1000, 2010.

[16] A. Farsi, Ö. Kayhan, C. Zamfirescu, I. Dincer, and G. F. Naterer, “Kinetic and hydrodynamic analyses of chemically reacting gas-particle flow in cupric chloride hydrolysis for the Cu-Cl cycle,” Int. J. Hydrogen Energy, vol. 44, no. 49, pp. 26783–26793, 2019.

[17] V. N. Daggupati, G. F. Naterer, K. S. Gabriel, R. J. Gravelsins, and Z. L. Wang, “Equilibrium conversion in Cu-Cl cycle multiphase processes of hydrogen production,” Thermochim. Acta, vol. 496, no. 1–2, pp. 117–123, 2009.

[18] A. Ozbilen, I. Dincer, and M. A. Rosen, “Environmental evaluation of hydrogen production via thermochemical water splitting using the Cu-Cl Cycle: A parametric study,” Int. J. Hydrogen Energy, vol. 36, no. 16, pp. 9514–9528, 2011.

[19] A. Ozbilen, I. Dincer, and M. A. Rosen, “Life cycle assessment of hydrogen production via thermochemical water splitting using multi-step Cu-Cl cycles,” J. Clean. Prod., vol. 33, pp. 202–216, 2012.

[20] G. F. Naterer, I. Dincer, and C. Zamfirescu, Hydrogen production from nuclear energy, vol. 9781447149. 2013.

[21] G. F. Naterer et al., “Advances in unit operations and materials for the Cu–Cl cycle of hydrogen production,” Int. J. Hydrogen Energy, vol. 42, no. 24, pp. 15708–15723, 2017.

[22] R. V. Singh et al., “Investigations on the hydrolysis step of copper-chlorine thermochemical cycle for hydrogen production,” Int. J. Energy Res., vol. 44, no. 4, pp. 2845–2863, 2020.

[23] K. Pope, Z. Wang, and G. F. Naterer, “Process integration of material flows of copper chlorides in the thermochemical Cu-Cl cycle,” Chem. Eng. Res. Des., vol. 109, pp. 273–281, 2016.

[24] A. Farsi, I. Dincer, and G. F. Naterer, “Second law analysis of CuCl2 hydrolysis reaction in the Cu–Cl thermochemical cycle of hydrogen production,” Energy, vol. 202, p. 117721, 2020.

[25] V. N. Daggupati, G. F. Naterer, and K. S. Gabriel, “Diffusion of gaseous products through a particle surface layer in a fluidized bed reactor,” Int. J. Heat Mass Transf., vol. 53, no. 11–12, pp. 2449–2458, 2010.

[26] M. S. Ferrandon, M. A. Lewis, F. Alvarez, and E. Shafirovich, “Hydrolysis of CuCl2 in the Cu-Cl thermochemical cycle for hydrogen production: Experimental studies using a spray reactor with an ultrasonic atomizer,” Int. J. Hydrogen Energy, vol. 35, no. 5, pp. 1895–1904, 2010.

[27] A. Farsi, Ö. Kayhan, C. Zamfirescu, I. Dincer, and G. F. Naterer, “Azeotropic pressure swing distillation of hydrochloric-water for hydrogen production in the Cu–Cl cycle: Thermodynamic and design methods,” Int. J. Hydrogen Energy, vol. 44, no. 16, pp. 7969–7982, 2019.

[28] Y. Haseli, I. Dincer, and G. F. Naterer, “Hydrodynamic gas-solid model of cupric chloride particles reacting with superheated steam for thermochemical hydrogen production,” Chem. Eng. Sci., vol. 63, no. 18, pp. 4596–4604, 2008.

[29] K. Pope, G. F. Naterer, and Z. L. Wang, “Nitrogen carrier gas flow for reduced steam requirements of water splitting in a packed bed hydrolysis reactor,” Exp. Therm. Fluid Sci., vol. 44, pp. 815–824, 2013.

[30] D. Thomas, N. A. Baveja, K. T. Shenoy, and J. B. Joshi, “Experimental Study on the Mechanism and Kinetics of CuCl2 Hydrolysis Reaction of the Cu-Cl Thermochemical Cycle in a Fluidized Bed Reactor,” Ind. Eng. Chem. Res., vol. 59, no. 26, pp. 12028–12037, 2020.

[31] M. Ferrandon, V. Daggupati, Z. Wang, G. Naterer, and L. Trevani, “Using XANES to obtain mechanistic information for the hydrolysis of CuCl2 and the decomposition of Cu2OCl2 in the thermochemical Cu-Cl cycle for H2 production,” J. Therm. Anal. Calorim., vol. 119, no. 2, pp. 975–982, 2015.

[32] G. D. Marin, Z. Wang, G. F. Naterer, and K. Gabriel, “Byproducts and reaction pathways for integration of the Cu-Cl cycle of hydrogen production,” Int. J. Hydrogen Energy, vol. 36, no. 21, pp. 13414–13424, 2011.

[33] T. Kekesi, K. Mimura, and M. Isshiki, “Copper Extraction from Chloride Solutions by Evaporation and Reduction with Hydrogen,” Mater. Trans. JIM, vol. 36, no. 5, pp. 649–658, 1995.

[34] Z. Wang, G. Marin, G. F. Naterer, and K. S. Gabriel, “Thermodynamics and kinetics of the thermal decomposition of cupric chloride in its hydrolysis reaction,” J. Therm. Anal. Calorim., vol. 119, no. 2, pp. 815–823, 2015.

[35] V. N. Daggupati, G. F. Naterer, K. S. Gabriel, R. J. Gravelsins, and Z. L. Wang, “Solid particle decomposition and hydrolysis reaction kinetics in Cu-Cl thermochemical hydrogen production,” Int. J. Hydrogen Energy, vol. 35, no. 10, pp. 4877–4882, 2010.

[36] D. Kunii and O. Levenspiel, “The Design of Noncatalytic Gas- Solid Reactors,” in Fluidization Engineering, 2nd ed., no. 1991, Stoneham: Butterworth - Heinemann, 2022, pp. 449–479.

[37] O. Levenspiel, “Fluid - Particle Reactions: Kinetics,” in Chemical Reaction Engineering, 3rd ed., vol. 566–588, New York: Wiley, 1999.

[38] J. Szekely and J. W. Evans, “A structural model for gas-solid reactions with a moving boundary,” Chem. Eng. Sci., vol. 25, no. 6, pp. 1091–1107, 1970.

[39] Y. Haseli, G. F. Naterer, and I. Dincer, “Fluid-particle mass transport of cupric chloride hydrolysis in a fluidized bed,” Int. J. Heat Mass Transf., vol. 52, no. 11–12, pp. 2507–2515, 2009.

[40] L. K. Ramachandran, P.A.; Doraiswamy, “Modeling of non-catalytic gas-solid reactions.,” AlChE J., vol. 28, no. April, pp. 881–900., 1982.

[41] A. Rahimi and A. Niksiar, “A general model for moving-bed reactors with multiple chemical reactions part I: Model formulation,” Int. J. Miner. Process., vol. 124, pp. 58–66, 2013.

[42] V. N. Daggupati, G. F. Naterer, and I. Dincer, “Convective heat transfer and solid conversion of reacting particles in a copper (II) chloride fluidized bed,” Chem. Eng. Sci., vol. 66, no. 3, pp. 460–468, 2011.

[43] L. Finney, K. Gabriel, and K. Pope, “A novel fluidized bed suitable for the hydrolysis step in CuCl hydrogen production cycle,” Int. J. Hydrogen Energy, vol. 47, no. 71, pp. 30378–30390, 2022.

[44] K. Pope, Z. L. Wang, and G. F. Naterer, “Measured steam conversion and chemical kinetics in a hydrolysis packed bed reactor for hydrogen production,” Energy Procedia, vol. 29, pp. 496–502, 2012.

[45] M. Li, F. Niu, X. Zuo, P. D. Metelski, D. H. Busch, and B. Subramaniam, "A spray reactor concept for catalytic oxidation of p-xylene to produce high-purity terephthalic acid," Chem. Eng. Sci., vol. 104, pp. 93–102, 2013.

[46] M. Shirzad, M. Karimi, J. A. C. Silva, and A. E. Rodrigues, "Moving Bed Reactors: Challenges and Progress of Experimental and Theoretical Studies in a Century of Research," Ind. Eng. Chem. Res., vol. 58, no. 22, pp. 9179–9198, 2019.

[47] A. Schwabauer, M. Mancini, Y. Poyraz, and R. Weber, "On the mathematical modelling of a moving-bed counter-current gasifier fuelled with wood-pellets," Energies, vol. 14, no. 18, 2021.

[48] C. Mandl, I. Obernberger, and F. Biedermann, "Modelling of an updraft fixed-bed gasifier operated with softwood pellets," Fuel, vol. 89, no. 12, pp. 3795–3806, 2010.

[49] S. M. Walas, "Reaction Kinetics for Chemical Engineers," in Reaction Kinetics for Chemical Engineers, S. D. KirkPatrick, Ed. McGraw-Hill, 1959, pp. 284–287.

[50] S. Catalano, A. Wozniak, and J. Holland, "Moving Bed Reactors," Visual Encyclopedia of Chemical Engineering. https://encyclopedia.che.engin.umich.edu/Pages/Reactors/MovingBed/MovingBed. html#:~:text=. (accessed Feb. 01, 2022).

[51] S. Arabi and H. Hashemipour Rafsanjani, "Modeling and simulation of noncatalytic gas-solid reaction in a moving bed reactor," Chem. Prod. Process Model., vol. 3, no. 1, 2008.

[52] M. Kulkarni and R. Ganguli, "Moving bed gasification of low rank alaska coal," J. Combust., vol. 2012, 2012.

[53] C. Di Blasi, "Modeling wood gasification in a countercurrent fixed-bed reactor," AIChE J., vol. 50, no. 9, pp. 2306–2319, 2004.

[54] J. Adánez and F. G. Labiano, "Modeling of Moving-Bed Coal Gasifiers," Ind. Eng. Chem. Res., vol. 29, no. 10, pp. 2079–2088, 1990.

[55] H. Krane, A. B. Groh, B. L. Schulman, and J. H. Sinfelt, "Reactions in catalytic reforming of naphthas," in 5Th World Petroleum Congress, 1959, pp. 39–54.

[56] P. M. Bijani and S. Sahebdelfar, "Modeling of a radial-flow moving-bed reactor for dehydrogenation of isobutane," Kinet. Catal., vol. 49, no. 4, pp. 599–605, 2008.

[57] S. Fujii, Y. Kanematsu, Y. Kikuchi, and T. Nakagaki, "Effect of multi-injection process on 'Zeolite boiler' in thermochemical energy storage and transport system

of unused heat from bagasse boiler," ASME 2017 11th Int. Conf. Energy Sustain. ES 2017, collocated with ASME 2017 Power Conf. Jt. with ICOPE 2017, ASME 2017 15th Int. Conf. Fuel Cell Sci. Eng. Technol. ASME 201, pp. 1–8, 2017.

[58] Z. Hongjun, S. Mingliang, W. Huixin, L. Zeji, and J. Hongbo, "Modeling and simulation of moving bed reactor for catalytic naphtha reforming," Pet. Sci. Technol., vol. 28, no. 7, pp. 667–676, 2010.

[59] J. Ancheyta-Juárez, E. Villafuerte-Macías, L. Díaz-García, and E. González-Arredondo, "Modeling and simulation of four catalytic reactors in series for naphtha reforming," Energy and Fuels, vol. 15, no. 4, pp. 887–893, 2001.

[60] M. Karimi, M. R. Rahimpour, R. Rafiei, A. Shariati, and D. Iranshahi, "Improving thermal efficiency and increasing production rate in the double moving beds thermally coupled reactors by using differential evolution (DE) technique," Appl. Therm. Eng., vol. 94, pp. 543–558, 2016.

[61] K. Pope, V. N. Daggupati, G. F. Naterer, and K. S. Gabriel, "Experimental study of gaseous effluent and solid conversion in a fluidized bed hydrolysis reactor for hydrogen production," Int. J. Hydrogen Energy, vol. 37, no. 21, pp. 16397–16401, 2012.

[62] M. S. Ferrandon et al., "The Hybrid Cu-Cl Thermochemical Cycle. I. Conceptual Process Design and H2a Cost Analysis. II. Limiting the Formation of CuCl during hydrolysis," no. January 2008, 2008.

[63] Ri. Felder, R. Rousseau, and L. Bullard, "Recycle and Bypass," in Elementary Principles of Chemical Processes, 4th ed., L. Ratts, Ed. Wiley, 2016, pp. 122–129.

[64] A. Farsi, Ö. Kayhan, C. Zamfirescu, I. Dincer, and G. F. Naterer, "Thermodynamic model of pressure swing distillation for a high-pressure process of hydrochloric/water separation and hydrogen production," Int. J. Hydrogen Energy, vol. 44, no. 7, pp. 3481–3491, 2019.

Chapter 3 - Hydrolysis Phase Equilibrium in Various Reactor Configurations

A modified version of this chapter has been published as: J. Broders, K. A. Hawboldt, K. Pope, G. F. Naterer. Equilibrium Analysis of Hydrolysis Conversion as a Function of Operating Conditions. International Journal of Hydrogen Energy (in press).

Abstract

This study examines the phase equilibrium trends of the hydrolysis process in the thermochemical Cu-Cl cycle of hydrogen production. Various temperatures, pressures, and steam to copper ratios are modelled within a single reactor configuration, to predict $CuCl_2$ conversion and progression of side reactions within the hydrolysis reactor. Optimal conversion of $CuCl_2$ and minimal by-product generation are obtained at a reactor temperature of 375°C and pressure of 1 bar, with improved conversion at higher temperatures and lower pressures. Improved reaction conversion is also identified at higher steam to copper ratios. A 10:1 steam to copper ratio was used for the remaining reactor configuration scenarios. Implementing the optimal design conditions, two novel reactor configurations, Multi-injection Moving Bed Reactors (MBRs) and outlet gas recirculation, are introduced to identify potential improvement in solid conversion and steam consumption within the hydrolysis reaction. Reactors in series were simulated to mimic the multi-injection MBR behaviour. Three reactors in series with 10 kmol total steam consumption showed better conversion of 1 kmol of $CuCl_2$ by 17% compared to the single reactor at the same conditions. Mitigation of $CuCl_2$ and Cu_2OCl_2 decomposition reactions was also observed. The outlet gas recirculation design improved the total desired product

yield, however, the maximum conversion of $CuCl_2$ was significantly impacted due to the high level of HCl concentrated steam. A combination of the gas outlet stream and reactors in series provide a method to improve the conversion rate. This reactor configuration is a challenging approach unless there is a separation technique to shift the reaction equilibrium or reduce HCl concentration within the gas stream.

3.1 Introduction

The Cu-Cl cycle is a favourable alternative to lower carbon footprint and increase conversion efficiency of hydrogen production. However, additional research is required to improve $CuCl_2$ conversion and steam consumption of the hydrolysis step. Introduction of novel reactor designs for the hydrolysis stage of the Cu-Cl Cycle requires preliminary examination of reaction progression and operating conditions to ensure feasibility of the new design before generation of a complete numerical model. Accumulation of the various operating conditions and reactor scenarios presented in previous literature will aid in the simulation of the hydrolysis process at different considerations, producing a set of operating conditions that will best suit the novel reactor design. These considerations include side reactions, temperatures, pressures, and steam to copper ratios (SCR).

Prior research identified several side reactions that can influence the hydrolysis solid conversion. However, there is limited numerical data and predictive models that presents side reactions involved in the hydrolysis stage. Daggupati et al. [1, 2] and Pope et al. [3] performed numerical modelling and experimental work, respectively, that neglected side reactions. Farsi et al. [4] presented a second law analysis of the hydrolysis stage within Aspen Plus which included the decomposition of $CuCl_2$ as a side reaction. Ferrandon et al.

[5], Thomas et al. [6], and Marin et al. [7] all performed experimental work identifying and investigating the impacts of common side reactions within the hydrolysis reaction. Introduction of these side reactions as a guide for the preliminary model will aid in generating accurate predictions of $CuCl_2$ conversion within the novel moving bed reactor (MBR) and gas recirculation design schemes.

Through the identification of the hydrolysis reaction operating ranges, phase equilibrium modelling can be exercised to produce high-level conversion and component yield predictions. There are various past studies that investigate phase equilibrium data for reaction predictions. Lee et al. [8] utilized thermodynamic software, HSC Chemistry, to predict gas compositions of biomass pyrolysis. The thermodynamic results were then implemented in kinetic simulations to predict realistic products of the pyrolysis reaction. Kim et al. [9] examined phase equilibria for predictions of behaviour of high temperature corrosion. These predictions were consistent with experimental results obtained in similar conditions. Wang et al. [10] predicted gaseous products of oil shale pyrolysis through a combination of kinetic and thermodynamic simulations. Predictions from thermodynamic equilibrium simulations of predominant gas species at different temperatures were then used as inputs for the simulation through the introduction of reaction kinetics. Similar trends for the hydrolysis reaction can identify ideal operating conditions and whether the multi-injection MBR or gas recirculation configurations have favourable potential for implementation into the hydrolysis reaction.

This chapter will investigate the impact of varying operating conditions (i.e., pressure, temperature, and steam consumption) on the hydrolysis reaction and side reactions, through the analysis of equilibrium conversion / concentrations trends within a single reactor

design. These results will be useful in the identification of conditions that favour the conversion of the $CuCl_2$ and minimize side reactions, with the overall goal of reducing steam requirements. Implementing these conditions, downdraft multi-injection MBR (modelled through reactors in series) and gas recirculation behaviour can be simulated for a preliminary assessment of these designs. This selection of reactor design and configuration through simulations will be used as a tool in improvement of the reactor bed design for the hydrolysis process and numerical modeling of the MBR configuration.

3.2 Formulation of Phase Equilibrium

The phase equilibrium simulations were performed using Equilibrium Modules of HSC Chemistry. The Equilibrium Module uses the Gibbs Energy Minimization method to predict the composition as a function of initial composition and specified temperature and pressure. The value of ΔG is minimized with the material balance as the objective function at isothermal and isobaric conditions [11]. With this approach, it is essential that all components, both reactant and product, are specified. This module does not predict possible component generation since chemical reactions are not modeled, thus emphasizing the importance of establishing possible by-product formations within the hydrolysis phase.

Several side reactions were identified within the literature review to have an impact on product yield, the most dominant being the decomposition of $CuCl_2$ and Cu_2OCl_2, occurring at temperatures around 400°C and higher. In this study, it is assumed that reactants and products were limited to those outlined in Equations (3-1) to (3-6). With typical hydrolysis operating conditions assumed as a pressure of 1 bar and temperatures between 375 – 400℃, as identified within the literature review [1, 12, 13].

$CuCl_2$ decomposition [7]:

$$2CuCl_2 \rightarrow 2CuCl_{(s)} + Cl_{2(g)} \quad (3\text{-}1)$$

Cu_2OCl_2 decomposition [6]:

$$Cu_2OCl_2 \rightarrow CuO + CuCl_2 \quad (3\text{-}2)$$

Oxygen generation [5]:

$$CuO + 0.5Cl_2 \rightarrow CuCl_2 + 0.5O_2 \quad (3\text{-}3)$$

Chlorine reaction with excess steam [7]:

$$Cl_{2(g)} + H_2O_{(g)} \rightarrow 2HCl_{(g)} + 0.5O_{2(g)} \quad (3\text{-}4)$$

$CuCl_2$/CuCl reaction [14]:

$$CuCl_{2(s)} + CuCl_2 \rightarrow CuCl_{2(s)} + CuCl_{(l)} \quad (3\text{-}5)$$

Melting of CuCl [8]:

$$CuCl_{(s)} \rightarrow CuCl_{(l)} \quad (3\text{-}6)$$

Component databases within HSC Chemistry contain the key thermochemical properties such as boiling and melting points, densities, and specific heat capacities. An exception was Cu_2OCl_2, which is not in the HSC Chemistry database. For this compound, thermophysical properties were obtained from Zamfirescu et al. [15], with Equation (3-7) used to calculate heat capacity.

$$Cp = a + bT + cT^2 + dT^3 \quad (3\text{-}7)$$

The constants in the equation are specified in Table (3-1). Zamfirescu [15] generated Eq. (3-7) through a comparison of results from Kawashima et al. [16] and Parry [17] to identify a practical and non-bias method for specific heat predictions of Cu_2OCl_2. The simulation modeled utilized a similar temperature-based approach for specific heat capacity

predictions. The coefficients from Table (3-1) were directly entered into the model. A decomposition temperature of 400℃, molar mass of 214 kg/kmol and density of 4080 kg/m^3, were also used based on the findings of Zamfirescu et al. [15].

Table 3-1: Coefficients for Cu_2OCl_2 heat capacity function [15].

Coefficient	Value
a	53.72
b	0.1670
c	-0.1740×10^{-3}
d	7.498×10^{-8}

The numerical predictions were presented in units of kmol, with a feed of 1 kmol of $CuCl_2$ over a specified temperature range and pressure. The conversion is calculated through Equation (3-8). Results were presented in terms of conversion to facilitate comparisons with existing hydrolysis data [18].

$$x = \frac{CuCl_2\ Initial\ - unreacted\ CuCl_2}{CuCl_2\ initial} \tag{3-8}$$

Equation. (3-9) was used in the experimental work of Singh et al. [13]. This equation was implemented to determine the percent conversion of the major products identified by XRD.

$$conversion(\%) = 100 \times \frac{moles\ of\ \text{hydrolysis}\ product\ obtained}{moles\ of\ CuCl_2} \tag{3-9}$$

Comparisons of phase equilibrium results from Equations (3-8) and Singh et al. [13] were performed to investigate the impact of the side reactions in modeling and validation.

3.3 Simulations

In reaction analysis using the Gibbs energy minimization approach, it is assumed the reactions have infinite time, i.e., there is no reaction rate, rather a final concentration of products based on the Gibbs free energy at that temperature and initial composition of

products. This is an important assumption as the predictions of some scenarios may not be achievable as they neglect the rate of reaction and mass transfer effects. Nonetheless, equilibrium trends provide useful insight into the extent of reaction(s) and can be used as a tool for predictions in experimental design and interpretation of results. The phase behaviour also plays a role in the Gibbs free energy values and hence product distribution. As such, the phase of the reactants and potential products were included [13]. Table (3-2) shows a list of the possible reactants/products in the hydrolysis stage based on the reactions outline in Eq. (3.1) – (3.6). Based on these inputs, the equilibrium simulations for this chapter were performed for three types of systems:

(i) Single reactor

(ii) Multiple reactors (multi-injection MBR simulations)

(iii) Gas recirculation for single and multi-injection reactors

Table 3-2: Potential reactants/products for equilibrium calculations

	Components
Main Reactants/products	$CuCl_{2(s)}$
	$H_2O_{(g)}$
	$Cu_2OCl_{2(s)}$
	$HCl_{(g)}$
Possible Side Products	$Cl_{(g)}$
	$Cl_{2(g)}$
	$O_{2(g)}$
	$H_{2(g)}$
	$H_{(g)}$
	$CuCl_2*2H_2O$
	$CuO_{(s)}$
	$Cu_2O_{(s)}$
	$HCl_{(aq)}$
	$CuCl_{(s)}$
	$CuCl_{(l)}$

3.3.1 Single Reactor Configuration

The first set of simulations were performed within the single reactor configurations, (i), as presented in Figure (3-1). Initial conditions were varied to identify the ideal temperature, pressure, and steam ratio to use in the reactors in series, (ii), and the re-circulation configuration, (iii). The temperature range of 300-550℃ for this simulation case was based on hydrolysis reactor temperature range established in previous work (300-400℃) and the overall operating temperature of the Cu-Cl cycle (500-550℃). This allowed for a wider scope to study both hydrolysis conversion within the ideal range (i.e., 370 - 400℃) and the formation of undesired by-product [12, 19, 20].

The typical operating pressure for the hydrolysis reaction is 1 bar [12, 19, 20]. Based on past experimental data (e.g., Ferrandon et al. [21]) varying reactor pressure can influence solid conversion and steam requirement. For this thesis, the pressures conditions selected were 0.1, 0.5, 1, 5, and 10 bar. Each pressure was studied over the stated temperature range (300-550℃).

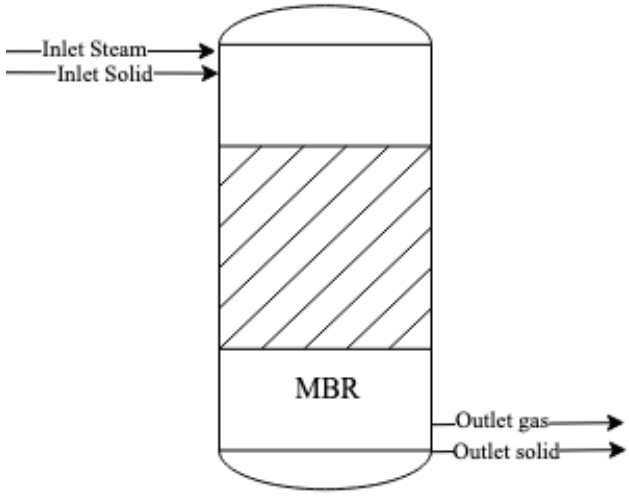

Figure 3-1: PFD for single injection downdraft reactor configuration (i) for hydrolysis operating condition simulations.

Additionally, the SCR was studied to determine the minimum SCR that would still achieve good conversion and minimize side reactions. Ferrandon et al. [21] and Lewis et al. [22] identified that the maximum conversion of $CuCl_2$ occurs when steam is supplied at approximately 20 times the stoichiometric value (i.e., 1 for H_2O). Thus, the SCR was varied from 1 to 20. These different operating scenarios resulted in a total of 100 simulations over the stated pressure, SCR, and temperature ranges, with the initial concentration of $CuCl_2$ as 1 kmol. Table (3-3) summarizes the simulation conditions.

Table 3-3: HSC simulation test conditions

Condition	Values	Units
Temperature	300 - 550	℃
Pressure	0.1 - 10	Bar
Steam to Copper Ratio	1 – 20	kmol/kmol
Inlet $CuCl_2$(s)	1	kmol
Inlet Cu_2OCl_2(s)	0	kmol
Inlet CuO(s)	0	kmol
Inlet CuCl(s)	0	kmol
Inlet Cu_2O(s)	0	kmol

3.3.2 Multiple Reactor Configuration

The multi-injection MBR design cannot be directly represented in HSC Chemistry, as such the MBR configuration was approximated via multiple reactors in series, (ii). A true reactor in series configuration consists of no side streams and all components entering the next reactor. However, in this set of reactions the concentration of HCl increases in each reactor, limiting the progression of the hydrolysis. Thus, in this work the solid stream from the previous reactor is combined with fresh steam and fed to each sequential reactor. Any gases produced are assumed to be not fed to the subsequent reactor (e.g. HCl). In theory this will eliminate the challenge of increasing HCl concentration, while shifting equilibrium

towards the reactant side for further solid conversion. The fresh steam entering each reactor was based on the total steam introduced in the single reactor simulations and dividing it by the number of reactors in series. The iterative pattern continued until either all the $CuCl_2$ was converted, or the available steam was fully used. This resulted in the same overall SCR for the reactor in series model as that of the single reactor model.

In previous work, three to four reactors in series have been used to simulate multi-injection MBR conditions. For instance, for the naphtha reforming process, Hongjun et al. [23] used four reactors, while Fazeli et al. [24] used three adiabatic reactors. For this work, three reactors in series are used to represent three injection points along the total reactor length. This acts as a basis for the preliminary model of the novel MBR design and solid conversion. Figure (3-2) outlines the PFD of reactors in series for multi-injection MBR simulation. This simulation used the ideal pressure, temperature, and SCR established from the single reactor simulations, (i). The conversion and component yields can then be compared with the single reactor configuration at the same conditions to identify any improvements.

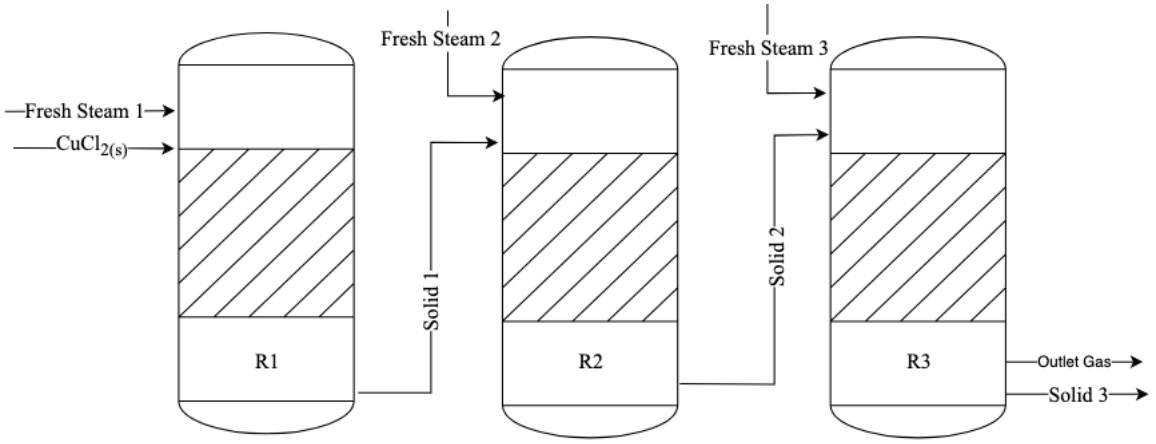

Figure 3-2: Process flow diagram for multi-injection downdraft MBR in series to simulate multi-injection behaviour (ii).

3.3.3 Gas Recirculation Configuration

Outlet gas recirculation, (iii), was added to both the single reactor, (i), and multiple reactor configuration, (ii), to assess the potential to reduce steam requirements by recycling any unreacted $H_2O_{(g)}$ after the hydrolysis reaction [21]. In the recirculation configuration the outlet gases (both new product and unreacted H_2O) from the first simulation are the feed for the next recirculation, with fresh steam add to maintain the overall SCR. This cyclic system continues until $CuCl_2$ conversion reached a plateau. Figure (3-3) outlines the single reactor gas recirculation.

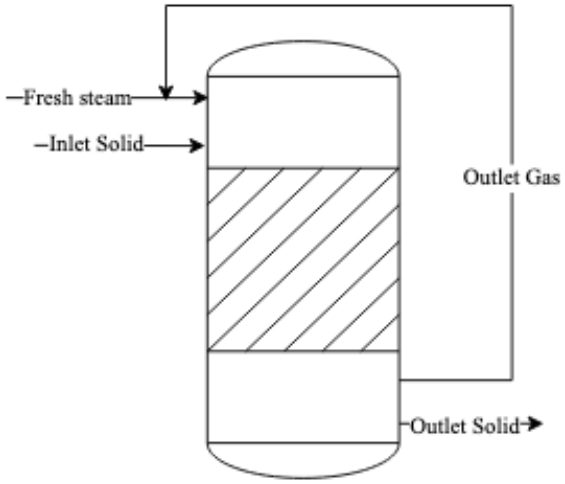

Figure 3-3: PFD of single hydrolysis reactor with outlet gas recirculation (iii).

Similarly, considering the multiple reactor configuration with gas recirculation, the outlet gas from the final reactor is recirculated to the initial reactor where sufficient fresh steam is injected to maintain the desired starting SCR as presented in Figure (3-4).

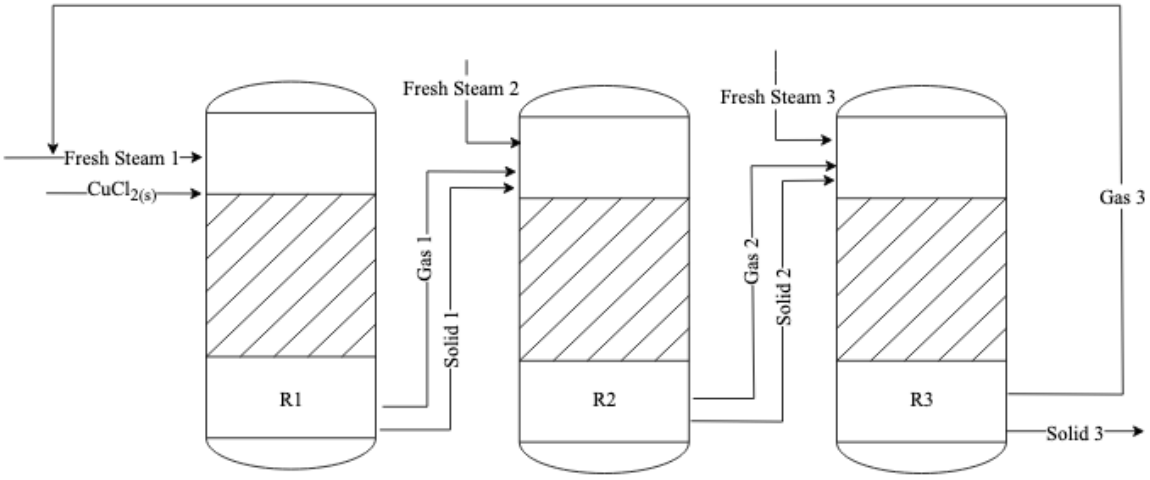

Figure 3-4: PFD for reactors in series with outlet gas recirculation.

3.4 Results and Discussion

3.4.1 Hydrolysis Operating Conditions

An objective of this research is to approximate ideal hydrolysis reactor conditions that will allow for maximum conversion and minimal excess steam requirements. The single reactor configuration was used to compare results from previous research and generate the "best" set of operating conditions for the multiple reactors, (ii), and gas recirculation simulations, (iii).

Through the single reactor design, the predictive equilibrium amounts of the component from Table (3-2) as a function of temperature for the varying pressures and SCR are generated. The $CuCl_2$ conversion for each simulation is calculated through Eq. (3-8), with the overall conversion based on all possible reactions associated with $CuCl_2$. Therefore, some scenarios may seem ideal, however, the conversion may be mainly associated with an undesired side reaction. Investigations of the main products of side reactions, specifically Cl_2, can reveal the impact, if any, of the side reactions on overall conversion

values. Figures (3-5) to (3-9) present the total conversion of $CuCl_2$ as a function of temperature for set pressures and SCRs.

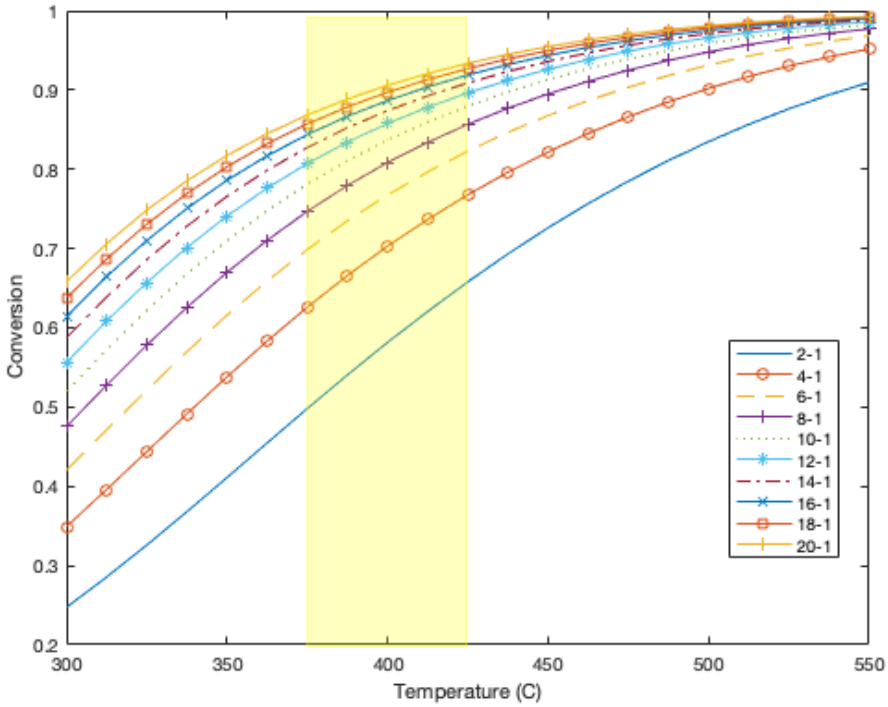

Figure 3-5: Conversion of $CuCl_2$ at a reactor pressure of 0.1 bar.

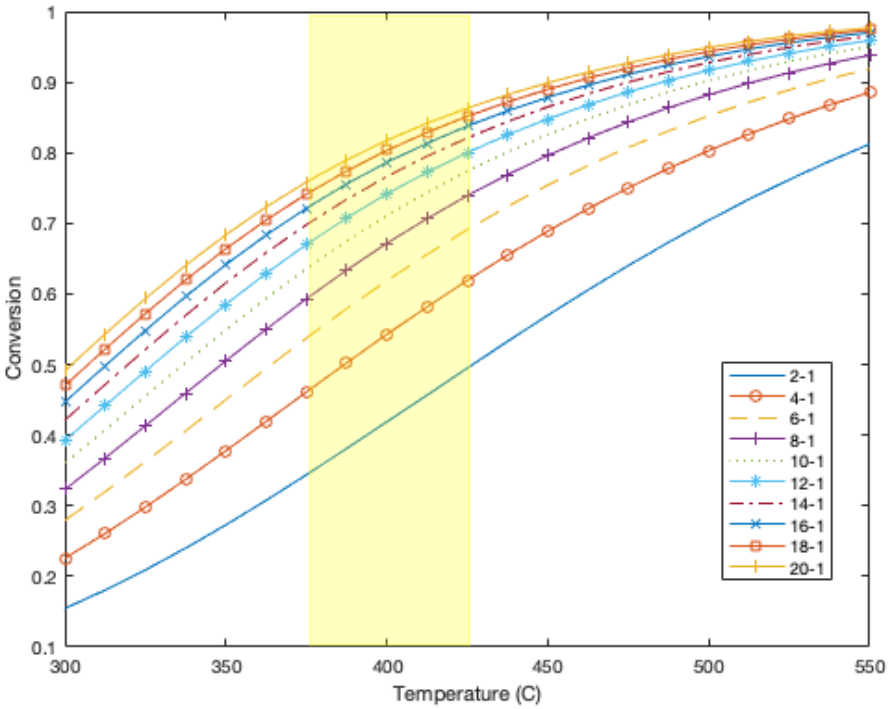

Figure 3-6: Conversion of $CuCl_2$ at a reactor pressure of 0.5 bar.

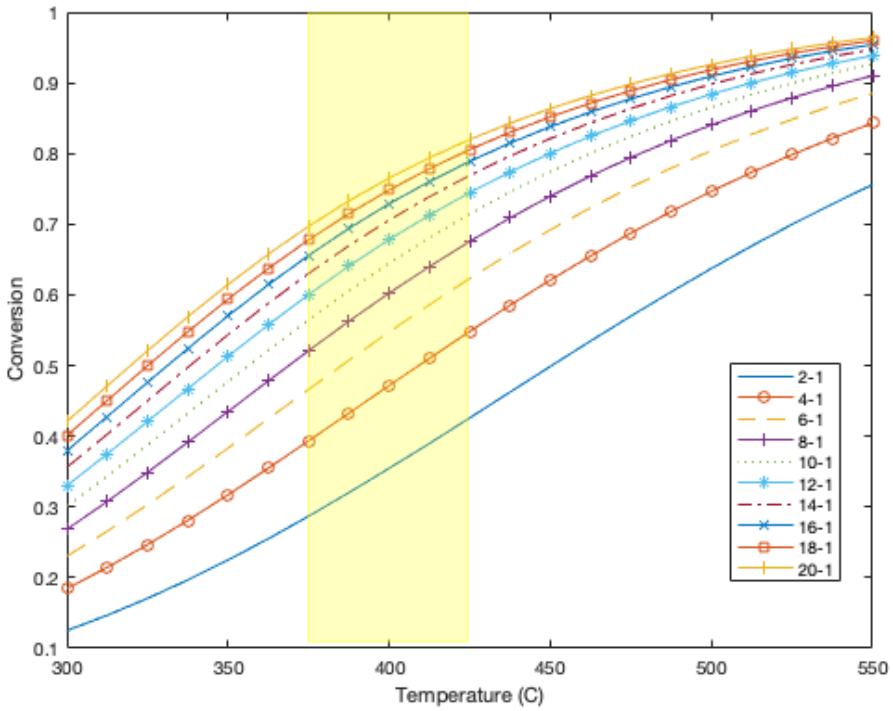

Figure 3-7: Conversion of $CuCl_2$ at a reactor pressure of 1 bar.

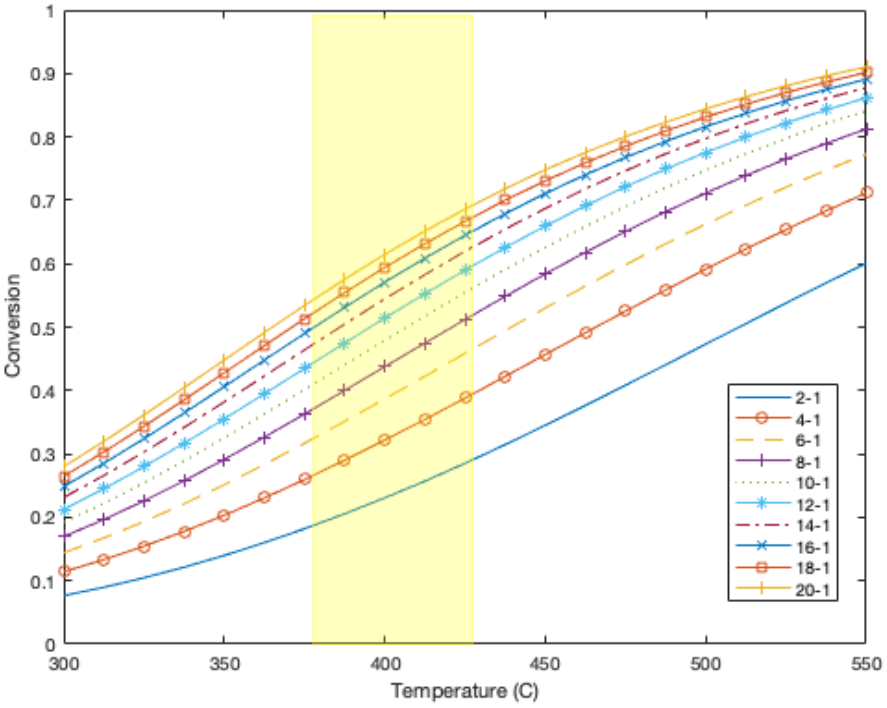

Figure 3-8: Conversion of $CuCl_2$ at a reactor pressure of 5 bar.

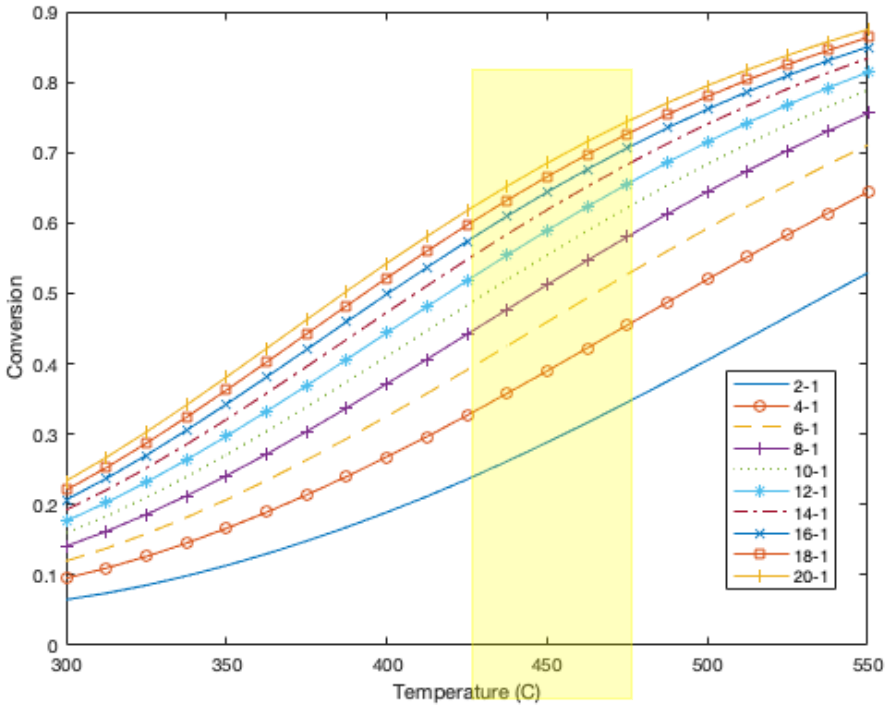

Figure 3-9: Conversion of $CuCl_2$ at a reactor pressure of 10 bar.

3.4.1.1 Pressure

Based on the single reactor simulations, lower operating pressures result in higher solid conversion at the same temperature and SCR. The highlighted zone in each figure is the typical operating range of the hydrolysis reactor from literature [6, 13]. Comparing conversions in this range shows a 30% increase in conversion as pressure is decreased from 10 bar to 0.1 bar. As the inlet is pure steam, the pressure of the system is the pressure of the inlet steam. However, the amount of steam and solid is constant (i.e., 1 k-mol). Therefore, the overall change in Gibbs energy (ΔG) of the system increases with increased pressure. Recalling that the equilibrium module is based on Gibbs energy minimization, this could potentially play a role in reduced $CuCl_2$ conversion, as higher value for ΔG would

limit product formation. Figure (3-10) shows the conversion as a function of pressure at a SCR of 10:1, which demonstrates the higher $CuCl_2$ conversion at lower pressure.

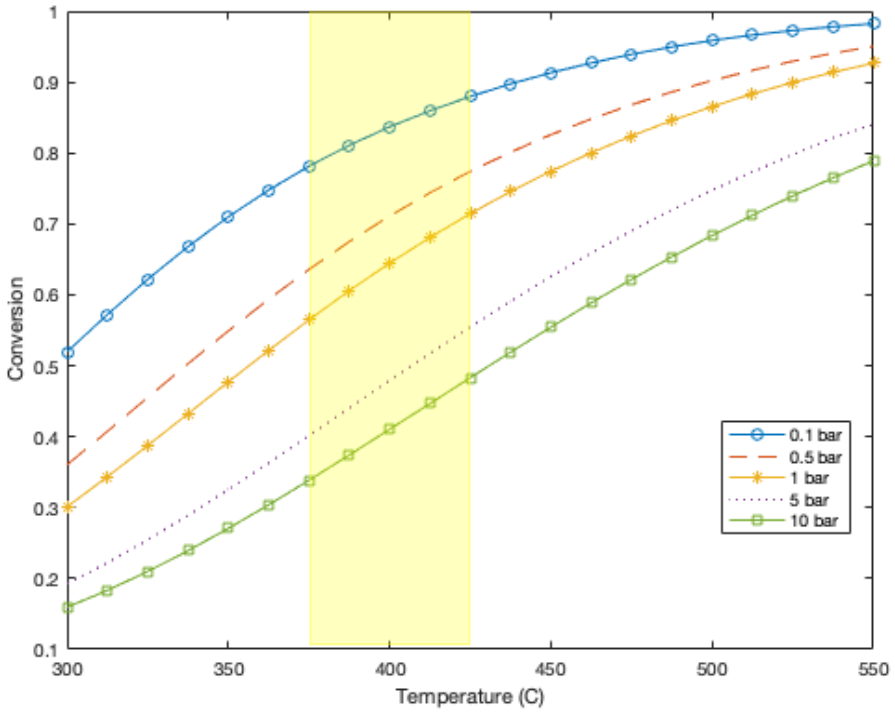

Figure 3-10: $CuCl_2$ conversion at 10:1 SCR at varying pressures and temperatures.

While $CuCl_2$ conversion is one indicator of process performance, the $CuCl_2$ can be converted to several products (i.e., through hydrolysis and $CuCl_2$ decomposition (Eq. (3-1))) and therefore does not completely reflect desired product formation. To determine the extent of other reactions occurring, the amount of Cl_2 produced (a product of $CuCl_2$ decomposition) was tracked to determine if the increase in conversion is due to hydrolysis or the decomposition of $CuCl_2$. Figure (3-11) presents a comparison of Cl_2 amounts at the varying pressure for a 10:1 SCR.

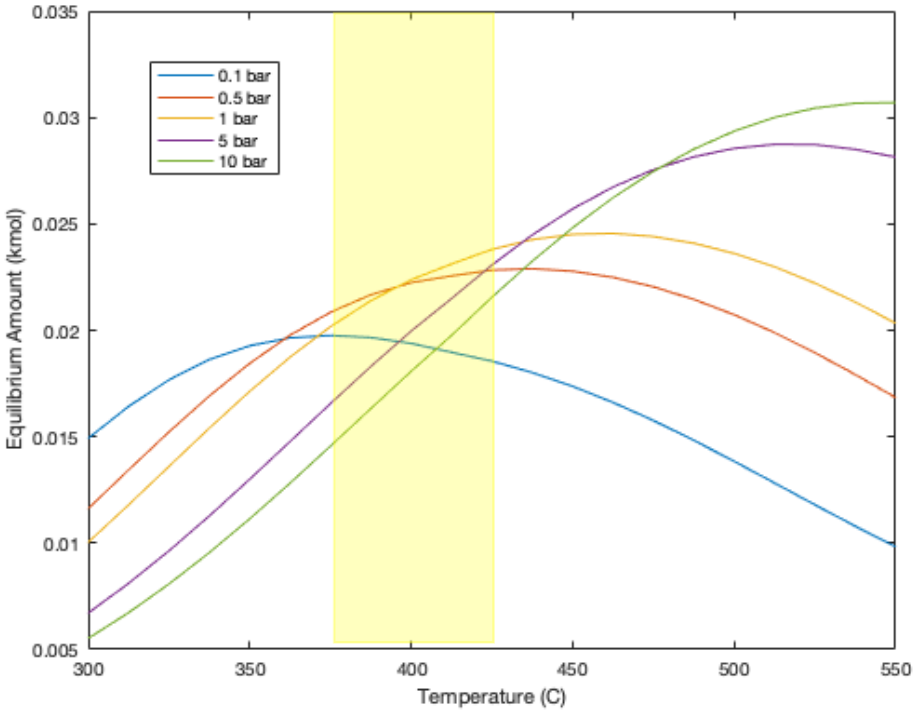

Figure 3-11: Comparison of Cl_2 equilibrium amount at varying pressures and temperatures at constant SCR=10:1.

Although the Cl_2 values are low (less than 6% of the total chlorine entering the reactor) there are still some interesting trends. In general, the influence of pressure on the generation of Cl_2 depends on the reactor temperature. At temperatures lower than the hydrolysis range (yellow zone), while Cl_2 increases with temperature, a decrease in generation with increasing pressure is observed. Within hydrolysis temperature range, two scenarios are present, (i) at very low pressures (0.1, 0.5 bar), Cl_2 is approximately constant or drops with temperature, and (ii) at P>1 bar Cl_2 generation increases with temperature. After the hydrolysis temperature range, another two scenarios are present, (i) for P<1 bar Cl_2 decreases with temperature and (ii) for P>1 bar Cl_2 increase with temperature. This further demonstrates the overall effect of pressure on the system. The low Cl_2 values at very high pressure and lower temperature indicate the impact of pressure on the ΔG of

system. As the temperature of the system increases, the impact of pressure on ΔG of system is mitigated. Therefore, an increase in Cl_2 production, especially at higher temperatures where the formation of Cl_2 is favoured, is observed. A similar trend is presented at lower system pressure, however at lower temperature range. This is due to the fact that for lower reactor pressures, the temperature effect occurs at lower temperatures compared to that of the high-pressure condition. This informs how one might operate the system based on steam, available pressure, and temperature in an industrial setting.

Pressure also impacts the steam requirement; the SCR required to achieve the same conversion drops as pressure is reduced. To achieve a 70% conversion at set temperature of 375℃ and pressure of 1 bar, a 20:1 SCR is required, whereas decreasing the pressure to 0.5 bar at the same temperature, requires a 15:1 SCR for the same conversion. This finding was supported by Ferrandon at al. [21], where in their experimental work, the conversion at P = 1 bar and SCR of 20:1 showed approximately the same conversion as P = 0.4 bar and SCR of 15:1. From this result, Ferrandon et al. [21] similarly concluded that reducing the pressure would allow operation at a lower SCR. While lower reactor pressures can improve solid conversion and steam requirements, the single reactor simulations indicated at P = 1 bar, conversion can be maximized without a high SCR. This is also a common pressure condition for the hydrolysis reactor in literature, supporting this pressure value as a basis for the remaining simulations [12, 13, 15].

3.4.1.2 Temperature

Increased temperature resulted in an increased conversion of $CuCl_2$ for the single reactor design. For all pressure scenarios (Figures (3-5) – (3-9)), the conversion of $CuCl_2$

increases with temperature - with almost complete conversion at temperatures greater than 500℃ for the higher SCR scenarios. This finding was support by the model results of Daggupati et al. [20], where they concluded based on predicted extent of reaction that conversion increased at a higher reactor temperature.

Further examining Figure (3-7), a constant reactor pressure of 1 bar, with respect to temperature and SCR, Table (3-4) summarizes the solid conversion at varying SCR and temperatures. For a SCR of 20:1 and a temperature of 375℃, the conversion of $CuCl_2$ is approximately 70%. If temperature is increased to 425℃, half the amount of steam would be required (SCR 10:1) to attain the same conversion. This indicates that the SCR required to achieve the equivalent conversion decreases with increased reactor temperature at a constant pressure.

Table 3-4: $CuCl_2$ conversion comparison at different reactor temperatures

Temperature	Steam to Copper Ratio	$CuCl_2$ Conversion
375 ℃	20:1	70 %
400 ℃	15:1	71.7 %
425 ℃	10:1	71.4 %

The temperature–SCR trend is more complex when one follows Cu_2OCl_2 generation (Fig. (3-12)). At temperatures greater than or equal to 400℃, Cu_2OCl_2 production drops, an unexpected result based on the increase in $CuCl_2$ conversion. This can in part be attributed to CuO production. There is an increase in CuO at temperatures above 400℃, suggesting that the decrease in Cu_2OCl_2 was associated with the decomposition of Cu_2OCl_2 to CuO (Eq. (3-2)) [13, 25].

The Cu_2OCl_2 amount initially increases with temperature to reach a maximum, then decreases with subsequent increase in temperature. The temperature for this maximum

Cu_2OCl_2 concentration, shifts with SCR. As SCR increases, the maximum concentration is observed at a lower temperature compared to lower SCRs. Recalling that there are multiple potential products depending on the Gibbs energy, the increase in the steam inlet feed (from 1 kmol to 20 kmol) impacts the decomposition of Cu_2OCl_2 by driving other gas phase reactions and potentially limits the decomposition. Additional research on Cu_2OCl_2 decomposition with steam injection would provide important new insights into this process.

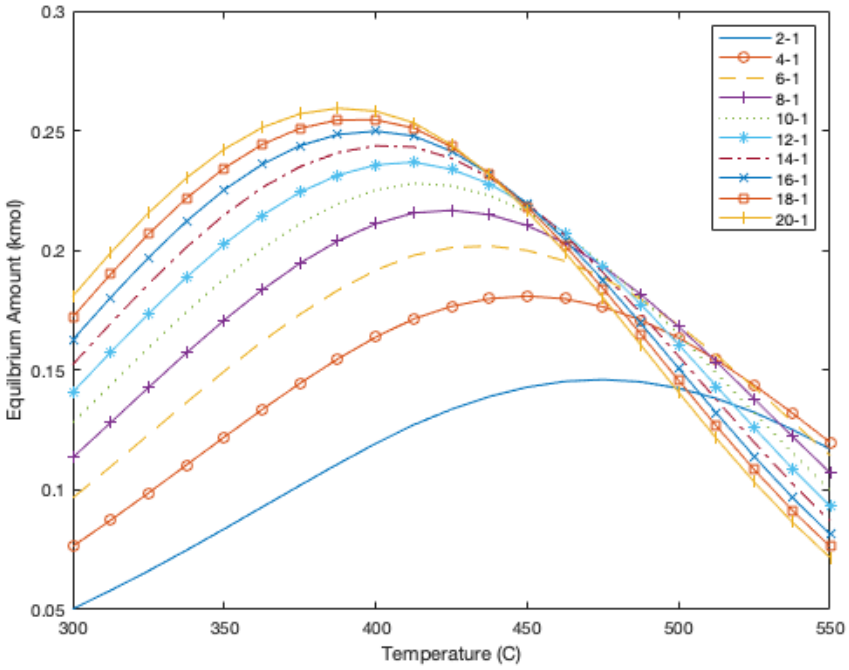

Figure 3-12: Equilibrium amount of Cu_2OCl_2 as a function of temperature at a constant P = 1 bar and varying SCR.

As previously stated, the Cl_2 generation provides insight on the influence of $CuCl_2$ decomposition on the total solid conversion. From Figure (3-13), Cl_2 increases with temperature, reaching a maximum at approximately 500°C. This indicates that the conversion of $CuCl_2$ at higher temperatures could be associated with the $CuCl_2$ decomposition reaction, which is not desired (Eq. (3-1)). This is further supported by Figure

(3-11), where more Cl_2 is generated at higher temperatures. Overall, higher conversion of $CuCl_2$ is achieved at temperatures of above 400℃, however undesired side reactions begin to impact the overall solid conversion and desired product. An ideal hydrolysis reactor temperature range of 375 - 400℃ was identified and the remaining simulations for this chapter and numerical model were done at 375℃.

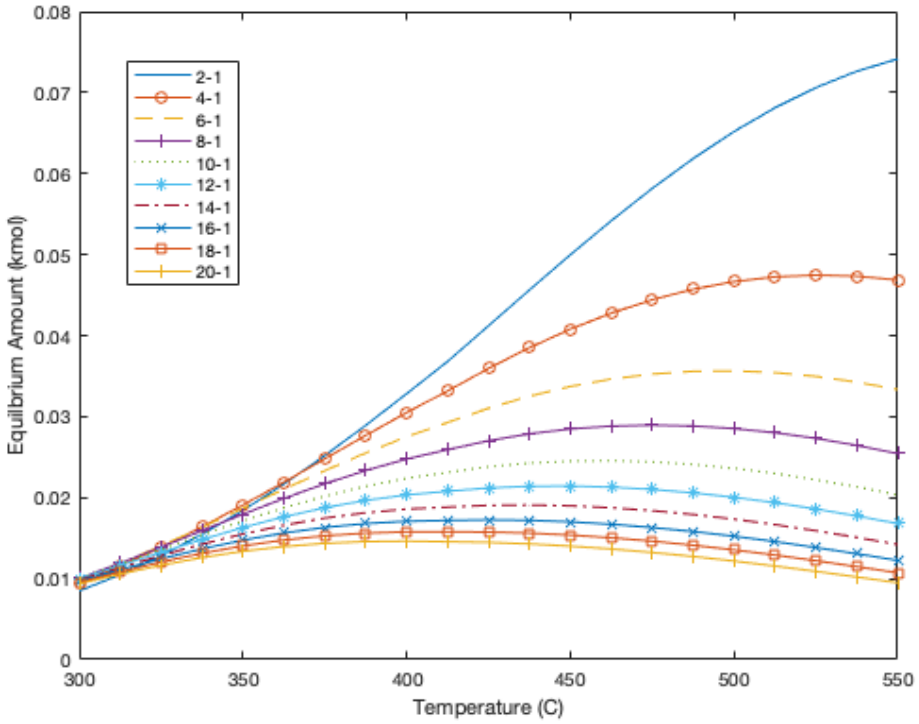

Figure 3-13: Cl_2 equilibrium amount as a function of temperature at a constant P =1 bar and varying SCR.

3.4.1.3 Steam to Copper Ratio

The SCR predictions were compared with experimental work of Singh et al. [13], in Table (3-5). The simulations and experiments both show an increase in $CuCl_2$ conversion with increased steam ratio. The higher values from the simulation are not unexpected as the maximum theoretical conversion may not have been achieved in experiments due to the

reaction time and transport phenomena. The conversion of $CuCl_2$ in simulations includes all possible conversion associated with side reactions, such as $CuCl_2$ decomposition, resulting in higher overall conversion values. Singh et al. [13] indicates the $CuCl_2$ decomposition was unlikely due to conditions of experiment. Despite the slight variation in conversion, the overall trends were the same.

Table 3-5: Conversion data with respect to steam to copper ratio variation.

Data Source	Reactor Temperature	Steam To Copper Ratio	Conversion %
Simulation Data	400	11:1	66%
		17:1	74%
Singh et al. [13]	400	11:1	45%
		17:1	65%

Based on the simulation results and the desire to decrease the steam consumption, a SCR of 10:1 was using for the remaining simulations. Table (3-6) outlines operating conditions (temperature, pressure, and SCR) used in the remaining simulations.

Table 3-6: Operating conditions from equilibrium simulations used in subsequent studies.

Parameter	Value
Temperature	375 ℃
Pressure	1 bar
Total Steam added	10 kmol for 1 kmol of $CuCl_2$

3.4.2 Multi-injection MBR Simulations

3.4.2.1 Reactors in Series

The results of three reactors in series with fresh steam injected at each inlet are summarized in Table (3-7). The conversion of $CuCl_2$ at a 10:1 SCR was 66%, a 17% increase compared to the single reactor simulations at the same temperature, pressure, and

total steam (Table (3-8)). To achieve the 66% conversion in a single reactor, a SCR between 16:1 - 17:1 would be required.

Table 3-7: Results of three reactors in series.

Iteration	Inlet $CuCl_2$ (kmol)	Cu_2OCl_2 Generated (kmol)	HCl Generated (kmol)	Inlet Steam (kmol)	Steam to Solid Ratio
1	1	0.160	0.407	5	5:1
2	0.567	0.209	0.140	2.52	3:1
3	0.432	0.242	0.103	2.48	3.1:1
FINAL	**0.338**	**0.242**	**0.65**	**10**	**-**

Table 3-8: Reactor in series $CuCl_2$ conversion comparison to single reactor conversion.

Configuration	Total Steam Input	$CuCl_2$ Conversion
Three reactors in series	10 kmol	66%
Single reactor	10 kmol	56.5%

With respect to undesired by-products, the total amount of Cl_2 generated after the three reactors in series was the same as the single reactor configuration. This indicated that the increase in $CuCl_2$ conversion for the reactors in series configuration was mainly associated with the hydrolysis reaction. Furthermore, CuO production indicated a minimal change (<2%) compared to that produced in the single reactor, demonstrating that the Cu_2OCl_2 decomposition reaction is not enhanced within this design scheme.

In general, these findings indicated the potential of reactors in series for MBR condition in the hydrolysis step, as side reactions and undesired by-product products were mitigated, along with the improved conversion and steam requirement reduction.

3.4.2.2 Gas Recirculation

The results for the outlet gas recirculation were obtained using the ideal operating conditions from Table (3-6). “Fresh” steam was added to maintain a steam input of 10 kmol

for each recirculation, along with fresh solid $CuCl_2$ feed (1 kmol). Table (3-9) shows the results of the gas stream recirculation into a single reactor design. After four iterations, there was no change in Cu_2OCl_2 and HCl production, and no increase in $CuCl_2$ conversion. This implied that the system would need to introduce a fresh stream of 10 kmol after the fourth recirculation of the high HCl concentrated outlet gas stream to offset equilibrium. This reintroduction of new steam would also be essential for the progression of the Cu-Cl cycle as the HCl accumulated over each iteration would be required for the electrolysis stage.

Table 3-9: Results of four iterations of gas stream recirculation

Iteration	**$CuCl_2$ Conversion (%)**	**Cu_2OCl_2 Generated (kmol)**	**HCl Generated (kmol)**	**Inlet Fresh Steam (kmol)**	**Inlet O_2 (kmol)**	**Inlet Cl_2 (kmol)**
1	56.5	0.211	0.561	10	-	-
2	40.3	0.147	0.911	0.280	0.016	0.020
3	32.2	0.114	1.172	0.175	0.020	0.057
4	27.4	0.095	1.385	0.058	0.021	0.094
TOTAL	**-**	**0.567**	**1.385**	**10.51**	**0.021**	**0.131**

Overall, for a 4.2% increase in steam consumption and only a fresh feed requirement after four recirculation, more than double the amount of desired products (Cu_2OCl_2 and HCl) were accumulated compared to a single reactor with no recirculation and the MBR model. However, the conversion of 1 kmol $CuCl_2$ decreases after each recirculation, resulting a significant portion of the $CuCl_2$ entering subsequent reactors not being converted. Thus, the maximum conversion potential of $CuCl_2$ was inhibited in each recirculation due to the increasingly concentrated HCl gas stream. As the exiting solid streams enters the next stage after each iteration, there will theoretically be more

unconverted $CuCl_2$ compared to the desired Cu_2OCl_2. This is not ideal as it could impede Thermolysis reaction progression and reduce overall process efficiencies and hydrogen yields.

To improve the conversion of $CuCl_2$ based on the results of the gas recycle, the reactor in series configuration, (ii), was combined with gas recirculation. In this scenario, the gas stream outlet was the inlet to the subsequent iteration (reactor). A potential issue of this reactor configuration was that the components reached equilibrium in the first reactor and further conversion would not occur in the additional reactor sequence. To mitigate conversion issues, fresh steam was added the gas stream to maintain the 10 kmol of steam in each reactor in series.

Table (3-10) demonstrates the results for this scenario, with conversion of $CuCl_2$ decreasing after three iterations (i.e., three reactors in series). The amount of products generated remained essentially the same. This indicated that the components were still in equilibrium as they moved into the next reactor and the addition of fresh steam was insufficient to shift equilibrium.

Table 3-10: Results of three reactors in series with gas recirculation

Iteration	**Inlet Unreacted $CuCl_2$ (kmol)**	**Cu_2OCl_2 Generated (kmol)**	**HCl Generated (kmol)**	**Inlet Fresh Steam (kmol)**	**Inlet O_2 (kmol)**	**Inlet Cl_2 (kmol)**
1	1	0.211	0.561	10	-	-
2	0.435	0.077	0.746	0.280	0.016	0.020
3	0.229	0.037	0.834	0	0.018	0.036
TOTAL	**-**	**0.344**	**0.879**	**10.28**	**0.019**	**0.046**

Comparing all components, the same decrease was observed, excluding steam in which the amount increased. This may indicate that a reverse reaction occurred. At this simulation

condition, the results indicate that this is not a viable option to improve conversion or steam consumption. However, it did lead to future consideration of a splitter scenario for the outlet gas stream as a potential to further shift equilibrium, similar to that presented by Finney et al. [26].

Overall, while the gas recirculation design requires additional research, the reactors in series configuration for multi-injection MBR behaviour presented encouraging potential to enhance $CuCl_2$ conversion within the hydrolysis reaction. When considering the reactors in series and the outlet gas recirculation scenarios, fast reactions in the gas phase may not be captured within the equilibrium trends. Therefore, further investigation is recommended, specifically with respect to the integration of reaction rate and reaction kinetics in the reactors in series design for more realistic predictive modelling.

3.5 Conclusions

This chapter analyzed three reactor configurations within the hydrolysis stage of the Cu-Cl cycle. Through the single reactor model, various temperature, pressure, and steam to copper ratio scenarios with respect to $CuCl_2$ conversion, progression of side reactions and by-product generation were examined. With respect to reactor pressure, decreasing reactor pressure increased solid conversion and mitigated side reaction progression. Additionally, similar conversion could be obtained at lower SCR when pressure was decreased. Through investigation of temperature and SCR, a proportional relationship with $CuCl_2$ conversion was observed - an increased temperature and increased SCR led to higher $CuCl_2$ conversion. The ideal hydrolysis reactor for the remaining simulations and future

MBR numerical modelling were identified as pressure equal to 1 bar, temperature of 375℃, and SCR of 10:1.

Simulation of the multi-injection MBR at these conditions through reactors in series demonstrated an increase of 17% in the overall conversion of $CuCl_2$ when compared to a single reactor at the same conditions. There was an observable decrease in undesired side product generation through the Cl_2 and CuO data, further indicating that the $CuCl_2$ conversion was associated with the hydrolysis reaction. This suggested that MBR is a viable configuration to improve conversion and side reaction mitigation, all while decreasing steam consumption.

In terms of gas stream recirculation, increased product generation was observed when introduced to a single reactor. This configuration was only viable after four iterations, as the conversion of $CuCl_2$ was negligible, which implied that a complete fresh stream of steam would be required. In an effort to improve the conversion of $CuCl_2$, the reactors in series approach was presented with the gas recirculation, with fresh steam only introduced to maintain the steam requirement of each reactor. This was found to be insufficient in shifting the equilibrium for further conversion of $CuCl_2$ and limited desired product generation was observed. Thus, the outlet gas recirculation was not an ideal configuration without the concentration reduction of HCl for total process integration.

Overall, these results have useful potential for conversion improvement within the hydrolysis process with respect to operating condition variation. The findings also highlight the potential for the MBR design within the hydrolysis stage and identified ideal reactor operating conditions for the introduction of reaction kinetics in the numerical model.

References

[1] V. N. Daggupati, G. F. Naterer, and K. S. Gabriel, "Diffusion of gaseous products through a particle surface layer in a fluidized bed reactor," *Int. J. Heat Mass Transf.*, vol. 53, no. 11–12, pp. 2449–2458, 2010.

[2] V. N. Daggupati, G. F. Naterer, K. S. Gabriel, R. J. Gravelsins, and Z. L. Wang, "Solid particle decomposition and hydrolysis reaction kinetics in Cu-Cl thermochemical hydrogen production," *Int. J. Hydrogen Energy*, vol. 35, no. 10, pp. 4877–4882, 2010.

[3] K. Pope, V. N. Daggupati, G. F. Naterer, and K. S. Gabriel, "Experimental study of gaseous effluent and solid conversion in a fluidized bed hydrolysis reactor for hydrogen production," *Int. J. Hydrogen Energy*, vol. 37, no. 21, pp. 16397–16401, 2012.

[4] A. Farsi, I. Dincer, and G. F. Naterer, "Second law analysis of $CuCl_2$ hydrolysis reaction in the Cu–Cl thermochemical cycle of hydrogen production," *Energy*, vol. 202, p. 117721, 2020.

[5] M. Ferrandon, V. Daggupati, Z. Wang, G. Naterer, and L. Trevani, "Using XANES to obtain mechanistic information for the hydrolysis of $CuCl_2$ and the decomposition of Cu2OCl2 in the thermochemical Cu-Cl cycle for H2 production," *J. Therm. Anal. Calorim.*, vol. 119, no. 2, pp. 975–982, 2015.

[6] D. Thomas, N. A. Baveja, K. T. Shenoy, and J. B. Joshi, "Experimental Study on the Mechanism and Kinetics of CuCl2 Hydrolysis Reaction of the Cu-Cl Thermochemical Cycle in a Fluidized Bed Reactor," *Ind. Eng. Chem. Res.*, vol. 59, no. 26, pp. 12028–12037, 2020.

[7] G. D. Marin, Z. Wang, G. F. Naterer, and K. Gabriel, "Byproducts and reaction pathways for integration of the Cu-Cl cycle of hydrogen production," *Int. J. Hydrogen Energy*, vol. 36, no. 21, pp. 13414–13424, 2011.

[8] D. H. Lee, H. Yang, R. Yan, and D. T. Liang, "Prediction of gaseous products from biomass pyrolysis through combined kinetic and thermodynamic simulations," *Fuel*, vol. 86, no. 3, pp. 410–417, 2007.

[9] D.-J. Kim, G.-G. Lee, S. W. Kim, and H. P. Kim, "The use of Thermodynamics and Phase Equilibria for Prediction of the Behavior of High Temperature Corrosion of Alloy 617 in Impure Helium Environment," *Corros. Sci. Technol.*, vol. 9, no. 4, pp. 164–170, 2010.

[10] S. Wang, L. Song, and X. Jiang, “Prediction of gaseous products from Dachengzi oil shale pyrolysis through combined kinetic and thermodynamic simulations,” *J. Therm. Anal. Calorim.*, vol. 134, no. 2, pp. 1129–1144, 2018.

[11] P. Kobylin, L. Furta, and D. Vilaev, “Equilibrium Model - Description of Menus and Options,” *Metso: Outotec*, p. 57, 2020, [Online]. Available: https://www.mogroup.com/globalassets/portfolio/hsc-chemistry/13-equilibrium-module.pdf.

[12] G. F. Naterer, I. Dincer, and C. Zamfirescu, *Hydrogen production from nuclear energy*, vol. 9781447149. 2013.

[13] R. V. Singh *et al.*, “Investigations on the hydrolysis step of copper-chlorine thermochemical cycle for hydrogen production,” *Int. J. Energy Res.*, vol. 44, no. 4, pp. 2845–2863, 2020.

[14] T. Kekesi, K. Mimura, and M. Isshiki, “Copper Extraction from Chloride Solutions by Evaporation and Reduction with Hydrogen,” *Mater. Trans. JIM*, vol. 36, no. 5, pp. 649–658, 1995.

[15] C. Zamfirescu, I. Dincer, and G. F. Naterer, “Thermophysical properties of copper compounds in copper-chlorine thermochemical water splitting cycles,” *Int. J. Hydrogen Energy*, vol. 35, no. 10, pp. 4839–4852, 2010.

[16] K. Kawashima *et al.*, “Antiferromagnetic ordering in Cu2OCl2 studied by the muon spin rotation/relaxation technique,” *J. Phys. Condens. Matter*, vol. 19, no. 14, pp. 2–7, 2007.

[17] T. J. Parry, “I. Thermodynamics and Magnetism of Cu2OCl2 II. Repairs to Microcalorimeter,” 2008.

[18] S. H. Fogler, *Fogler - Elements of Chemical Reaction Engineering 5th Edition*. Pearson, 2016.

[19] A. Farsi, C. Zamfirescu, I. Dincer, and G. F. Naterer, “Thermodynamic assessment of a lab-scale experimental copper-chlorine cycle for sustainable hydrogen production,” *Int. J. Hydrogen Energy*, vol. 44, no. 33, pp. 17595–17610, 2019.

[20] V. N. Daggupati, G. F. Naterer, K. S. Gabriel, R. J. Gravelsins, and Z. L. Wang, “Equilibrium conversion in Cu-Cl cycle multiphase processes of hydrogen production,” *Thermochim. Acta*, vol. 496, no. 1–2, pp. 117–123, 2009 .

[21] M. S. Ferrandon, M. A. Lewis, F. Alvarez, and E. Shafirovich, “Hydrolysis of CuCl2 in the Cu-Cl thermochemical cycle for hydrogen production: Experimental

studies using a spray reactor with an ultrasonic atomizer," *Int. J. Hydrogen Energy*, vol. 35, no. 5, pp. 1895–1904, 2010.

[22] M. A. Lewis, M. Serban, and J. Basco, "Hydrogen Production at 550 C using a low temperature thermochemical cycle," in *Proceedings of the OECD/NEA Meeting*, 2003, pp. 145–156.

[23] Z. Hongjun, S. Mingliang, W. Huixin, L. Zeji, and J. Hongbo, "Modeling and simulation of moving bed reactor for catalytic naphtha reforming," *Pet. Sci. Technol.*, vol. 28, no. 7, pp. 667–676, 2010.

[24] A. Fazeli, S. Fatemi, M. Mahdavian, and A. Ghaee, "Mathematical modeling of an industrial naphtha reformer with three adiabatic reactors in series," *Iran. J. Chem. Chem. Eng.*, vol. 28, no. 3, pp. 97–102, 2009.

[25] J. Ancheyta-Juárez, E. Villafuerte-Macías, L. Díaz-García, and E. González-Arredondo, "Modeling and simulation of four catalytic reactors in series for naphtha reforming," *Energy and Fuels*, vol. 15, no. 4, pp. 887–893, 2001.

[26] L. Finney, K. Gabriel, and K. Pope, "A novel fluidized bed suitable for the hydrolysis step in CuCl hydrogen production cycle," *Int. J. Hydrogen Energy*, vol. 47, no. 71, pp. 30378–30390, 2022.

Chapter 4 – Kinetic Model of Multi-Injection Moving Bed Reactor with Downdraft

A modified version of this chapter will be submitted for journal publication. It has been proofread and revised by Dr. Kevin Pope, Dr. Greg F. Naterer and Dr. Kelly A. Hawboldt.

Abstract

This chapter presents numerical modelling of the hydrolysis stage of the copper-chlorine (Cu-Cl) thermochemical cycle using a downdraft multi-injection moving bed reactor (MBR), modelled through reactors in series. In the previous chapter, an equilibrium approach was used to predict gas and solid compositions as a function of temperature, partial pressure, and steam to copper ratio (SCR) in a MBR with a series of sequential steam injection points along the total reactor length. The work showed potential improvement in $CuCl_2$ conversion and a reduction in the SCR using this configuration. In this chapter, the equilibrium approach is replaced with hydrolysis step reaction rate equations. The multi-injection MBR is modelled through reactor in series and combined with reaction rates based on the shrinking core model (SCM). The reactors in series, are modelled as isothermal and isobaric plug flow reactors. The model showed an approximately 23% increase in $CuCl_2$ conversion for the multi-injection MBR when compared to a single reactor design and 8% increases when compared to experimental results of a fluidized bed reactor at the same conditions.

Variations of reactor design parameters, including reactor volume, injection point location, and amount of steam injection, were conducted to study the maximum achievable solid conversion within the MBR design. Through the analysis, four combinations of

injection spacing, and two combinations of steam injection amounts presented solid conversion higher than the base condition. A combination of the two best configurations presented a further 8.8% increase in total $CuCl_2$ conversion. From an asymptotic analysis, a maximum conversion is obtained after a certain number of increasing injection points. This relationship held true regardless of reactor conditions. Overall, these analyses highlighted the importance of reactor design conditions to achieve the best reactor yields for the desired scale of solid conversion.

4.1 Introduction

Reiterated throughout this thesis, hydrogen presents good opportunities to decarbonize energy systems, with the Cu-Cl thermochemical water splitting cycle (TWSC) as a low-temperature, high conversion, and environmentally friendly hydrogen production alternative. However, it is not without challenges, specifically with respect to the high steam requirement of hydrolysis step – decreasing overall process efficiencies [1]. This chapter investigates kinetic modeling of the downdraft multi-injection moving bed reactors (MBR) in the hydrolysis stage of the Copper-Chlorine (Cu-Cl) thermochemical cycle to increase conversion and improve steam consumption. Prior work in literature has demonstrated that generation of reaction kinetic models based on phase equilibrium predictions show accurate results when compared to measured data [2, 3]. The previous chapter presented an equilibrium approach to simulate reaction progression and phase behavior. The results indicated conceivable improvement in $CuCl_2$ conversion, as well as a reduction in the steam to copper ratio (SCR) through an MBR with multiple steam injection points (i.e., multi-injection MBR). Through the literature review, Singh et al. [4]

and Haseli et al. [5] both concluded that the shrinking core model (SCM) presented more accurate prediction to experimental results, advocating its use within this work. In this chapter, the phase equilibrium model generated in Chapter 3 is improved by replacing the Gibbs Free Energy minimization approach with reaction rate(s) represented by the SCM.

In the first part of the study, a SCM model for a single reactor is developed through MatLAB and compares past work by Daggupati et al. [6], Ferrandon et al. [7], and Thomas et al. [8]. Daggupati et al. [6] developed a numerical model based on experimental results from Ferrandon et al. [7] for a packed bed system. Thomas et al. [8] performed experimental studies within a fluidized bed at lower reactor temperatures (300 – 375℃) and steam mole fractions. The purpose of this research was to quantify reaction rate constants and identify ideal validation data for the kinetic model.

There are several studies that have examined the reaction kinetics of the hydrolysis reaction. Ferrandon et al. [7] performed experiments using a packed bed reactor for the hydrolysis stage at higher steam to copper ratios (27:1 - 66:1). Daggupati et al. [9] and Naterer et al. [10] referenced this experimental work, [7], in their models and literature review. Singh et al. [4] performed experimental tests for fixed bed hydrolysis, where they investigated various particle sizes (0.02 - 0.045 μm) and reactor temperatures (370 – 400℃) to derive kinetic parameters, rate constants and activation energy.

While these are all suitable experimental tests to obtain reaction rate data, when creating an accurate numerical model, it is important to utilize experimental data that reflects the operating conditions to be studied. This is especially important for the novel MBR design, as there are no known experimental results for this design in Cu-Cl cycle literature. Past

work has resulted in different reaction rates expressions depending on the experimental range of temperature, pressure and SCRs studied, as presented in Chapter 2. This presents difficulty in generating a single reaction rate constant that accurately reflects the hydrolysis reaction over the wide range of possible operating conditions.

In the second part of this work, based on the developed rate constants from the selected published reaction rate data, a single plug flow reactor (PFR) was modelled using MatLAB software. Plug flow is a common assumption within MBR models to simplify model equations. Wolff et al. [11] utilized a plug flow for solid movement of alumina particles within a novel circulating crossflow moving bed reactor system. Arabi et al. [12] simulated the reduction of porous iron ore pellets to sponge iron in a countercurrent MBR model with plug flow assumption. Arce et al. [13] also assumed gas and solid phase plug flow for a parametric study of a non-catalytic heterogenous MBR. A PFR numerical model for a single reactor was first tested using published experimental data to ensure the model was accurate. With the single reactor model validated, the multi-injection downdraft MBR condition was developed through the reactors in series approached presented in Chapter 3.

There are several past studies that utilized reactors in series to mimic multi-injection MBR conditions, specifically within catalytic naphtha reforming processes. Hongjun et al. [14] utilized four reactors in series to generate a kinetic model for continuous catalysis reforming processes. The results demonstrated good agreement of compositions at the exit of the final reactor between the simulated values and the plant data. Karimi et al. [15] utilized four adiabatic reactors in series to simulate an MBR for endothermic naphtha reforming. This model showed a reduction in operational costs as well as enhancement in plant net profit when compared to non-optimized and conventional models.

A sensitivity analyses and optimization of reactor design parameters was also performed. Zang et al. [16] used a parametric sensitivity analysis (PSA) of chemical reaction systems and showed small changes in critical operating parameters can have large effects. It provided insight to the theoretical assessment of thermal runaway. Kumar et al. [17] performed a sensitivity analysis with respect to reaction kinetics of biomass gasification to optimize gasifier temperatures and syngas composition. The sensitivity analysis established the optimized kinetic parameters for the homogenous reactions. Therefore, performing a sensitivity analysis on MBR design in this work can provide insight to each reactor scenario and its limitations.

Overall, in this chapter, plug flow reactors in series under isobaric and isothermal conditions are numerically modeled to investigate hydrolysis reaction progression and $CuCl_2$ conversion for multi-injection downdraft MBR behaviour. The relationship between SCR and $CuCl_2$ conversion is used to further assess the MBR design. The conversion of $CuCl_2$ with respect to the reactor residence time and reactor length are monitored. Variable flow rates, steam to copper ratios and reactor dimensions are investigated to identify their impact on the hydrolysis reaction process. A sensitivity analysis with respect to reactor volume, injection spacing and steam injection amount, will be implemented to determine the maximum conversion at a specific reactor condition. Asymptotic conditions of solid conversion in terms of number of injection sites along the length will also be assessed for a comprehensive examination of conversion limitations. Varying injection parameters, such as initial SCR, will provide further insight to reactor progression at various conditions. Overall, the numerical modelling and design analysis will inform optimal reactor design conditions and further improve bed reactor design for the hydrolysis process.

4.2 Model Development

The hydrolysis reaction is a non-catalytic gas-solid endothermic reaction step within the Cu-Cl cycle (Eq. (2-1)). Chapter 3 provided insight to the feasibility of the novel multi-injection MBR design within the hydrolysis reaction through equilibrium simulations. Introduction of reaction kinetics will present enhanced predictive data for this configuration and supply further insight to design constraints. Numerical modelling of the MBR permits establishing additional reactor conditions (i.e., reactor size, reaction time, component flowrates), that were not introduced in the previous phase equilibrium simulations. Figures (2-5) and (2-6) outline the reactor(s) configurations for the single and sequential reactor systems. Three scenarios were used to study the novel system:

(i) Numerical modeling of reaction rate equations and SCM for the hydrolysis stage in a single reactor,

(ii) Numerical modeling of multi-injection MBR to present conversion as a function of reactor length. This is generated in two parts, (i) single PFR validation and (ii) PFR in series to simulate MBR behaviour,

(iii) Sensitivity and asymptotic analysis of the MBR model to assess limitations of the MBR condition.

To compare $CuCl_2$ conversion in the single and sequential scenarios, the same total amount of steam was used in both reactor configurations. This is achieved by setting a base inlet molar flow rate and overall SCR to determine the total steam obtainable for the reactor models. All available steam will be provided into the single reactor scenario, while in the sequential reactors, the steam is distributed throughout all reactors, to simulate multiple

injection sites. Completion of the numerical models will allow for the sensitivity and asymptotic analysis of the MBR design.

4.2.1 Reaction Rate Models

The model considers the endothermic hydrolysis reaction, represented by Equation (2-1). It is assumed that the decomposition of $CuCl_2$ and other side reactions in hydrolysis occur at temperatures higher than 400°C based on the results from Chapter 3, allowing for side reactions to be neglected at this phase. It is also assumed, based on the assumptions of SCM established in the literature review, that the operation will run under steady-state conditions with a constant spherical particle size. The numerical model is generated in two parts. Firstly, the reaction kinetics are modelled in a single reactor to investigate past experimental data for suitable reaction rate constant generation. Evolving from the reactor kinetic model, with plug flow assumptions, the novel multi-injection downdraft MBR model is generated through a series of PFRs to realistically capture hydrolysis reaction behaviour.

4.2.1.1 Reactor Kinetic Model

For the SCM model, reaction rate can be represented through various equations. For this preliminary model, the surface reaction rate kinetics expression for the gas phase can be written in terms of partial pressure as presented in Equation (4-1) [6],

$$r_{H_2O} = k_1 \left(p_{H_2O} - \frac{p_{HCl}^2}{K_1} \right) \tag{4-1}$$

where K_1 is the equilibrium constant for the hydrolysis reaction, obtained from the Gibbs free energy (via the heat of reaction), and k_1 is the reaction rate constant. The partial

pressure of the gaseous components can be written in terms of conversion (x) and SCR (S) as seen in Equations (4-2) and (4-3) [6].

$$p_{H_2O} = \frac{s - x}{s + x} P \tag{4-2}$$

$$p_{HCl} = \frac{2x}{s + x} P \tag{4-3}$$

The chemical reaction control equation from the SCM is represented by Equation (4-4), with Equation (4-5) indicating complete conversion of $CuCl_2$ through the relationship of decreasing solid radius (r_c) and fractional conversion [18].

$$\frac{dr_c}{dt} = \frac{-ak_1 C_b}{\rho'_A} \tag{4-4}$$

$$1 - \frac{r_c}{R_p} = 1 - (1 - x)^{1/3} \tag{4-5}$$

Solving Equation (4-5) for x and combining with Equations (4-1) and (4-4), generated the overall fractional conversion expression for $CuCl_2$ as an ordinary differential equation (ODE), represented by Equation (4-6).

$$\frac{dx}{dt} = \frac{3a(1 - x)^{2/3}}{R_P \rho'_A} k_1 \left[\left(\frac{s - x}{s + x} P \right) - \frac{1}{K_1} \left(\frac{2x}{s + x} P \right)^2 \right] \tag{4-6}$$

4.2.1.2 Downdraft Moving Bed Reactor Model

The model is based on reaction rate kinetic equations above (shrinking core model equations) and general plug flow equations. The mole balance for a plug flow reactor is defined by Equation (4-7) [19].

$$F_{i|V} - F_{i|V+\Delta V} + r_i \Delta V = 0 \tag{4-7}$$

Differentiating with respect to volume and combining with the volume of a cylinder, provides the change in specific molar flow rate with respect to the length of reactor (Equation (4-8)).

$$\frac{dF_i}{dL} = -\pi R^2 r_i \tag{4-8}$$

The reaction rate for the MBR model is based on past studies [7] as a function of gaseous reactant concentration and unreacted solid in the hydrolysis reaction, as presented in Equation (4-9).

$$r_{H_2O} = akC_A C_B \tag{4-9}$$

The concentration of H_2O is related through the ideal gas law and partial pressure in the bulk phase [6]. The concentration of $CuCl_2$ relates to the volumetric flowrate and molar flowrate of $CuCl_2$ within the reactor. These equations yield a set of differential equations for each species of the hydrolysis reaction which is solved numerically. Equations (4-10) and (4-11) are compare the results in terms of overall conversion.

$$n_A = n_{A,i} - x n_{A,i} \tag{4-10}$$

$$X = \frac{n_i - n_o}{n_i} \tag{4-11}$$

4.2.1.3 Numerical Solution

The PFR model is created using a non-stiff ODE solver in MatLAB to solve the set of differential equations (Eq. (4-6) and (4-8)) for solid $CuCl_2$ conversion with respect to time within a single reactor configuration. From the isothermal and isobaric assumption, temperature and pressure remain constant at the inlet and outlet for both the gas and solid phases. Table (4-1) presents the initial conditions and constant boundary conditions for the model.

Table 4-1: Reactor conditions for single PFR model validation [8].

Variable	Value	Units
Reactor Temperature	300	℃
Reactor Pressure	1	bar
Reactor Length	1	m
Reactor Diameter	0.05	m
Steam mole fraction	0.5	%
Inlet Solid	0.0034	mol/s

The work from Daggupati et al. [6], Ferrandon et al. [7] and Thomas et al. [8] was used to investigate the reaction constants and initial model validation. Two comparisons of $CuCl_2$ conversion predictions were performed, (i) through the established SCM model from Daggupati et al. [6] and the experimental results of Ferrandon et al. [7], and (ii) though the experimental work of Thomas et al. [8]. It is essential that the experimental validation data has operating conditions within the desired range for this work. The SCR range, temperature, and pressure all impact reaction time, which in turn influences the reaction rate constant for the hydrolysis phase. This will further investigate the accuracy of the predictive results when compared to experimental data and identify potential gaps in literature with respect to reaction constant generation. Based on the PFR model, the

experimental conditions and results of Thomas et al. [8] are utilized for the modeling of the MBR condition through the sequential reactor approach. Their experimental work within a fluidized bed investigated various ranges of SCR and temperatures, which suits the desired operating temperature, pressure and SCR established in Chapter 3. Utilizing their experimental data, a reaction rate constant was calculated, ($k = 0.0006112\ m^3/mol\text{-}s$) and implemented into the model at the same reactor dimensions, as presented in Table (4-1).

The multi-injection reactor configuration is modelled through the same iterative approach as presented in Chapter 3, where the outlet flowrates of each species from the previous reactor are set as the inlet parameters for the next reactor. All reactor operating conditions and dimensions remain constant, with the individual reactor length representing the spacing between each injection site, as presented in Figure (4-1). At each sequential reactor, the inlet steam amount will change to account for the additional injected steam. Three reactors in series will be utilized for this work to compare the reaction model to the results of the initial multi-injection MBR model from the phase equilibrium simulations. This will provide an understanding of the importance of reaction kinetics to the reaction modeling and reactor design. Additionally, there are various ways in which the steam can be divided along the injection points. The total amount of available steam is determined through the molar SCR and inlet molar flowrate of $CuCl_2$. For the base model, the total available steam is divided based on halve, 50% of the total steam enters the first reactor, 50% of the remaining fresh steam enters the second reactor, and all remaining fresh steam enters the third. At the end of the sequential reactors, the total amount of steam injected will be the same as in a single injection reactor.

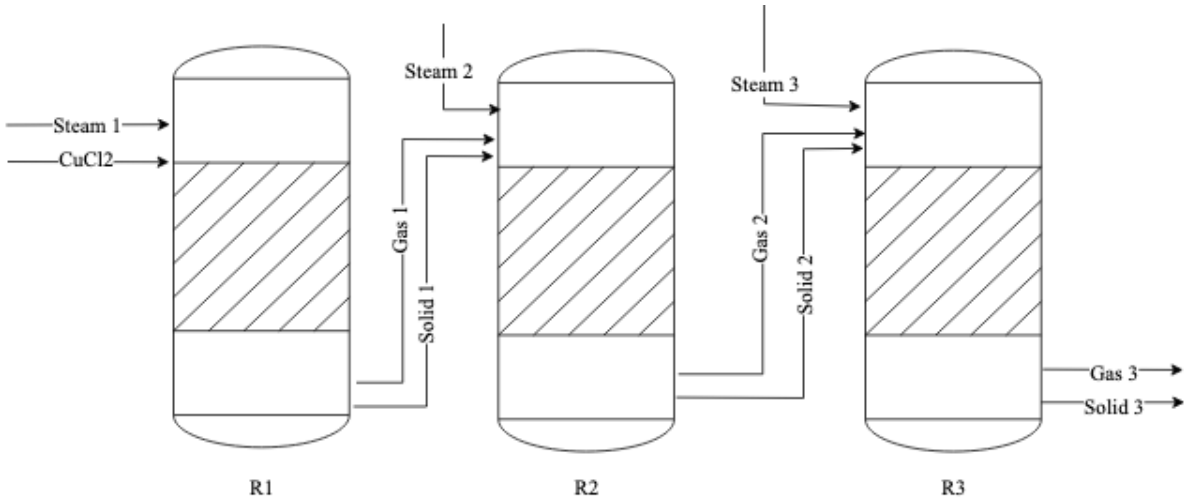

Figure 4-1: Plug flow reactors in series configuration to simulate multi-injection downdraft MBR behaviour. Each single reactor length represents the injection spacing along total reactor length.

4.2.2 Sensitivity and Asymptotic Analysis

Understanding the influence of different variables is important in establishing feasible reactor configurations and maximizing conversion. Five analyses are performed for the multi-injection MBR model, four sensitivity and one asymptotic. Each sensitivity analysis is compared to the results of the base reactor in series (MBR) model to identify potential improvement in solid conversion and reactor configuration optimization. Table (4-2) demonstrates the variations of the reaction conditions for each sensitivity analysis. While the asymptotic analysis allowed for the examination of various scenarios, both realistic and unrealistic, to identify the limiting behaviour of the MBR reactor design.

The first analysis is performed with respect to the reactor volume, specifically investigating the impact of total reactor length on solid conversion. The original model has a total reactor length with three injection sites equally spaced (i.e., length of each individual reactor in series). Two variations are performed: (i) double the total reactor length and (ii)

half of the total reactor length. All other parameters remain the same, as well as the condition of equally spaced injection points. In theory, the longer reactor length will provide an increase in reactor volume, increasing the solid conversion [20]. Analysis of the reactor diameter variation was not performed in this case, as based on the equation for the volume of a cylinder, the diameter would have similar effects on the reaction conversion.

The second analysis is through variations of injection point location (i.e., injection spacing). This is accomplished by changing the individual reactor lengths, or the distance between each injection point. The different reactor lengths could increase or decrease conversion depending on the entering steam and unconverted solid, allowing for more or less time at that reaction condition. In this analysis, nine combinations (C# in Table (4-2)) of injection points are investigated over a total reactor length to identify the potential maximum achievable solid conversion.

The third sensitivity analysis considers the steam input at each injection. In this test, the total steam consumption over the three reactors remains the same, however the amount at each injection point varies (IA# in Table (4-2)). Varying steam inputs along the length of the reactor can suggest the sequence for total steam injection that provides the highest solid conversion. The reactor dimensions, SCR and inlet solid flowrate are maintained at the original conditions.

The two final analyses performed are, (i) a combination of the best conversion conditions from the injection spacing and injection amount to predict maximum achievable solid conversion, and (ii) the asymptotic analysis of the number of injections along the reactor length with respect to solid conversion. Different reactor conditions, such as SCR, are also manipulated to further identify the limiting behaviour of the reactor configuration.

Table 4-2: Sensitivity Analysis Parameters

Analysis	Total Reactor Length	Total Reactor Diameter	R1 Length	R2 Length	R3 Length	Injection 1 amount	Injection 2 amount	Injection 3 amount
Base	0.15	0.026	0.05	0.05	0.05	0.0168	0.0084	0.0084
L1	0.30	0.026	0.1	0.1	0.1	0.0168	0.0084	0.0084
L2	0.075	0.026	0.025	0.025	0.025	0.0168	0.0084	0.0084
C1	0.15	0.026	0.1	0.025	0.025	0.0168	0.0084	0.0084
C2	0.15	0.026	0.025	0.025	0.1	0.0168	0.0084	0.0084
C3	0.15	0.026	0.025	0.01	0.025	0.0168	0.0084	0.0084
C4	0.15	0.026	0.075	0.05	0.025	0.0168	0.0084	0.0084
C5	0.15	0.026	0.075	0.025	0.05	0.0168	0.0084	0.0084
C6	0.15	0.026	0.025	0.05	0.075	0.0168	0.0084	0.0084
C7	0.15	0.026	0.025	0.075	0.05	0.0168	0.0084	0.0084
C8	0.15	0.026	0.05	0.025	0.075	0.0168	0.0084	0.0084
C9	0.15	0.026	0.05	0.075	0.025	0.0168	0.0084	0.0084
IA1	0.15	0.026	0.05	0.05	0.05	0.0168	0.0126	0.0042
IA2	0.15	0.026	0.05	0.05	0.05	0.0202	0.0067	0.0067
IA3	0.15	0.026	0.05	0.05	0.05	0.0202	0.0101	0.0340
IA4	0.15	0.026	0.05	0.05	0.05	0.0134	0.0101	0.0101
IA5	0.15	0.026	0.05	0.05	0.05	0.0134	0.0151	0.0050

4.3 Results and Discussion

As stated, initial investigation of reaction rate equations and rate constants were performed through past work of Daggupati et al. [6], Ferrandon et al. [7] and Thomas et al. [8]. Figure (4-2a) compares $CuCl_2$ conversion of this work with [6] and [7]. Overall, good agreement is observed between this work and the model presented by Daggupati et al. [6]. For a longer reaction time, both models agree well with the experimental data of Ferrandon [7]. However, it should be noted, ideally the rate constant is derived where the rate is changing the most (i.e., steepest part of the curve). This is not the case here; the rate constant value was derived by fitting the model equations of [6] to the experimental data of [7], which as presented in Figure (4-2a), only demonstrates conversion for longer reaction times (time > 20 minutes). Therefore, more experimental work is required to verify the rate constant from [7].

Further examining the experimental conditions for the experiments of Ferrandon et al. [7], presented high SCR (22:1 – 68:1) compared to those desired for this model. Thus, the experimental data from Thomas et al. [8] was selected for reaction constant calculations as the experiments were performed within the desired MBR model conditions range (i.e., low SCR, temperature of 375℃ and pressure of 1 bar). Figure (4-2b) presents a comparison of the predictive model and the experimental data. The predictive results reflected good agreement with experimental data. However, again, there is limited available data for the total reaction progression. Investigating why this disparity occurred with a different set experimental data presented that past experimental conversion results have been presented in terms of the final solid conversion at a specific reaction time for multiple different

reaction conditions. Therefore, when conversion vs time plots are generated, they are presented as distinct points at certain times, and not capturing the complete reaction progression.

Overall, the model demonstrated the importance of utilizing validation data that is generated from similar operating conditions as those desired for the model. A rate constant derived at very high conversions means its application is limited to these conditions. There is limited experimental data within the hydrolysis Cu-Cl cycle literature that provides a comprehensive data set over the total reaction progression. This creates challenges when developing reaction kinetic predictive models, as presented in in Figure (4-2). This is a significant challenge in the generation of the multi-injection MBR model as there is no available experimental data for this reactor configuration. Through the limited application range, the experimental work from Thomas et al. [8] was selected based on the reactor operating conditions and better agreement between predictive and experimental data.

(a)

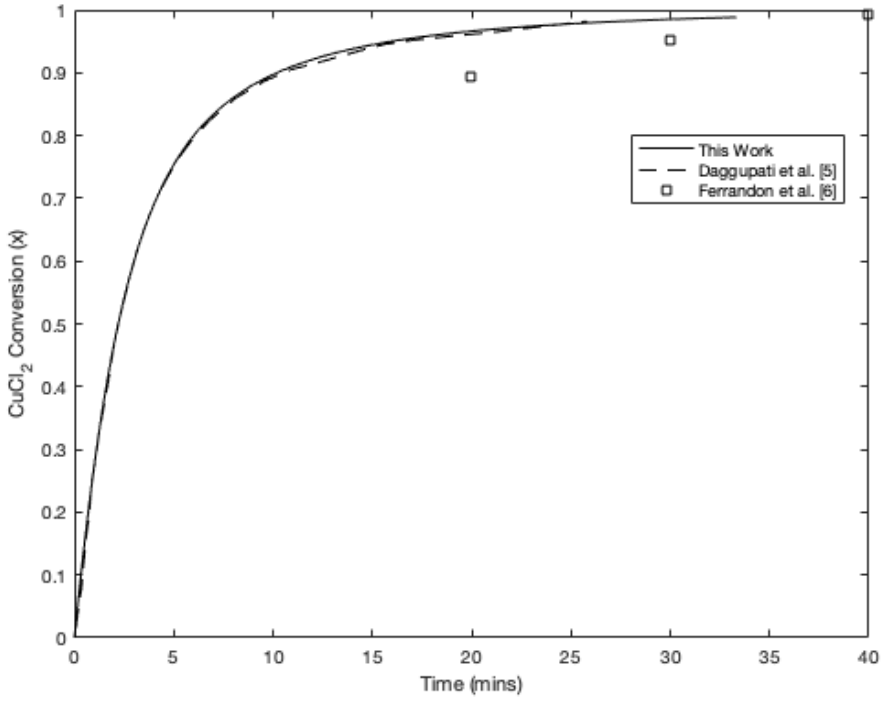

(b)

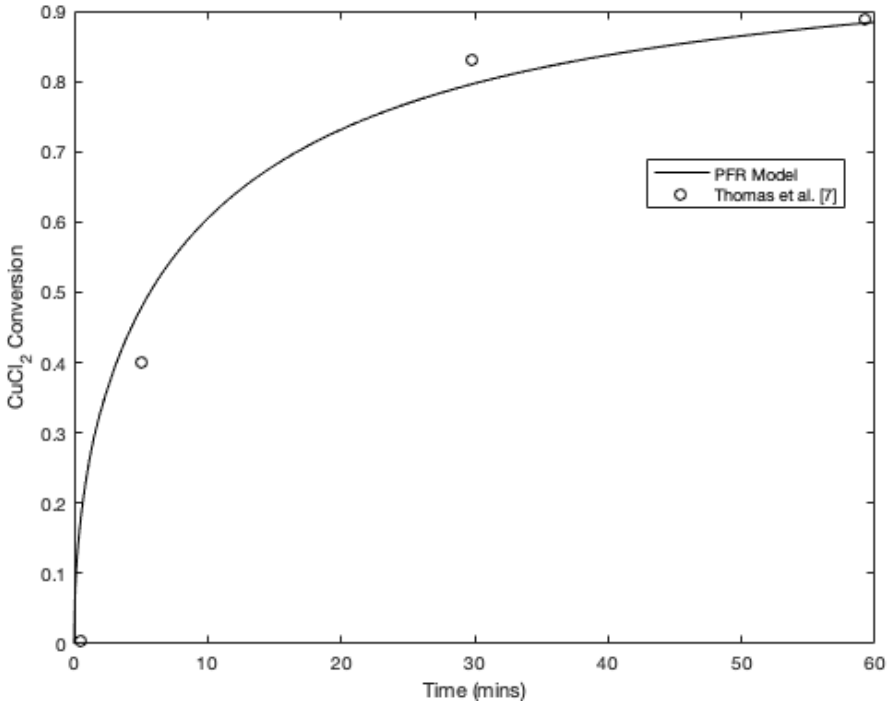

Figure 4-2: $CuCl_2$ conversion comparison between (a) SCM model in this work, model from Daggupati et al. [6] and experimental work of Ferrandon et al. [7]. (b) between model in this work and experimental results of Thomas et al. [8]

Table (4-3) presents a comparison of the single PFR model results and the experimental results from the validation data [8]. The experimental results of Thomas et al. [8] are utilized to generate reaction rate constants for this model, (0.0006112 m^3/mol-s).

Table 4-3: PFR model validation

Reference Work	**Operating Temperature (℃)**	**Maximum $CuCl_2$ conversion (%)**	**Reaction time (mins)**	**Steam mole fraction**
This work	300	88.3	57	0.5
	375	65	34	0.62
Thomas et al. [8]	300	88	60	0.5
	375	75	35	0.62

Similar conversion is achieved for the 300℃ and 0.5 steam mole fraction reactor conditions in the numerical model compared to a similar reaction time to the experimental results of Thomas et al. [8]. Further examination was also performed at a higher reaction temperature of 375℃ - the desired operating temperature for the MBR model established in the previous chapter. The experimental results were extrapolated for this temperature, as there was not a full data set presented at this condition within the reference material. A slightly lower solid conversion was achieved for the 375℃ case. This is anticipated as additional to reaction kinetics, experimental results are also influenced by transport phenomena, such as heat and mass transfer, which were not considered in the model. Furthermore, the limitation associated with the generated rate constant values and the partial data presented for the 375℃ experiment in the reference work could be cause for the deviation.

Additionally, from the phase equilibrium results in Chapter 3, at higher reactor temperatures, side reactions are more likely, specifically when considering the decomposition of $CuCl_2$. Thomas et al. [8] also concluded that at higher temperatures, $CuCl_2$ decomposition becomes more prominent. Therefore, this side reaction could further account for the higher conversion in Thomas et al. [8], as the current numerical model neglected side reactions at this temperature. Overall, the reaction constant calculated through the experimental results of Thomas et al. [8] presented favourable predictive results for the numerical model. Figure (4-3) presents the $CuCl_2$ conversion along the reactor length for the single PFR model at 375℃.

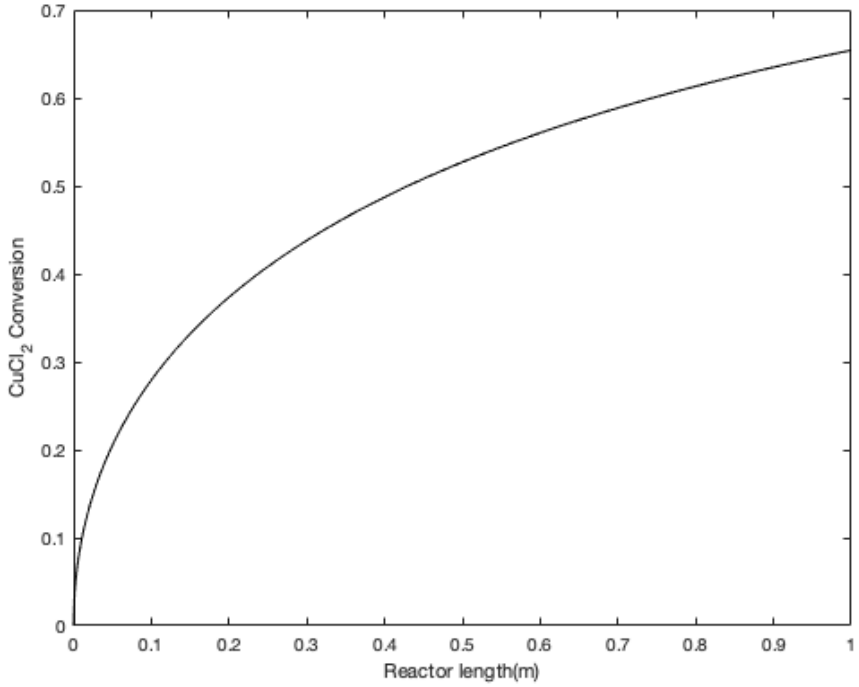

Figure 4-3: $CuCl_2$ conversion along reactor length for validation of singular PFR at 375℃.

From the validated PFR model, multi-injection MBR condition is simulated at 375℃. The reactor dimensions from Thomas et al. [8] were used, with each individual reactor in series having a length 1/3 of the total reactor length. Figure (4-4) presents a comparison of solid conversion along the reactor length between the MBR model and the single PFR for the same reactor conditions. From Figure (4-4), each change in conversion from the MBR model trend indicates a new reactor (i.e., steam injection point). A total solid conversion of approximately 80.7% is observed; a 23.4% increase compared to the single injection model. Further comparing to the experimental fluidized bed results of Thomas et al. [8] from Table (4-2), this MBR model show an approximate 8% increase in conversion. This suggests that the fresh steam injection along the reactor length is sufficient to increase $CuCl_2$ conversion.

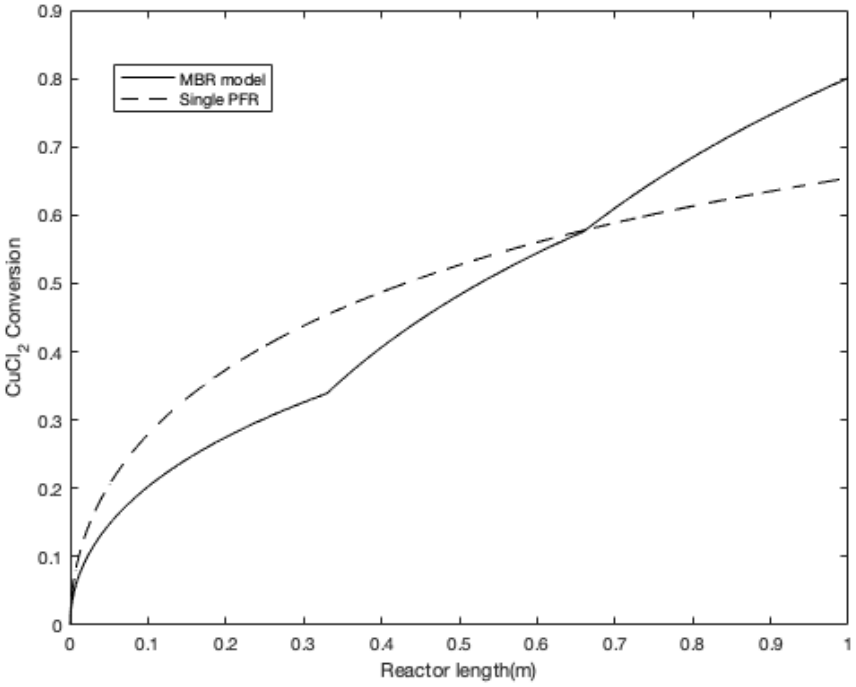

Figure 4-4: $CuCl_2$ conversion comparison between single PFR and PFR in series to simulation multi-injection MBR condition.

A new base model for the MBR condition is generated to compare this kinetic model with the previous phase equilibrium simulation results. The main changes are with respect to the inlet steam to create the 10-1 SCR and the size of the reactor (i.e., reactor length). There is limited literature that investigates the impact of reactor dimensions on the hydrolysis reaction. Therefore, taking the dimensions of a smaller scale reactor from past literature, Table (4-4) presents the base model conditions, with Figure (4-5) showing solid conversion along the reactor length [5].

Table 4-4: Base model reactor conditions for smaller lab scale reactor dimensions [5].

Variable	Value	Unit
Reactor length	0.15	m
Reactor Diameter	0.026	m
SCR	10:1	-
Inlet solid	0.0034	mol/s

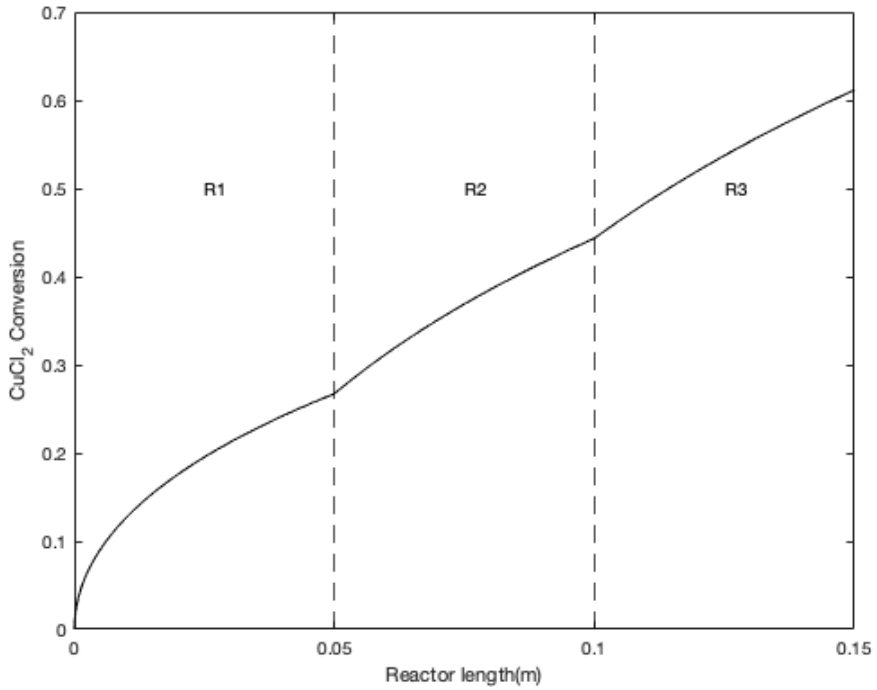

Figure 4-5: $CuCl_2$ conversion along reactor length for multi-injection downdraft MBR base model parameters.

From Figure (4-5), comparing with the conversion achieved with the reactor conditions for Figure (4-4), a lower solid conversion is achieved with the smaller reactor dimensions. This is expected as the volume of the reactor is now smaller, along with a shorter residence time. Comparing this scenario to the phase equilibrium simulation results in the previous chapter, a lower solid conversion is achieved in the kinetic model of the multi-injection MBR. The equilibrium simulation showed total conversion of 66% at the same reactor conditions, compared to 61.1% here. This result was anticipated as the numerical model introduced reaction rates, which are a function of time and temperature. The equilibrium results are independent of residence time and are only a function of temperature. Additionally, the equilibrium model included all possible side reactions, including the decomposition of $CuCl_2$, which can increase the overall conversion of $CuCl_2$. In this work,

the side reactions were neglected at the reactor temperature. Nonetheless, the reactor rate and reactor design in this study translated to a better representation of the reaction through the additional constraints.

Overall, the multi-injection downdraft MBR model present favourable conversion for $CuCl_2$ in the hydrolysis phase. The predictions indicate an improved conversion through the shifting of equilibrium when compared to the single PFR model as well as the experimental fluidized bed data from Thomas et al. [8].

4.3.1 Sensitivity Analysis

Each sensitivity analysis calculates solid conversion as a function reactor length to compare the conversion result with the base model (Fig. 4-5). Table (4-2) presents the varying reactor parameters for sensitivity analyses with respect to reactor length, injection spacing and injection amount (16 variations in total).

4.3.1.1 Reactor Length

The first analysis of total reactor length shows an increased solid conversion can be achieved within a longer reactor at the same reactor operating conditions (i.e., temperature, pressure, flowrate, SCR, equal injection spacing). This indicates the reactor length is within a length that the reverse reaction is not favoured and as expected conversion increases with time (length) [5]. Figure (4-6) shows $CuCl_2$ conversion as a function of reactor length, with Table (4-5) comparing the final solid conversion at different lengths.

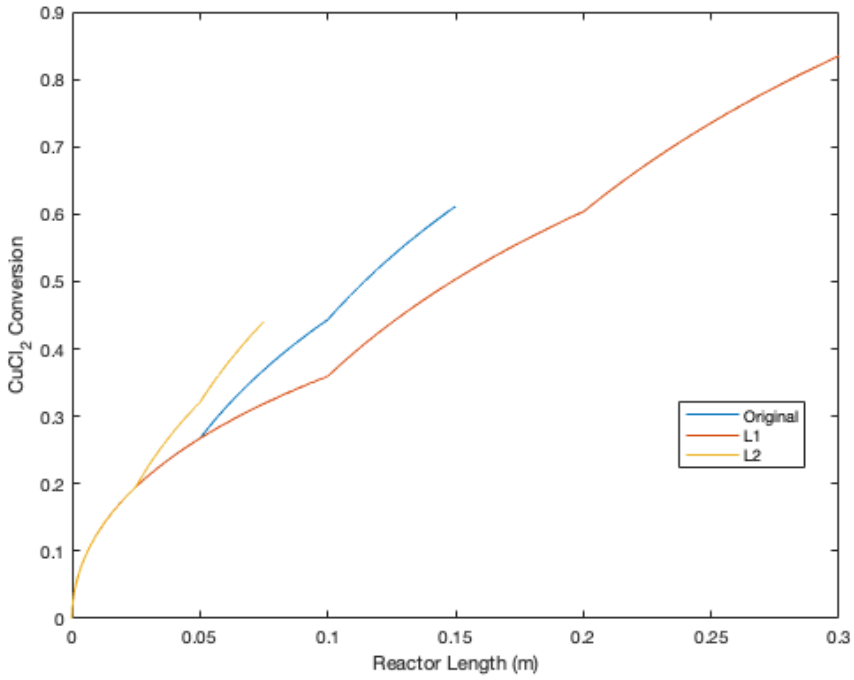

Figure 4-6: $CuCl_2$ conversion along reactor length at vary total reactor lengths for multi-injection downdraft MBR. With Original = 0.15m, L1 =0.3, and L2 = 0.075m.

Table 4-5: Solid conversion comparison for different reactor lengths

Combination	Conversion (%)
Original	61.1
L1	83.5
L2	44.0

The variation of reactor length, and thus reaction time, is an important parameter to consider when studying equipment design, costs, and downstream processes. From Figure (4-6), the same solid conversion is achieved at the end of the 0.15 m reactor length with 3 injections, as after two injections at the 0.3 m reactor length. This indicates that for potentially less steam injection and longer reaction time (i.e., longer distance between the injection sites), higher solid conversion is observed. However, when choosing between these different design configurations, feasibility of the design from a sizing, costs, and

efficiency perspective are important to consider. While an approximate 20% increase in solid conversion is seen as favourable, the increased size of the reactor may decrease process efficiency or be too costly for implementation. Consideration of downstream implications is also important, especially with respect to impurity tolerance for later reactions within the Cu-Cl cycle. The longer residence time associated with the large volume could result in progression of undesired side reactions and by-product generation. Whereas low solid conversion presented with small reactor volumes may also not be suitable for later reaction stages. Therefore, additional research is required to identify the ideal product composition for thermolysis and electrolysis step of the Cu-Cl cycle for successful integration of the hydrolysis step.

Overall, through this reaction time/reactor length analysis, essential insight is provided with respect to the relationship between $CuCl_2$ conversion and reactor volume. Further emphasizing the importance of reactor design parameters for successful process integration, optimization, and process scaling.

4.3.1.2 Injection Point Location

For the injection point location analysis, or injection spacing, nine combinations were simulated by varying the individual reactor lengths from Table (4-2). This sensitivity analysis provided insight on reactor configurations that could achieve maximum $CuCl_2$ conversion at a set temperature, pressure, and SCR. Figures (4-7) – (4-9) demonstrate each variation.

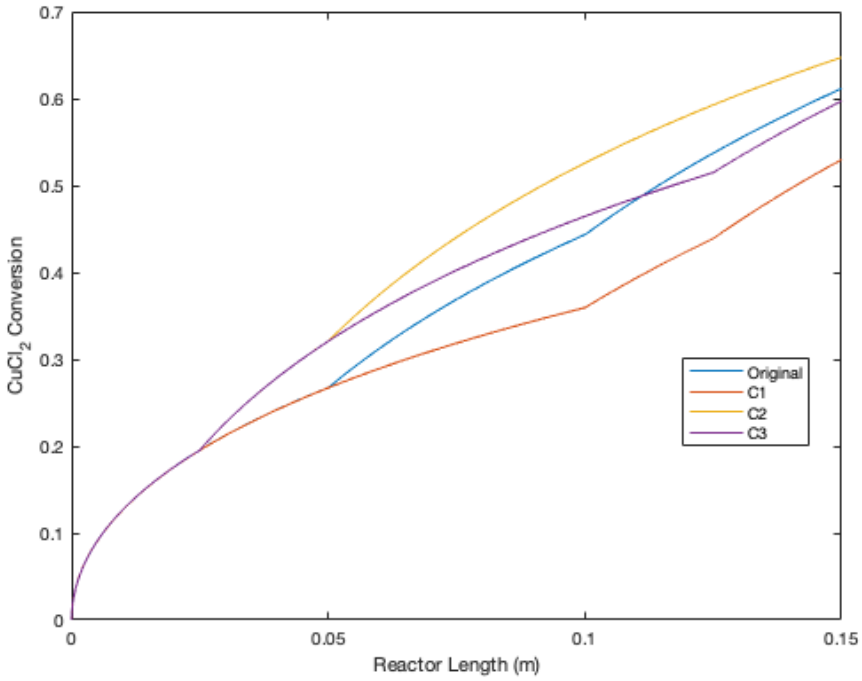

Figure 4-7:Comparison of base model $CuCl_2$ conversion to $CuCl_2$ conversion at varying to injection spacing, C1- C3, along total reactor length.

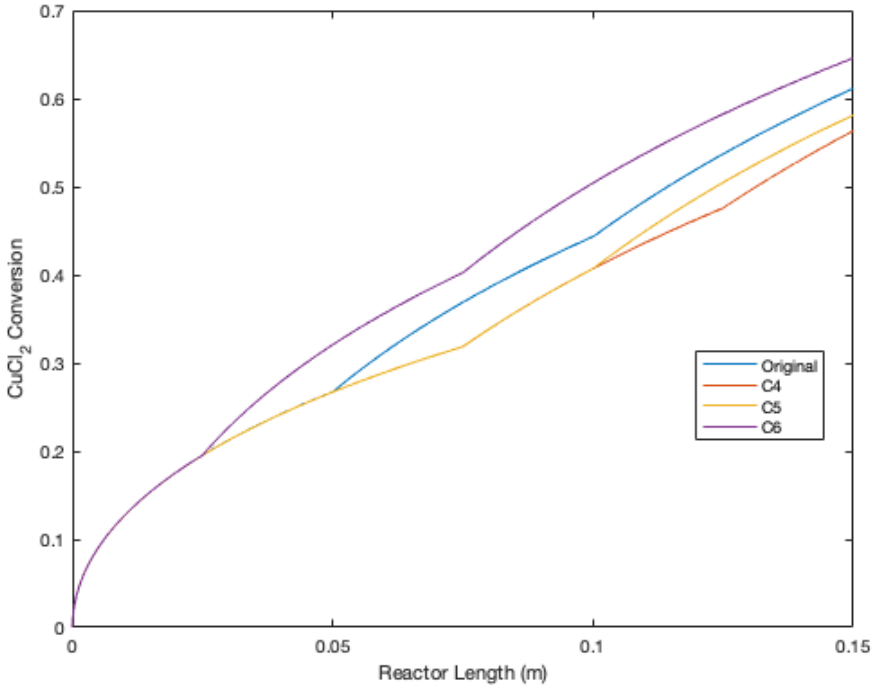

Figure 4-8:Comparison of base model $CuCl_2$ conversion to $CuCl_2$ conversion at varying injection spacing, C4 - C6, along total reactor length.

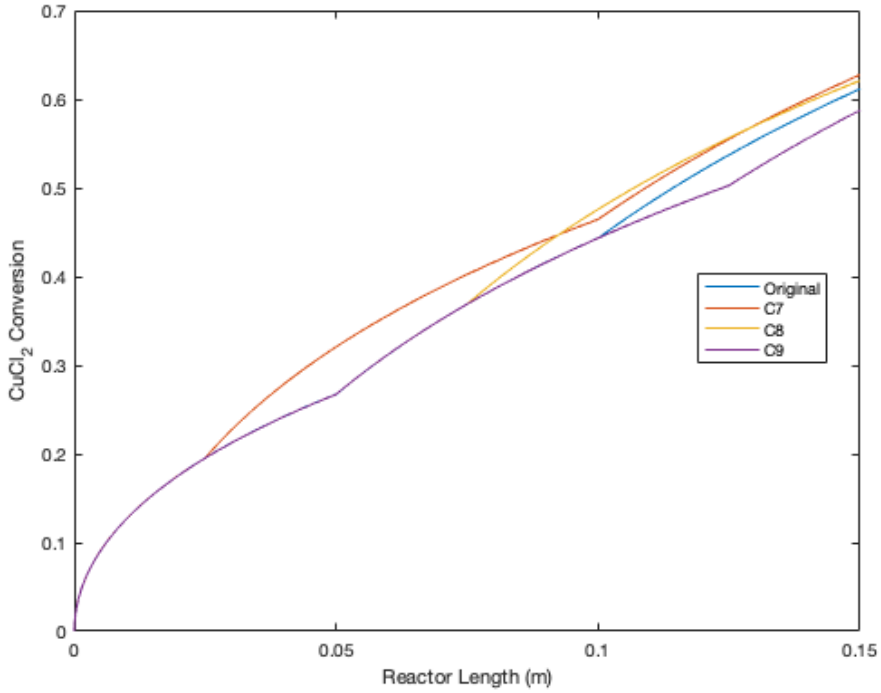

Figure 4-9:Comparison of base model $CuCl_2$ conversion to $CuCl_2$ conversion at varying injection spacing, C7 - C9, along total reactor length.

Table (4-6) presents a conversion comparison of the combinations. Combinations 2, 6, 7 and 8 demonstrate solid conversion greater than or equal to the original mode. Performing the same analysis at a higher SCR (15:1) indicated that the same combinations have higher solid conversion. From the four variations, C2 and C6 pose the largest increase in solid conversion. Both C2 and C6 have the longest reactor length (i.e., longest distance between injection points or outlet) after the last injection site. This suggests that a longer length (i.e., longer time) during the end of the sequence can increase solid conversion for this condition. This can be due to the notion that all of the steam has enter the reactor at the time last injection, thus allowing for a longer reaction time at a condition with more steam.

Considering C7 and C8, C7 has the longest reactor length at the last injection, while C8 had the longest in the middle condition and the second longest at the end. This further

supports that a longer time between injection points during the last sites can increase conversion. The remaining injection site variations produce conversions 2 – 15% smaller than the original model. The majority have the longest distance between the first and second steam injection sites.

Table 4-6: Solid conversion comparison at different injection spacings

Combination	Conversion (%)
Original	61.1
C1	53.0
C2	64.7
C3	59.7
C4	56.3
C5	58.1
C6	64.6
C7	62.8
C8	62.1
C9	58.7

While these are not a significant increase or decrease in solid conversion, this is expected as the amount of steam entering the reactor does not change. Therefore, higher conversion differences would not be obtained as only the injection spacing is changing slightly. The objective of this sensitivity analysis is to determine the ideal configuration that would maximize solid conversion at the specific operating conditions.

4.3.1.3 Injection Amount

The final analysis presented conversion data with respect to the varying steam injection amount at each site. In the original condition, the initial reactor has 50% of the available fresh steam injected (same as IA1). IA2 and IA3 have 60% of the fresh steam injected and IA4 and IA5 have 40%. Additionally, the steam input for the second reactor was either 50% or 75% of the remaining fresh steam. Figures (4-10) and (4-11) present the five variations.

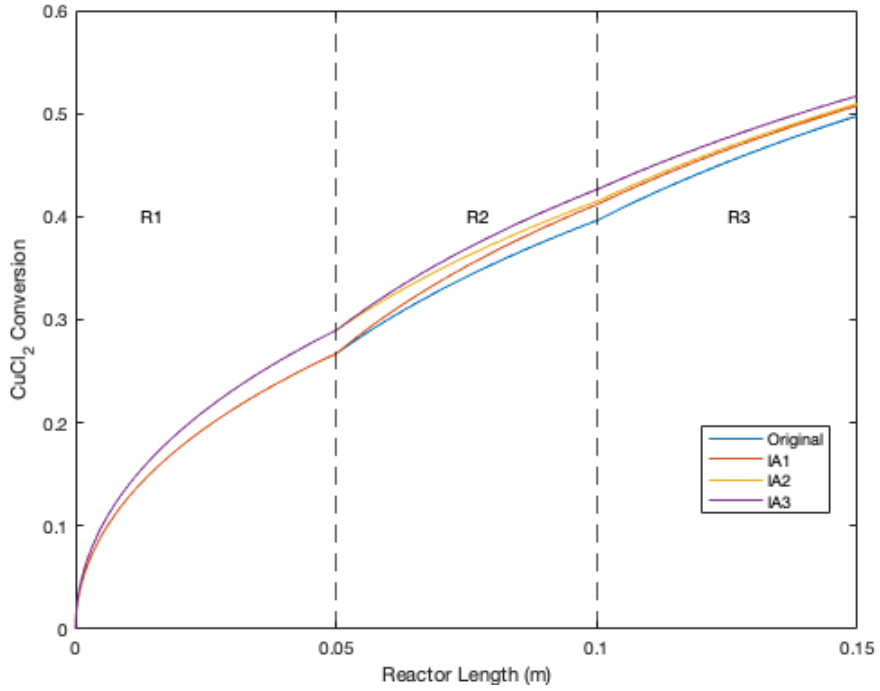

Figure 4-10: Comparison of base model $CuCl_2$ conversion to $CuCl_2$ conversion at varying injection amounts, IA1 – IA3, along total reactor length.

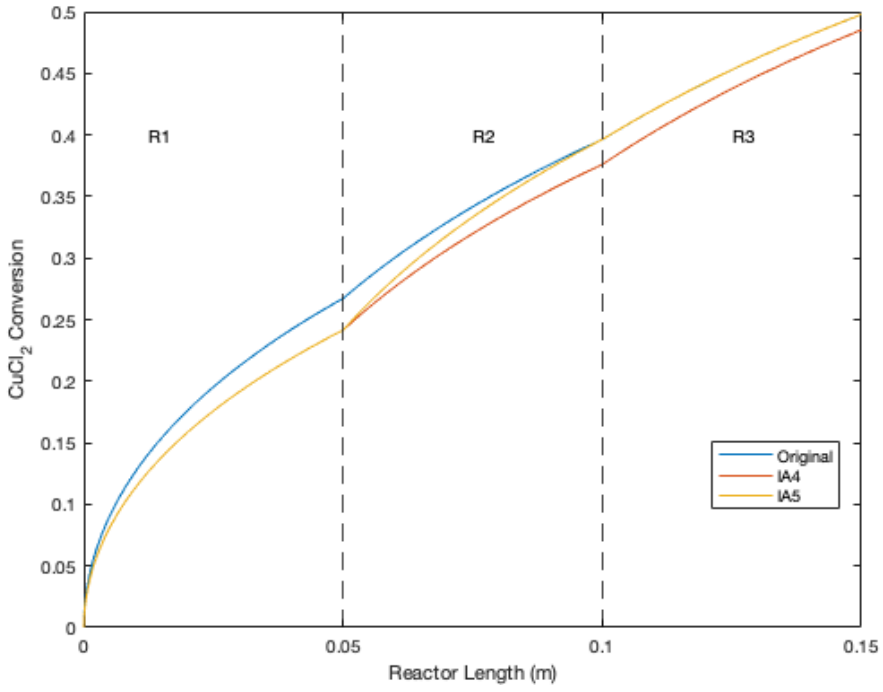

Figure 4-11: Comparison of base model $CuCl_2$ conversion to $CuCl_2$ conversion at varying to injection amounts, IA4 and IA5, along total reactor length.

From the figures, more steam input within the first two injection points allows for further conversion of $CuCl_2$. A higher SCR will theoretically allow for more conversion. As the solid enters the third reactor there will also be less unreacted $CuCl_2$ for conversion, thus, maintaining a high SCR even though the amount of steam entering is lower compared to 1st injection. Table (4-7) presents a comparison between steam injection amounts with the original condition data. IA3 presents the highest total solid conversion with the most steam entering the first and second reactors (approximately 5% increase). In general, there is a not a large increase in solid conversion at the varying injection conditions. Again, the total amount of steam entering the reactor has not changed, therefore it is not expected that significant change in solid conversion would be presented.

Table 4-7: Conversion comparison between different steam injection amounts.

Combination	Conversion (%)
Original	61.1
IA1	62.8
IA2	62.8
IA3	64.1
IA4	59.4
IA5	61.4

4.3.1.4 Ideal Analysis

Considering the trials with the highest solid conversion, a final analysis is performed to combine the best conversions for the injection site and injection amount trials. Based on Table (4-6) and (4-7), the higher solid conversion conditions are from analysis C6 and IA3. Table (4-8) presents all the variables for this final analysis.

Table 4-8: Reactor parameters for best conversion data for sensitivity analysis 2 and 3.

Variable	Value
Total reactor length (m)	0.15
R1 length (m)	0.025
R2 length (m)	0.025
R3 length (m)	0.1
IA1 (mol/s)	0.0202
IA2 (mol/s)	0.0101
IA3 (mol/s)	0.00336

The conversion of this ideal trial is presented in Figure (4-12), with comparison to the original C2 and IA3 trials. An 8.8% increase in solid conversion is achieved through the ideal conditions when compared to the base model data. Further evaluating against all sensitivity analysis results, this is the highest $CuCl_2$ conversion achieved, indicating these conditions maximize solid conversion with this MBR design.

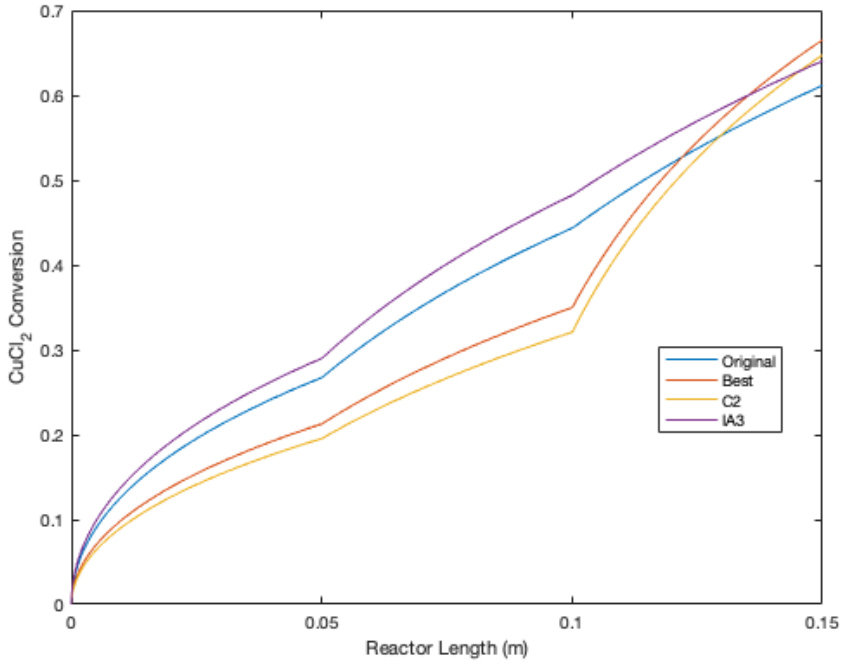

Figure 4-12: $CuCl_2$ conversion comparison along total reactor length at varying reactor configurations to identify highest final conversion.

This result also suggests that there is no relationship between injection spacing and injection amount. Regardless of the location of the injection sites, more steam entering the first part of the reactor will increase solid conversion. Similarly, having a longer distance between the last injection and reactor outlet will achieve higher $CuCl_2$ conversion regardless of the amount of steam entering each injection site. However, a combination of both conditions will increase overall conversion more than one condition alone.

Again, a large increase in conversion is not achieved, nor expected, at the different injection conditions, as the amount of overall steam injected, or total reactor volume did not change. The purpose was to identify the relationship between reactor configuration and solid conversion in order to achieve the maximum possible solid conversion at a designated design condition, which was achieved. Overall, the ideal reactor configuration is dependent on the scale of the system, which impacts the reactor volume and inlet reactant flowrates. This signifies the importance of design conditions and parameters analysis for the successful implementation of the MBR design in experimental settings.

4.3.2 Asymptotic Analysis

The final analysis for the MBR behaviour is with respect to asymptotic conditions to investigate the limitations of solid conversion. Modifying the model to generate data for solid conversion at an increasing number of injection sites along the reactor length presented asymptotic conditions for solid conversion. Figure (4-13) demonstrates the solid conversion with respect to increase injection sites.

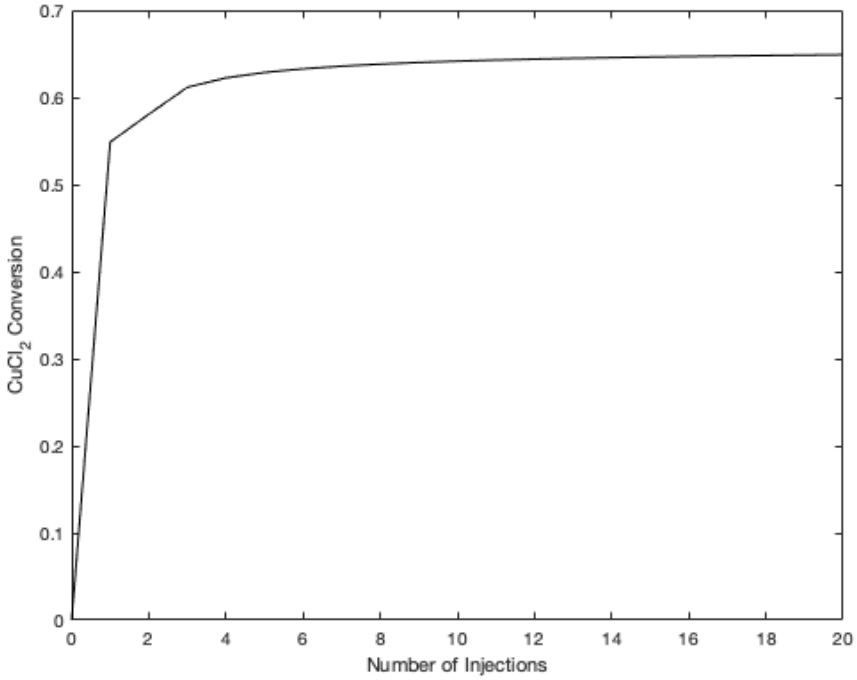

Figure 4-13: Asymptotic analysis of solid $CuCl_2$ conversion with respect to number of steam injections along reactor.

It is observed that after approximately 12-15 injection along the reactor, a maximum solid conversion is achieved, i.e., no further conversion is obtained. This maximum conversion is 65%, a 6.4% increase compared to the base amount of 61.1% with three injection sites. The difference between the final conversion values is insignificant; again, the amount of steam entering the reactor has not changed, just the number of fresh steam injection sites, thus a large change in solid conversion would not be obtained.

Based on the asymptotic model, changes of the operating conditions can be performed to identify limitations for other reactor scenarios and determine if the trend holds regardless of operating conditions. With respect to varying SCR, Figure (4-14) presents the trends for SCR of 5, 10, and 15, with all remaining conditions the same. The same asymptotic trend observed in each condition. The maximum total solid conversion achieved increases with

increasing SCR. This is anticipated as data from this Chapter 3 and previous literatures [6,7,9] support that increasing the SCR increases the total $CuCl_2$ conversion within the hydrolysis reactor. Furthermore, considering all three trend lines, for higher SCR, the asymptotic condition establishes after more injections. For the 5:1 SCR condition, there is no improvement in conversion between 1 and 2 injections, with asymptotic conditions establishing after 3 injections. Whereas for the 15:1 SCR, an asymptotic is established around 20 injections. Overall, the asymptotic analysis demonstrated that there is a maximum conversion that can be achieved within the MBR design, regardless of the SCR and number of injections. These results further underline the need for design analysis to understand the limitations for novel reactor design and maximum desired yields.

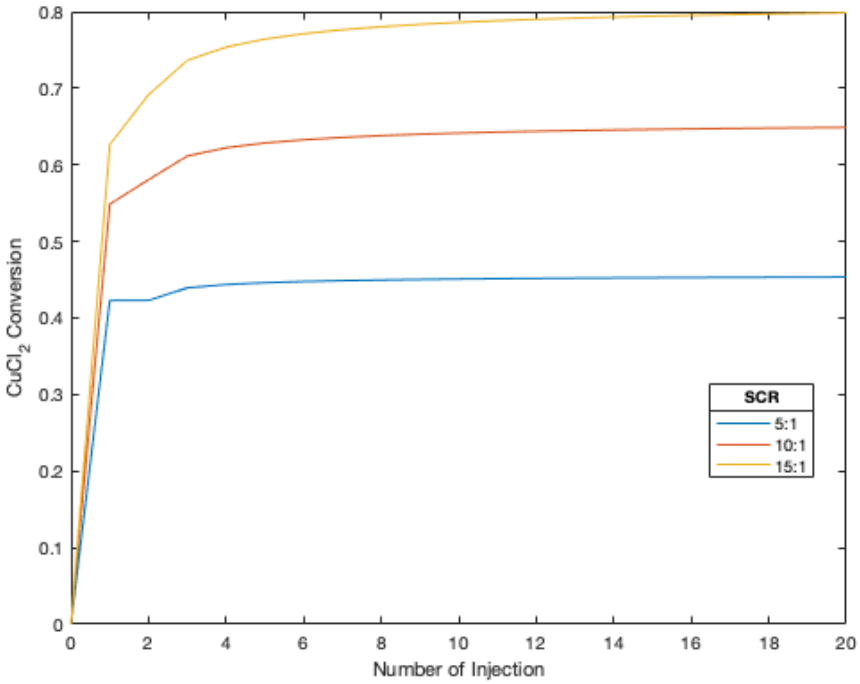

Figure 4-14: Asymptotic relationship for solid $CuCl_2$ conversion at various SCR, with increasing number of injections.

4.4 Conclusions

This chapter examined a novel multi-injection MBR reactor design and its relationship with $CuCl_2$ conversion in the hydrolysis process of the Cu-Cl cycle. Numerical modeling of reaction kinetics and plug flow conditions yielded solid conversion that was comparable to experimental data. Proportional relationships between SCR and $CuCl_2$ conversion were observed, with the steam mole fraction meeting the minimum requirement for the higher desired product yield established in past literature. Through the combination of the validated PFR model and reactor parameters including dimensions and operating conditions, the downdraft multi-injection MBR model was established. Favourable solid conversion was achieved when compared to past work within a fluidized bed reactor, with a 23.4% increase from the single model and an 8% increase from experimental data.

Furthermore, when implementing the same conditions as the preliminary phase equilibrium simulations, the numerical model presented conversions lower than the preliminary equilibrium model. However, the incorporation of reaction rates and reactor design parameters translated to a better representation of reaction progression. Overall, the model indicated that the MBR design has a potential to enhance hydrolysis conversion with a lower steam requirement through improved reactant contact and enhanced heat and mass transfer between the particles.

This study also assessed the impact of different variables on $CuCl_2$ conversion within the MBR model. The three sensitivity analyses investigated variations in reactor volume, injection site locations, and inlet steam flowrate, in comparison to conversion results of the base MBR model. Through total reactor volume alternatives, a higher solid conversion was

achieved at larger reactor volumes. Larger discrepancies in conversion were predicted to be achieved when adjusting the reactor diameter through the squared relationship with reactor volume. Injection location, altered through sequential reactor length, yielded varying results with respect to solid conversion. Of the nine trials, four exhibited conversions greater than or equal to the base model, all of which had the largest reactor length after the final injection site. Similarly, the injection amount in each site also impacted the maximum achievable conversion at the specific reactor conditions, with more steam at the beginning injections presenting higher overall conversion.

An investigation of the best conversion results from the injection location and amount sensitivity analyses demonstrated that a combination of the best conversion configurations within each analysis predicted an 8.8% increase in the maximum achievable solid conversion. Finally, the asymptotic analysis demonstrated that there is a limitation to the maximum possible attainable conversion through the number of injections, with a maximum conversion of approximately 65%. At varying SCR, the same relationship is observed, with increasing SCR resulting in increased solid conversion. Overall, different reactor operating conditions can influence the impact that the reactor configuration will have on total solid conversion.

References

[1] M. F. Orhan, I. Dinçer, and M. A. Rosen, "Efficiency comparison of various design schemes for copper-chlorine (Cu-Cl) hydrogen production processes using Aspen Plus software," Energy Convers. Manag., vol. 63, pp. 70–86, 2012.

[2] D. H. Lee, H. Yang, R. Yan, and D. T. Liang, "Prediction of gaseous products from biomass pyrolysis through combined kinetic and thermodynamic simulations," *Fuel*, vol. 86, no. 3, pp. 410–417, 2007.

[3] D.-J. Kim, G.-G. Lee, S. W. Kim, and H. P. Kim, "The use of Thermodynamics and Phase Equilibria for Prediction of the Behavior of High Temperature Corrosion of Alloy 617 in Impure Helium Environment," *Corros. Sci. Technol.*, vol. 9, no. 4, pp. 164–170, 2010.

[4] R. V. Singh *et al.*, "Investigations on the hydrolysis step of copper-chlorine thermochemical cycle for hydrogen production," *Int. J. Energy Res.*, vol. 44, no. 4, pp. 2845–2863, 2020.

[5] Y. Haseli, G. F. Naterer, and I. Dincer, "Fluid-particle mass transport of cupric chloride hydrolysis in a fluidized bed," *Int. J. Heat Mass Transf.*, vol. 52, no. 11–12, pp. 2507–2515, 2009.

[6] V. N. Daggupati, G. F. Naterer, K. S. Gabriel, R. J. Gravelsins, and Z. L. Wang, "Solid particle decomposition and hydrolysis reaction kinetics in Cu-Cl thermochemical hydrogen production," *Int. J. Hydrogen Energy*, vol. 35, no. 10, pp. 4877–4882, 2010.

[7] M. S. Ferrandon *et al.*, "The Hybrid Cu-Cl Thermochemical Cycle. I. Conceptual Process Design and H2a Cost Analysis. II. Limiting the Formation of CuCl during hydrolysis," no. January 2008, 2008.

[8] D. Thomas, N. A. Baveja, K. T. Shenoy, and J. B. Joshi, "Experimental Study on the Mechanism and Kinetics of CuCl2 Hydrolysis Reaction of the Cu-Cl Thermochemical Cycle in a Fluidized Bed Reactor," *Ind. Eng. Chem. Res.*, vol. 59, no. 26, pp. 12028–12037, 2020.

[9] V. N. Daggupati, G. F. Naterer, and K. S. Gabriel, "Diffusion of gaseous products through a particle surface layer in a fluidized bed reactor," *Int. J. Heat Mass Transf.*, vol. 53, no. 11–12, pp. 2449–2458, 2010.

[10] G. Naterer *et al.*, "Recent Canadian advances in nuclear-based hydrogen production and the thermochemical Cu-Cl cycle," *Int. J. Hydrogen Energy*, vol. 34, no. 7, 2009.

[11] E. H. P. Wolff, "A novel circulating cross-flow moving bed reactor system for gas-solids contacting," *Chem. Eng. Sci.*, vol. 49, no. 24, pp. 5427–5438, 1994.

[12] S. Arabi and H. Hashemipour Rafsanjani, "Modeling and simulation of noncatalytic gas-solid reaction in a moving bed reactor," *Chem. Prod. Process Model.*, vol. 3, no. 1, 2008.

[13] P. E. Arce, O. M. Alfano, I. M. B. Trigatti, and A. E. Cassano, "Heterogeneous Model of a Moving Bed Reactor. 2. Parametric Analysis of the Steady-State Structure," *Ind. Eng. Chem. Res.*, vol. 28, no. 2, pp. 165–173, 1989.

[14] Z. Hongjun, S. Mingliang, W. Huixin, L. Zeji, and J. Hongbo, “Modeling and simulation of moving bed reactor for catalytic naphtha reforming,” *Pet. Sci. Technol.*, vol. 28, no. 7, pp. 667–676, 2010.

[15] M. Karimi, M. R. Rahimpour, R. Rafiei, A. Shariati, and D. Iranshahi, “Improving thermal efficiency and increasing production rate in the double moving beds thermally coupled reactors by using differential evolution (DE) technique,” *Appl. Therm. Eng.*, vol. 94, pp. 543–558, 2016.

[16] N. Zang, X. M. Qian, C. M. Shu, and D. Wu, “Parametric sensitivity analysis for thermal runaway in semi-batch reactors: Application to cyclohexanone peroxide reactions,” *J. Loss Prev. Process Ind.*, vol. 70, no. February, p. 104436, 2021.

[17] U. Kumar and M. C. Paul, “Sensitivity analysis of homogeneous reactions for thermochemical conversion of biomass in a downdraft gasifier,” *Renew. Energy*, vol. 151, pp. 332–341, 2020.

[18] O. Levenspiel, “Fluid - Particle Reactions: Kinetics,” in *Chemical Reaction Engineering*, 3rd ed., vol. 566–588, New York: Wiley, 1999.

[19] S. H. Fogler, *Fogler - Elements of Chemical Reaction Engineering 5th Edition*. Pearson, 2016.

[20] V. Manokaran, T. Sengupta, S. Narasimhan, and N. Bhatt, “Analysis of Experimental Conditions, Measurement Strategies, and Model Identification Approaches on Parameter Estimation in Plug Flow Reactors,” *Ind. Eng. Chem. Res.*, vol. 58, no. 30, pp. 13767–13779, 2019.

Chapter 5 - Conclusions and Recommendations

Development of cleaner fuel alternatives is critical for the future sustainability of the energy industry. While there are various hydrogen generation methods, thermochemical water splitting cycles, like the Cu-Cl cycle, can reduce emissions compared to other conventional methods [1, 2]. The hydrolysis reaction is a challenging step of the Cu-Cl cycle. Improvement of $CuCl_2$ conversion and reduction of steam requirements are essential for process integration and large-scale production [3, 4].

In this thesis, simulations of the critical operating conditions of the hydrolysis reaction have been presented in a single reactor configuration to gain a better understanding of the limitations of hydrolysis reaction and identify ideal operating scenarios that will allow for maximum solid conversion. These simulations involved component compositions in a range of temperatures (300 – 550℃), pressures (0.5 – 10 bar) and steam to copper ratios (SCR) (1:1 - 20:1). Analysis of all product generation, both desired and undesired, emphasized reactor operating conditions between 375 – 400℃ and 1 bar. These achieved the most solid conversion through the hydrolysis reaction while mitigating the influence of undesired side reactions. A final operating condition of 375℃, 1 bar and a 10:1 SCR was chosen for the remaining simulations, as these results and past studies indicate that the main side reactions within the hydrolysis stage occur at temperatures 400℃ and greater [5, 6].

A study of novel reactor design configurations was also presented in this thesis, specifically multi-injection moving bed reactors (MBR) simulated through reactors in series. Through the Gibbs energy minimization method and an iterative approach, the

multi-injection MBR design was first simulated to determine the feasibility in the hydrolysis stage and identify any improvements to SCR or solid conversion. These simulations indicated promising potential for the MBR design, with a 17% increase in overall solid conversion when compared to a single injection design at the same operating conditions.

Another reactor configuration investigated outlet gas recirculation. The goal of this design was to recycle the unreacted outlet steam, with only enough fresh steam added to maintain the original SCR. It was found that this configuration was only viable for four recirculations, after which a completely fresh stream of steam would be required. While this arrangement minimized the required steam input into the reactor, the maximum achievable solid conversion with each iteration decreased, due to the increasing concentration of HCl gas. Therefore, the outlet gas recirculation scheme was not ideal without the concentration reduction of HCl for total process integration.

An important assumption used within the equilibrium simulations was infinite time. Since no reaction kinetics or reactor details (i.e., reactor type, dimensions, flow configurations, etc.) were defined within this first model, the predicted equilibrium amounts were solely a function of temperature. Based on the phase equilibrium results, a numerical model was generated to integrate reaction kinetics and reactor design components to accurately reflect the hydrolysis reaction progression. From a literature review, the reaction rate equations and rate constants were identified for this reaction model. This study highlighted a key gap within the experimental hydrolysis reaction literature, namely a discrepancy with respect to reaction kinetic values. Depending on the reactor conditions implemented in past literature, different kinetic values could be

generated. This was also true for the case of the MBR design, as there are currently no experimental results available to the author's knowledge for this configuration. Therefore, ensuring that validation data was generated from the same operating conditions as the model was essential.

The numerical multi-injection MBR model presented favourable results for integration into the hydrolysis reaction. When compared to experimental results of a fluidized bed reactor at the same conditions, the MBR design presented a 23.4% increase in solid conversion. Further evaluation of the phase equilibrium model results yielded a 6.8% decrease in solid conversion within the kinetic model. However, through the incorporation of reaction kinetics and design parameters, the numerical model translated to a more accurate representation of the hydrolysis reaction. A series of sensitivity analyses was performed with this model to detect limitations of the design at different configurations through the variation of reactor length, injection spacing and steam injection amount. It was found that the maximum achievable conversion was 66.5%, for an 8.8% increase compared to the base model conditions. Additionally, through asymptotic assessment, regardless of the number of injections, the MBR reaches a maximum solid conversion that varies based on other conditions, such as reactant input, reactor dimensions and injection conditions.

Overall, these models indicated that the downdraft multi-injection MBR design has promising potential for implementation into the hydrolysis reactor of the Cu-Cl cycle. The model provided predictive trends for reaction progression and identified that, through the reactors in series approach, the multi-injection behaviour can achieve higher $CuCl_2$ conversions at lower SCR. The results of this thesis also emphasized the importance of

design considerations and operating conditions to ensure accurate modelling and optimal yield.

5.1 Future Recommendations

The MBR, and specifically the multi-injection configuration, is a largely unexplored reactor design for the hydrolysis reaction. Additional research is recommended to better understand the reaction kinetics and progression of the hydrolysis reaction within the moving bed reactor design. Future recommendations for this work are summarized as follows.

- The phase equilibrium simulation demonstrated the possible side reaction and by-product generation within the hydrolysis reactor and the impact that different operating conditions can have on their progression. However, the kinetic model neglected the influence of side reactions at the prescribed temperature conditions. Integration of the major side reactions, such as the decomposition of $CuCl_2$ and Cu_2OCl_2, could lead to a better predictive model of the hydrolysis reaction.
- Based on the results of the gas recirculation simulations, further details to effectively identify potential strategies and technologies to incorporate this concept within the reactor configuration would be beneficial to reduce steam consumption and improve overall system efficiency.
- The kinetic model in this thesis assumed isothermal conditions. Integration of the heat of reactions and energy balances could further optimize the model and provide insight to the influence of temperature on the endothermic reaction.

- Due to the varying experimental data in past literature, additional experimental validation would improve the numerical model by providing reaction kinetic data at various operating conditions. As previously mentioned, it is important that the experimental results encompass the entire hydrolysis reaction progression within the reactor to ensure accurate reflection within the established rate constants.
- Due to novelty of the multi-injection MBR design for the Cu-Cl cycle, construction of a lab scale reactor, based model results, would allow for further validation of design. This process would include exploring scalability of the MBR design, investigation of material (i.e., durability, performance efficiency, corrosion resistances, etc.), energy efficiency, and economic feasibility.

References

[1] L. C. Brown *et al.*, "High efficiency generation of hydrogen fuels using nuclear power.," 2003. [Online]. Available: http://www.osti.gov/servlets/purl/814014-tdQyiq/native/%0Ahttps://fusion.gat.com/pubs-ext/AnnSemiannETC/A24285.pdf.

[2] B. W. Mcquillan *et al.*, "High efficiency generation of hydrogen fuels using solar thermal-chemical splitting of water (Solar thermo-chemical splitting for H2)," 2010.

[3] G. Naterer *et al.*, "Recent Canadian advances in nuclear-based hydrogen production and the thermochemical Cu-Cl cycle," *Int. J. Hydrogen Energy*, vol. 34, no. 7, 2009.

[4] A. Farsi and A. Science, "Development and Modeling of a Lab-scale Integrated Copper-Chlorine Cycle for Hydrogen Production," no. August, 2020.

[5] M. Ferrandon, V. Daggupati, Z. Wang, G. Naterer, and L. Trevani, "Using XANES to obtain mechanistic information for the hydrolysis of CuCl2 and the decomposition of Cu2OCl2 in the thermochemical Cu-Cl cycle for H2 production," *J. Therm. Anal. Calorim.*, vol. 119, no. 2, pp. 975–982, 2015.

[6] R. V. Singh *et al.*, "Investigations on the hydrolysis step of copper-chlorine thermochemical cycle for hydrogen production," *Int. J. Energy Res.*, vol. 44, no. 4, pp. 2845–2863, 2020.

Appendix A: MATLAB Codes

Reaction Kinetic Model - Function and Script

```
function X = CuCl_reversible(t, x, N, Dp)
%Constants
T = 375+273.15; %R
R1 = 8.314472*(10^-5); %m3-bar/mol-K
Ps = Dp;%0.0002; %m
R = (Ps/2);%particle radius in m
MM = 134.45; %g/mol
p = 3390*1000; %g/m3
dens = p/(MM); % molar density, mol/m3
N2 = 3*N; %steam to copper ratio
P = 1; %bar
%yh2o = 0.21
%p_h2o = P*yh2o;
p_h2o = (((N-x(1)))./((N)+x(1))).*P;
p_hcl = ((2.*x(1))./((N)+x(1))).*P;
k1 = 0.0022; %mol/m2-s-bar
%k2 = 0.0001; %m/s
K1 = 0.00259; %bar
C_h2o = p_h2o/(R1*T); %mol/m3 - concentration h2o
b = 2;

dxdt = ((3.*b.*((1-x).^(2/3)))./(R.*dens)).*(k1).*((p_h2o)-((1/K1).*((p_hcl)^2)));

%dx2dt = ((3.*b.*((1-x).^(2/3)))./(R.*dens)).*k2.*C_h2o;

X =[dxdt];

%Script code
%Initial Conditions

% Single Reactor
tspan = 0:2000; %time in seconds
xinit = 0;
N = 40;
Dp = 0.0002; %m, particle diameter

[t1,x] = ode45(@(t, x)CuCl_reversible(t,x,N,Dp), tspan, xinit);

time = t1/60;


% Daggupati Data
% without inert N2
xdata2 = [0.079709228
```

0.198712345
0.357383168
0.446854764
0.581816979
0.767704535
0.848017621
1.079295154
1.245959904
1.512395379
1.791042201
1.954989591
2.237494393
2.495140383
2.81719787
3.203666855
3.590135839
4.041016321
4.556308301
5.200423276
6.059243242
6.810710712
8.098940661
9.558934603
10.93304655
12.0495125
14.26097392
15.57067437
16.98772731
18.98448373
21.11006315
22.2694701
25.81210246];

ydata2 =[0.016702457
0.047230513
0.079677086
0.112431484
0.158241395
0.20245409
0.243495969
0.286917131
0.328173585
0.373743689
0.424542517
0.460436801
0.504277899
0.536397336
0.578470254
0.621601073
0.658636353
0.693024916
0.725791444
0.762118834
0.798469373

```
0.824088598
0.859166964
0.886601432
0.905332377
0.914194785
0.934138622
0.945099888
0.951701711
0.95829438
0.964614314
0.969218043
0.98178779];

%Ferrandon Experimental Data
xdata3 = [19.918375915760844
29.95414492667638
39.91360671430544];

ydata3 = [0.892669691724751
0.9515357855547963
0.9914875458807451];

%PLOTS

plot(time,x, 'color','k')
hold on
plot(xdata2, ydata2,'--', 'color','k')
plot(xdata3,ydata3, 'square','color','k')
legend('This work','Daggupati et al. [4]', 'Ferrandon et al. [16]')
xlabel('Time (mins)')
ylabel('CuCl_2 Conversion (x)')
```

MBR model

Function Code

```
function dydl = pfr_edits(L,x,Pf,N,D)
%UPDATED VERSION
%V =  volume of pfr
%X = concentration of specific components (A (CuCl2), B(H2O), C(Cu2OCl2), D(HCL)
% AND Temperatures (Ts, Tg)
%Pf = pressure and flow rate of inert gas (not using inert nitrogen in
%this case yet)

%REACTION
%2CuCl2 + H2O = Cu2OCl2 + 2HCl
% aA + bB = = cC + dD

%CONSTANTS
a = 2;% stoic coefficient of the solid reactant
P = Pf(1); % bar
d = D;%0.012; %reactor diameter, m
n = N;
```

```
r = d/2; %reactor radius
FN2 = Pf(2); % flow rate of inert nitrogen
Ts = x(5); %Reactor temp, K
Tg = x(6); %Gas Temp, K
R = 8.314472e-5;%m3-bar/mol-k
MMa = 0.13445; %g/mol of Cucl2
MMc = 213.999; %g/mol of Cu2OCl2
xa = x(1)/(x(1)+x(2)+x(3)+x(4)+FN2); % mole fraction of CuCl2
xb = x(2)/(x(1)+x(2)+x(3)+x(4)+FN2); % mole fraction of H2O
xc = x(3)/(x(1)+x(2)+x(3)+x(4)+FN2); % mole fraction of Cu2OCl2
xa_s = x(1)/(x(1)+x(3));
xc_s = x(1)/(x(1)+x(3));
pa = 3390; %kg/m3 dens of CuCl2
pc = 4080; %kg/m3 dens of Cu2OCl2
p_avg = (xa_s.*pa)+(xc_s.*pc); % kg/m3 - average solid density - assumption
MMs = (xa*MMa)+(xc*MMc); %Average molar mass of solids, g/mol
Fs = x(1)+x(3); %solid moar flow rate, mol/s
Vs = ((Fs)*MMs)/(p_avg)/(1000); % total Volumetric flow rat,m3/s
C_a = x(1)/Vs; %concentration of CuCl2, mol/m3

%PARTIAL PRESSURE CALCS
C_b = xb*(P)/(R*Tg);%(P*xb)/(R*Tg);


k1 =  0.0006115;%0.00164;%0.0006115;%0.0000265;% rate constant as a function of
temperature, m3/mol-s, daggupati diffusion paper/ferradon

%CUCL2 DATA
 A_cucl2 = -16.3596145;
 B_cucl2 = 0.75069416;
 C_cucl2 = -0.00256737967;
 D_cucl2 = 0.00000462107127;
 E_cucl2 = -0.00000000424415987;
 F_cucl2 = 0.0000000000157231689;
 Cp_a =
A_cucl2+(B_cucl2*Ts)+(C_cucl2*(Ts^2))+(D_cucl2*(Ts^3))+(E_cucl2*(Ts^4))+(F_cucl2*(Ts^5));
% Heat capacity, J/mol-K

%H2O DATA
 A_h2o = 30.092;
 B_h2o = 6.832514;
 C_h2o = 6.793435;
 D_h2o = -2.53448;
 E_h2o = 0.082139;
 Cp_b =
A_h2o+(B_h2o.*(Tg./1000))+(C_h2o.*((Tg./1000).^2))+(D_h2o.*((Tg./1000).^3))+(E_h2o./((Tg./10
00).^2)); % Heat capcity of H2O, J/mol-K

%HCl DATA
 A_hcl = 32.12392;
 B_hcl = -13.45805;
 C_hcl = 19.86852;
 D_hcl = -6.853936;
 E_hcl = -0.049672;
```

```
 Cp_d =
A_hcl+(B_hcl.*(Tg/1000))+(C_hcl.*((Tg/1000)^2))+(D_hcl.*((Tg/1000)^3))+(E_hcl/((Tg/1000)^2));
%heat capacity of HCl J/mol*K

%Cu2OCl2 DATA SOLID
 A_cu2ocl2 = 53.7166572;
 B_cu2ocl2 = 0.334033497;
 C_cu2ocl2 = -0.00052212794;
 D_cu2ocl2 = 0.000000299950910;
 Cp_c = A_cu2ocl2+(B_cu2ocl2.*Ts)+(C_cu2ocl2.*(Ts^2))+(D_cu2ocl2.*(Ts^3)); %heat capacity
of Cu2OCl2 J/mol*K

%N2 DATA
 A_n2 = 19.59583;
 B_n2 = 19.88705;
 C_n2 = -8.598535;
 D_n2 = 1.369784;
 E_n2 = 0.527601;
 Cp_n2 =
A_n2+(B_n2*(Tg/1000))+(C_n2*((Tg/1000)^2))+(D_n2*((Tg/1000)^3))+(E_n2*((Tg/1000)^2)); %
Heat capacity of N2, J/mol-K

% REACTION RATES

Hrxn = 113000;

ra = -(a.*k1*C_b*C_a.*4*pi()*(0.000175^2));%-(a.*k1.*C_b.*C_a);%(a/C_a).*rh2o1
%(a*k1*C_b*C_a); % <-- this is another reaction rate equation also sued be Daggupati
dFadl = ra;%(pi()*(r^2)).*ra;
dFbdl = 0.5*ra;%(pi()*(r^2)).*ra;
dFcdl = 0.5*(-ra);%(pi()*(r^2)).*(-ra);
dFddl = -ra;%(pi()*(r^2)).*(-ra);
dTsdl = (pi()*(r^2)).*(-ra.*(-Hrxn))./(((x(1).*Cp_a)+(x(2).*Cp_c)));
dTgdl = (pi()*(r^2)).*(-ra.*(-Hrxn))./(((x(2).*Cp_b)+(x(4).*Cp_d)+(FN2.*Cp_n2))); %+ x(2)*Cp_b+
x(4)*Cp_d

Da = (-ra)*(pi()*(r^2)*(L))./(x(1));%+x(2)+x(3)+x(4));

dydl = [dFadl; dFbdl; dFcdl; dFddl; dTsdl; dTgdl;Da];
```

Script Code

```
% Injection Number connector loop
steam = 10; %initial SCR
count = 3; % total number of injections
inj = 1; % initiation for number of injections
conv_tot = zeros(count,1);
```

```
for j = 1:count
%injection loop
L_tot = 0.15; %m total reactor length
n = inj(j); %number of injections along the length
l = L_tot/n; %each individual reactor length
Fa = 0.00336; %initial CuCl2 flow rate
SCR_tot = steam;% total mbr SCR
steam_tot = SCR_tot*Fa; %total available steam for injection
SCR_r1 = 5; %inital reactor SCR

Fc = 0; %inital Cu2OCl2 flow rate
Fd = 0; %Intital HCl flow rate
Tg = 375+273.15; %Inital gas temp
Ts = 375+273.15; %initial solid temp
%conv_a = zeros(1000,1);
iter = 1000;
m = n*iter;
if n == 1
   Fb = steam_tot;%SCR_tot*Fa; % initial reactor steam input
else
   Fb = 0.5*steam_tot;
end

steam_rem = steam_tot-Fb; %Remaining steam after first reactor ALWAYS
ratio = (Fb/(n-1))/Fb;
conv_x = zeros(m,1);
l_r = zeros(m,1);
Y = linspace(0,l,iter)';

for i = 1:n
length=linspace(0,l,iter); %time, s
Fa0 = Fa(i);
N = 10; %steam to copper ratio
steam0 = N*Fa(1); %total Steam consumption
Fb0 = Fb(i); %mol/s
Fc0 = Fc(i);%Fc(i);%mol/s
Fd0 = Fd(i); %mol/s
Ts = 375+273.15; %Solid temp, K
Tg = 375+273.15; %Gas temp, K
D = 0.026; %Reactor Diameter, m
pf=[1,0.002422]; %Constant pressure 162atm and N2 flowrate is zero
initial_values=[Fa0, Fb0, Fc0, Fd0, Ts, Tg,0]; % values of X at V=0
[L1,X1] = ode45(@(L,x,Pf)pfr_edits(L,x,Pf,N,D), length, initial_values,[], pf); %ODE solver

Xa = X1(:,1)./(X1(:,1)+X1(:,2)+ X1(:,3)+X1(:,4)+pf(2));
Xb = X1(:,2)./(X1(:,1)+X1(:,2)+ X1(:,3)+X1(:,4)+pf(2));
Xc = X1(:,3)./(X1(:,1)+X1(:,2)+ X1(:,3)+X1(:,4)+pf(2));
Xd = X1(:,4)./(X1(:,1)+X1(:,2)+ X1(:,3)+X1(:,4)+pf(2));

Fa(i+1) = X1(end,1);
Fc(i+1) = X1(end,3);
Fd(i+1) = X1(end,4);

if i<n-1
```

```
   steam_used = ratio*steam_rem(i);
   steam_rem(i+1) = steam_rem(i)-steam_used;
   Fb(i+1) = Fb(i)+steam_used;

else if i==(n-1)

            Fb(i+1) = Fb(i)+steam_rem(i);
end

end

 X = (Fa(i)-X1(:,1))./Fa(i);
 if i==1
    conv_x = X;
 else
    conv_x = [conv_x; X+conv_x(end)];

 end
end

count_tot1 = linspace(0,count,count+1)';
length_tot1 = linspace(0,L_tot,m)';


plot(length_tot1,conv_x)
xlabel('Reactor Length (m)')
ylabel ('CuCl_2 Conversion')

figure()
plot(count_tot1', conv_tot)
xlabel('Number of Injections')
ylabel('CuCl_2 Conversion')
```